CHARACTERIZATION AND RELAXATION DYNAMICS OF THE NONLINEAR OPTICAL PROPERTIES OF THIOPHENE BASED POLYMERS

by

David Harris

A dissertation submitted to the Graduate Faculty in Engineering in partial fulfillment of the requirements for the degree of Doctor of Philosophy. The City University of New York.

1998

This manuscript has been read and accepted for the Graduate Faculty in Engineering in satisfaction of the dissertation requirement for the degree of Doctor of Philosophy.

10/29/97
Date

Chair of Examining Committee

Dr. Roger Dorsinville
Professor, Department of Electrical Engineering, The City College of the City University of New York.

10/29/97
Date

Executive Officer

Dean G. Lowen

Dr. Mohamed Ali — Professor, Department of Electrical Engineering, The City College of The City University of New York.

Dr. Shahab Etemad — Member of Technical Staff, Bellcore, Morristown, NJ 07960.

Dr. Ping-Pei Ho — Professor, Department of Electrical Engineering, The City College of The City University of New York.

Dr. Vladimir Petricevic — Assistant Professor, Department of Physics, The City College of The City University of New York.

Dr. Ardie Walser — Associate Professor, Department of Electrical Engineering, The City College of The City University of New York.

Supervisory Committee

THE CITY UNIVERSITY OF NEW YORK

Abstract

CHARACTERIZATION AND RELAXATION DYNAMICS OF THE NONLINEAR OPTICAL PROPERTIES OF THIOPHENE BASED POLYMERS

by

David L. Harris

Advisor: Professor Roger Dorsinville

Conjugated polymers are fast becoming more complex with greater potential for a host of important effects such as light emission and detection. They can also be processed at room temperature and coated virtually on any surface.

In this thesis, picosecond and femtosecond laser pulses are used to study the magnitude, dynamics and sign of the third order nonlinear optical susceptibility $\chi^{(3)}$ in a series of oligothiophenes using degenerate four-wave mixing and z-scan techniques. The effects of conjugation length, quantum confinement, and packing on the third order nonlinearity are investigated for the first time. Fluence effects on the dynamics of nonlinear optical properties of thiophene polymer films are reported. A detailed model of the diffusion processes in polydithieno(3,2-b: 2',3'-d)thiophene (PDTT) thin films is given.

Dedicated to
my parents
Richard and Rowena Harris
and
my wife
Vanessa Harris

Acknowledgments

I would like to take this opportunity to thank my parents, Richard and Rowena Harris, and my family for their continued support. My parents instilled in me the correct training and discipline necessary for me to continue toward this degree. My mother made many sacrifices throughout my years in primary school, high school and college, for which I am most grateful. Her prayers have been with me continuously through it all. I will always be grateful to my parents for their love and support of me.

A special thank you to my thesis advisor Professor Roger Dorsinville for taking me under his wings and providing guidance, encouragement, training, counseling, and support during my thesis research project. Also, Dr. Shahab Etemad for giving me the opportunity as an undergraduate to work on my first research project and for his continued support, advice and encouragement, and Professor Mohamed Ali for the many helpful discussions. I would like to acknowledge the Center for Analysis of Structures and Interfaces for providing financial support, the Department of Electrical Engineering of the City College of New York, for providing me with the theoretical knowledge, and the Program for the Retention of Engineering Students and Dean Ramona Brown for their continued support. I would like to thank my committee members, Professor Ardie Walser, Professor Ping Pi Ho, Professor V. Petricevic, Professor Mohamed Ali, and Dr. Shahab

Etemad of Bellcore. I would also like to thank my fellow graduate and undergraduate students for their kindness and helpfulness.

Finally, I would like to thank my wife, Vanessa Harris, for her love, patience, understanding and continued support.

Table of Content

Abstracts iv

Dedication v

Acknowledgments vi

List of Figures xii

List of Tables xvii

Chapter I. Introduction 1

1.2) Nonlinear Optics 5

1.3) Thesis Statement 9

1.4) Thesis Organization 10

Chapter II. Experimental Methods 14

2.1) Introduction 14

2.2) The Laser Systems 15

2.3) Degenerate Four-Wave Mixing 18

2.3.1) Magnitude Measurement 24

2.3.2) Time Resolved Measurements 26

2.4) Z-Scan 28

Chapter III. Dynamics and Magnitude of the Nonlinear Optical Response.....40

3.1) Introduction.....40

3.2) Dynamics of the Nonlinear Optical Response in Conjugated Polymers.....40

3.2-1) Relaxation of Self-Trapped Excitons in Conjugated Polymers.....44

3.3) Magnitude of the Nonlinear Optical Response.....47

3.3-1) Packing.....47

3.3-2) Quantum Confinement in One Dimensional Systems.....50

3.3-3) Length Dependence in Conjugated Systems.....52

3.3-4) Phonon Resonance.....55

Chapter IV. Excited-State Dynamics of Thiophene Thin Films Studied by Time-Resolved Degenerate Four-Wave Mixing.....62

4.1) Introduction.....62

4.2) Experimental Set-up.....64

4.3) Results and Discussion.....65

4.4) Conclusion.....75

Chapter V. Nonlinear Optical Anisotropy and Molecular Orientational Distribution in Poly[3-(6-tetrahydro-pyraniloxyhexyl)]-2,5-thienylene Langmuir Blodgett Films.....78

5.1) Introduction....78

5.2) Sample....80

5.3) Experimental Techniques....81

5.4) Results and Discussion....85

5.4-1) Third-order nonlinear optical responses....85

5.4-2) Anisotropy and packing effects....91

5.5) Conclusion....94

Chapter VI. Nonlinear Optical Analysis of a Series of Oligothiophenes: Length Dependence of the Third Order Nonlinear Susceptibility in Conjugated Organic Molecules....96

6.1) Introduction....96

6.2) Sample....98

6.3) Experimental Set-up....101

6.4) Results....103

6.5) Discussion....108

6.6) Conclusion....115

Chapter VII. Time-resolved Degenerate Four-wave Mixing in Solution of Oligothiophenes....118

7.1) Introduction....118

7.2) Degenerate Four-wave Mixing Experimental Results.....119

7.3) Conclusion.....125

Chapter VIII. Summary and Future Directions.....127

8.1) Summary.....127

8.2) Future Directions.....128

8.2-1)Enhanced of the third-order nonlinear susceptibility in thiophene based block conjugated copolymers.....128

Appendix. The Genkin-Mednis Approach.....132

Bibliography.....139

List of Figures

Chapter 1

1.1 Waveforms associated with the atomic response.....4

Chapter 2

2.2.1 Set up of the amplified laser system.....17

2.3.1 Shows the geometry and energy diagrams describing degenerate four-wave mixing.....19

2.3.2 Degenerate four-wave mixing setup: M -mirror, BS -beam splitter, L -Lens, S -sample, A -aperture, D - detector, Sig. -Signal beam.....21

2.3.3 **k**-vector diagram for the folded boxcar geometry.....22

2.3.4 Schematic of the optical beam geometry in the plane of the material for the DFWM process. The dashed and solid line represent the two population gratings produced by beams 1 and 2 and beams 1 and 3 respectively.....23

2.4.1 Single Beam Z-scan Set-up.....29

2.4.2 Curves of the calculated Z-scan transmittance for third order nonlinearity with either a negative or positive polarity and a small aperture.....36

Chapter 3

3.2.1 The schematic diagram of polythiophene in which the ground state degeneracy is weakly lifted, energetically form A and B are not equal as shown in the diagram at the bottom of the figure where a plot of the energy versus the distortion parameter u..... 42

3.2.2 Shows the molecular structure of self-trapped exciton, polaron (P^+ and P^-)and bipolaron (BP^{++}) in polythiophene. ⊖ and ⊕. represent an electron - hole pair, double dots ":" represents a lone pair, and single dot "•" represents a unpair electron.....43

3.2.4 Model of the relaxation kinetics and adiabatic potential surface of excitons in polythiophene. Numbers 1, 2, and 3 indicates FE, and STE before the emission of phonons, and STE after the phonon emission. G - ground state,FE - free exciton, STE - and self-trapped exciton.....46

3.3.1 Schematic showing a four-wave mixing process with $\omega_1 - \omega_2$ at resonance.....56

Chapter 4

4.1 Molecular structure of Polydithieno(3,2-b; 2',3'-d)-thiophene (PDTT).....63

4.2 Time dependence of the DFWM in PDTT thin films are plotted with a

XXXX (solid) and (XYXY (broken) configuration. The inset shows a semi-log plot of the XYXY configuration with (9±1) ps and 40 ps.....66

4.3 The fluence dependence of the early temporal response of the NLO signal of PDTT at 635 nm. The following laser fluences were used (top to bottom) 0.51, 1.34, 2.74, and 5.54 mJ/cm^2 68

4.4 Temporal resolution of the bimolecular reaction (solid) fitted to the experimental data (dots), pulse energy of 1.7 mJ.....70

4.5 A model of the diffusion processes in polydithieno(3,2-b; 2'3'-d)-thiophene thin films. Free excitons (FE), self-trapped excitons (STE) S^0, S^1 and S^2 are different energy levels.....72

Chapter 5

5.2.1 Molecular structure of PTHT LB film.....80

5.3.1 A Y-type multilayered film (centrosymmetric) where stacking of the layers is head to head or tail to tail.....81

5.3.2 UV-Visible spectra of 8 layers of PTHT LB film measured with light polarization parallel with (||) and perpendicular to ($\perp$) the dipping direction.....82

5.3.3 Fig. 5.3.3 shows a plot of the ratio between $A_{//}$ and $A_{\perp}$ versus temperature.....83

5.4.1 Shows the observed DFWM signal as a function of time delay, and with the electric vectors of all the waves parallel to the draw direction. Pulse limited subpicosecond (<500 fsec) time response is measured.....84

5.4.2 Shows a plot of $\chi^{(3)}$, the square root of the DFMW signal intensity as a function of the film rotation with respect to the incident electric field vector. The dots represent the number of data scans, the solid line represents the average of all scan.....86

5.4.3 A stereoscopical view of the molecular structure after the transfer process.....87

5.4.4 The polarization dependence of the D4WM signal generated from an aligned sample. An error bar of ~0.2 x 10^{-8} esu was obtained base on the repeatability of the results from measurement to measurement.....89

Chapter 6

6.2.1 Molecular structure of PBC10, PTC10, PQC10, PPC10.....98

6.2.2 Absorption spectra of PBC10, PTC10, PQC10, and PPC10.....99

6.4.1 Normalized transmittance of Z - scan measurements from $CHCl_3$ and CS_2 at 800-nm.....103

6.4.2 Normalized transmittance of Z-scan measurements from PBC10 at 800-nm, with I_0= 6.25 GW/cm^2.....104

6.5.3(a) Third order nonlinear optical coefficient versus delocalization.....109

6.5.3(b) Semi-log plot of $\chi^{(3)}$ versus N_d for PBC10, PTC10, PQC10 and PPC10. The solid line is a theoretical fit for $\chi^{(3)} \sim (N_d)^4$.....111

Chapter 7

7.2.1 The degenerate four-wave mixing signal as a function of delay time for oligothiophenes in a solution of chloroform.....119

Chapter 8

8.1 Molecular structure of (a) T_6B_2 and (b) T_8B_2, T stands for thyenilenic rings, and B stands for benzenic rings.....130

List of Tables

Chapter 3

Table 3.2.1 The formation time τ_f(fs) and decay τ_d (ps) of Self-Trapped (ST) Excitons.....45

Chapter 6

Table 6.2.1. Photophysical properties of PBC10, PTC10, PQC10, and PPC10.....100

Table 6.4.2. Listed the concentrations and calculated values of $\chi^{(3)}$.....106

Chapter 7

Table 7.2.1 Nonlinear Coefficient $\chi^{(3)}$ versus delocalization length.....122

Chapter 1

1.1 Introduction

Nonlinear optics is the study of phenomena that occurs because of the modification of the optical properties of a material system by the presence of light. The concept of nonlinear optics is considerably older than the lasers. Interactions involving two or more quanta, eg. two-photon absorption and stimulated Raman scattering were described theoretically as early as 1931 by Goeppert-Mayer. However, the advents of high power laser pulses four decades ago have produced fascinating effects and have contributed greatly to our knowledge about the interaction of light with matter, and created a revolutionary change in optics and photonics. Nonlinear optics was first observed in second harmonic generation by Franken and coworkers in 1961[1], and since then has grown continuously. The field of nonlinear optics now ranges from fundamental studies of the interaction of light with matter to applications such as laser frequency conversion and optical switching. Nonlinear optical phenomena are "nonlinear" in the sense that they occur when the response of a material system to an applied optical field depends in a nonlinear manner upon the strength of the optical field. For example, second and third harmonic generation depend quadratically and cubically on the strength of the applied optical fields.

respectively. The importance of nonlinear optical processes in optoelectronics and/or photonics will be realized in the twenty-first century, the same way that nonlinear electronic processes such as modulation or frequency multiplication are key phenomena in well-developed electronics.

Among various possibilities of materials to be used in devices in optoelectronics and photonics, conjugated polymers have many advantages such as large optical nonlinearity, ultrafast response, processability, high optical stability, and chemical stability.

The nonlinear optical response can be described by expressing the polarization P(t) or the dipole moment per unit volume as a power series in the field strength E(t) as

$$P(t)=\chi^{1}E(t)+\chi^{2}E^{2}(t)+\chi^{3}E^{3}(t)+\chi^{4}E^{4}(t)+\chi^{5}E^{5}(t)+\cdots \qquad (1.1.1)$$

In the case of conventional (i.e. linear) optics, the induced polarization depends linearly upon the electric field (Fig. 1.1 b) where $\chi^{(1)}$ is the constant of proportionality. The quantities $\chi^{(2)}$, $\chi^{(3)}$, $\chi^{(4)}$, and $\chi^{(5)}$ are known as second-, third-, fourth-, and fifth-order nonlinear susceptibility, respectively. For simplicity, we have taken the fields $\tilde{P}(t)$ and $\tilde{E}(t)$ to be scalar quantities in writing Equ. 1.1.1. The nonlinear optical interactions described in terms of the nonlinear polarization given in Equ. 1.1.1 apply only to lossless and

dispersionless materials. In the more general cases of materials with dispersion and/or losses, the polarization and field are vectors: $\chi^{(1)}$ is a second rank tensor. $\chi^{(2)}$ is a third rank tensor, etc.

The physical processes that occur as a result of second-order polarization $\tilde{P}^{(2)}(t) = \chi^{(2)}\tilde{E}^{2}(t)$ are distinct from those that occur as a result of the third-order polarization $\tilde{P}^{(3)}(t) = \chi^{(3)}\tilde{E}^{3}(t)$. Second-order nonlinear optical interactions can only occur in noncentrosymmetric materials. that is. materials that do not display inversion symmetry (Fig. 1.1 d). Second-order nonlinearity is responsible for second harmonic generation. sum and difference-frequency generation. rectification. two photon absorption. optical parametric oscillation and amplification, and Pockels electro optical effects. On the other hand. third-order nonlinear optical interactions (ie. , those described by a $\chi^{(3)}$ susceptibility) can occur both from centrosymmetric (Fig. 1.1c) and noncentrosymmetric (Fig. 1.1d) material. Typical third order nonlinear processes are third harmonic generation, phase conjugation, two-photon absorption. Raman scattering. self-focusing, Kerr effects, four-wave mixing. self-phase modulation (SPM) and cross-phase modulation (XPM).

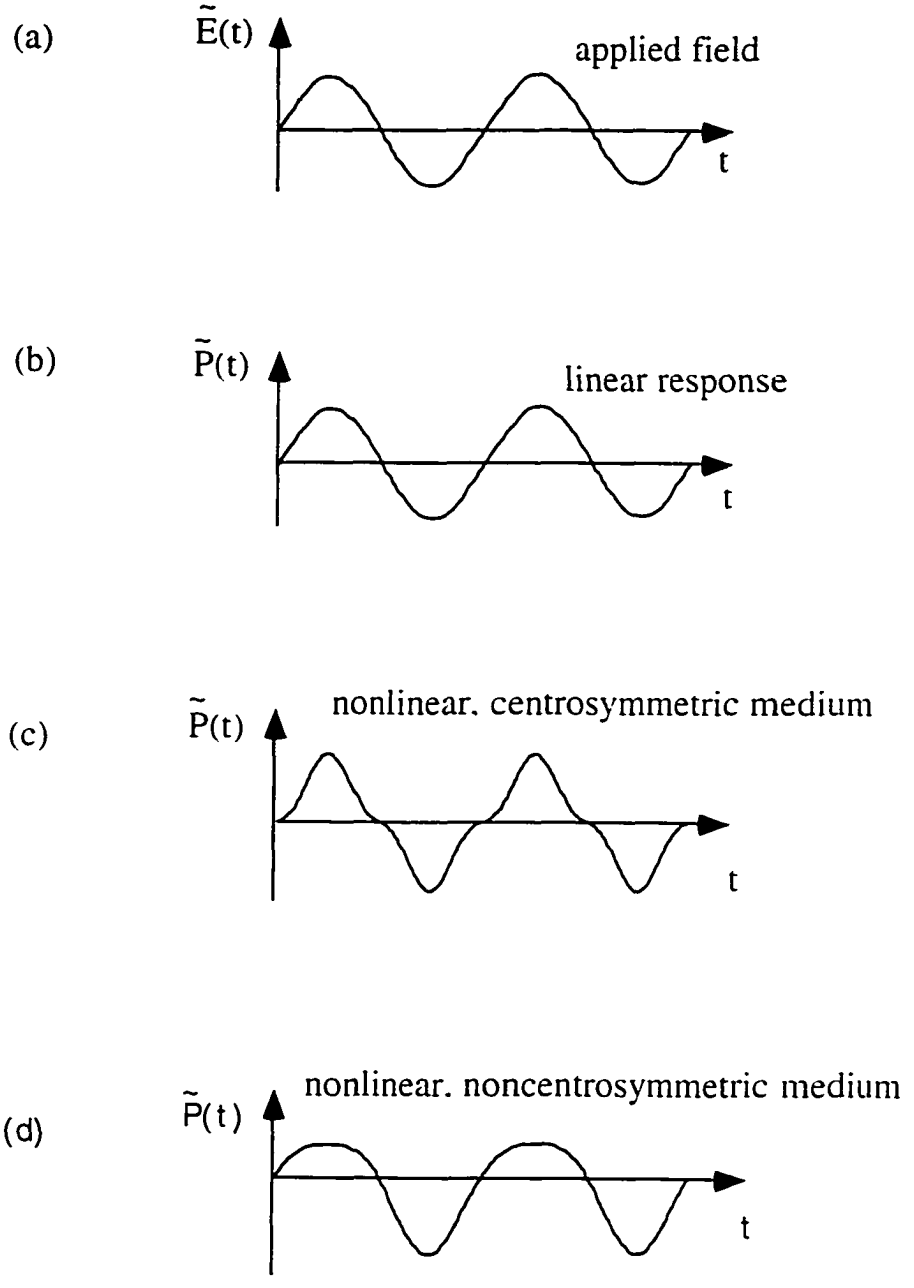

Figure 1.1 Waveforms associated with the atomic response[2]

In section 1.2, we introduce the nonlinear polarization and nonlinear optical susceptibilities. Section 1.3 gives the thesis statement, and section 1.4 describes the thesis organization.

1.2 Nonlinear Optics

An optical pulse propagating in a nonlinear medium is governed by Maxwell's equations for the electric and magnetic fields $\mathbf{E}(\mathbf{r},t)$ and $\mathbf{B}(\mathbf{r},t)$[3]:

$$\begin{aligned} \nabla \times \mathbf{E} &= -\frac{1}{c}\frac{\partial \mathbf{B}}{\partial t}, \\ \nabla \times \mathbf{H} &= \frac{1}{c}\frac{\partial \mathbf{D}}{\partial t} + \frac{4\pi}{c}\mathbf{J}, \\ \nabla \cdot \mathbf{D} &= 4\pi\rho, \\ \nabla \cdot \mathbf{B} &= 0 \end{aligned} \tag{1.2.1}$$

where $\mathbf{J}(\mathbf{r},t)$ and $\rho(\mathbf{r},t)$ are the free current and charge densities, respectively. In nonlinear optics, we are often interested in the solution of Maxwell's equations in regions of space that contain no free charges and currents, so that $\mathbf{J}(\mathbf{r},t) = 0$ and $\rho(\mathbf{r},t) = 0$. For nonmagnetic materials, we also have $\mathbf{B} = \mathbf{H}$.

The electric displacement $\mathbf{D}(\mathbf{r},t)$ is given by the constitutive equations[4]

$$\mathbf{D} = \varepsilon\mathbf{E} = \mathbf{E} + 4\pi\mathbf{P}, \tag{1.2.2}$$

where the constitutive parameter ε is known as permittivity tensor, and **P** is the electric polarization. From the first two equations in Equ. (1.2.1), the wave equation that governs optical wave propagation in the medium can be obtained:

$$\left(\nabla x(\nabla x)+ \frac{1}{c^2}\frac{\partial^2}{\partial t^2}\right)\mathbf{E}(r,t) = -\frac{4\pi}{c^2}\frac{\partial^2}{\partial t^2}\mathbf{P}(r,t) \qquad (1.2.3)$$

where **P** is a function of spatial coordinates and time, and is the only time-varying source term.

When the electric and magnetic fields are not strong, the quantity ε can be assumed independent of the fields. That is the case of linear optics.

In this case, **P** takes a simple linearized form

$$\mathbf{P}(\mathbf{r},t)= \int_{-\infty}^{\infty} \chi^{1}(\mathbf{r}-\mathbf{r}',t-t')\cdot\mathbf{E}(\mathbf{r}',t')d\mathbf{r}'dt' \qquad (1.2.4)$$

where $\chi^{(1)}$ is the linear susceptibility. If **E** is a monochromatic plane wave with

$$\mathbf{E}(\mathbf{r},t) = \mathbf{E}(\mathbf{k},\omega)=\mathbf{A}(\mathbf{k},\omega)\exp(i\mathbf{k}\cdot\mathbf{r}-i\omega t) \qquad (1.2.5)$$

then Fourier transform of (1.2.3) yields the relation

$$\mathbf{P}(\mathbf{k},\omega)=\chi^{(1)}(\mathbf{k},\omega)\cdot\mathbf{E}(\mathbf{k},\omega)$$

with

$$\chi^{(1)}(\mathbf{k},\omega)=\int_{-\infty}^{\infty}\chi^{(1)}(r,t)\exp(-i\mathbf{k}\cdot\mathbf{r}-i\omega t)d\mathbf{r}dt \qquad (1.2.6)$$

The linear dielectric constant $\varepsilon(\mathbf{k},\omega)$ is related to $\chi^{(1)}$ by

$$\varepsilon(\mathbf{k},\omega)=1+4\pi\chi^{(1)}(\mathbf{k},\omega) \qquad (1.27)$$

In the electric dipole approximation, $\chi^{(1)}(\mathbf{r},t)$ is independent of $\mathbf{r}$, and hence both $\chi^{(1)}(\mathbf{k},\omega)$ and $\varepsilon(\mathbf{k},w)$ are independent of $\mathbf{k}$.

In the nonlinear case, the electric polarization $\mathbf{P}$ can be expanded into a power series of $\mathbf{E}$:[5]

$$\begin{aligned}P(r,t)=&\int_{-\infty}^{\infty}\chi^{(1)}(t-t')\cdot\mathbf{E}(\mathbf{r},t')dt'\\&+\int_{-\infty}^{\infty}\chi^{(2)}(t-t_1;t-t_2)\cdot E(\mathbf{r},t_1)E(\mathbf{r},t_2)dt_1dt_2\\&+\int_{-\infty}^{\infty}\chi^{(3)}(t-t_1;t-t_2;t-t_3)\cdot E(\mathbf{r},t_1)E(\mathbf{r},t_2)E(\mathbf{r},t_3)dt_1dt_2dt_3+\cdots\end{aligned} \qquad (1.2.8)$$

where $\chi^{(n)}$ is the nth-order nonlinear susceptibility. If $\mathbf{E}$ can be expressed as

$$\mathbf{E}(\mathbf{r},t)=\int_{-\infty}^{\infty}\mathbf{E}(\mathbf{r},\omega)d\omega \quad \text{with } \mathbf{E}(\mathbf{r},\omega)\propto\exp(-i\omega t), \qquad (1.2.9)$$

then, the induced polarization in a medium can be expressed as

$$\mathbf{P}(\mathbf{r},t)=\mathbf{P}^{(1)}(\mathbf{r},t)+\mathbf{P}^{(2)}(\mathbf{r},t)+\mathbf{P}^{(3)}(\mathbf{r},t) \qquad (1.2.10)$$

where

$$\mathbf{P}(\mathbf{r},t)=\int_{-\infty}^{\infty}\chi^{(1)}(t-t')\cdot\mathbf{E}(\mathbf{r},t')dt',$$

$$\mathbf{P}^{(n)}(\mathbf{r},t)=\int_{-\infty}^{\infty}\chi^{(n)}(t-t_1;t-t_2;\cdots t-t_n)\cdot\mathbf{E}(\mathbf{r},t_1)\mathbf{E}(\mathbf{r},t_2)\cdots\mathbf{E}(\mathbf{r},t_n)dt_1dt_2\cdots dt_n$$

$$=\int_{-\infty}^{\infty}\chi^{(n)}(\omega=\omega_1+\omega_2+\cdots\omega_n):\mathbf{E}(\omega_1)\mathbf{E}(\omega_2)\cdots\mathbf{E}(\omega_n)d\omega_1d\omega_2\cdots d\omega_n. \tag{1.2.11}$$

and the nth-order susceptibility is

$$\chi^{(n)}(t-t_1;t-t_2;\cdots;t-t_n)=\int_{-\infty}^{\infty}\chi^{(n)}(t-t_1;t-t_2;\cdots;t-t_n)\exp\left[i\omega_1(t-t_1)\right.$$
$$\left.+i\omega_2(t-t_2)+\cdots+i\omega_n(t-t_n)\right]d\omega_1d\omega_2\cdots d\omega_n. \tag{1.2.12}$$

we note that, strictly speaking, only for a set of applied monochromatic fields can we write

$$\mathbf{P}^{(n)}(\mathbf{r},\omega)=\chi^{(n)}(\omega=\omega_1+\omega_2+\cdots+\omega_n):\mathbf{E}(\omega_1)\mathbf{E}(\omega_1)\cdots\mathbf{E}(\omega_n) \tag{1.2.13}$$

In the case of instantaneous response (corresponding to a dispersionless medium)

$$\mathbf{P}^{(n)}(\mathbf{r},t)=\chi^{(n)}\cdot\left[\mathbf{E}(\mathbf{r},t)\right]^n \tag{1.2.14}$$

The linear and nonlinear susceptibilities characterize the optical properties of a medium. If $\chi^{(n)}$ is known for a given medium, the n-th order nonlinear optical effects in this medium can be predicted from Maxwell's equations. Physically, $\chi^{(n)}$ is related to the microscopic structure of the medium and can be properly evaluated with a full quantum mechanical calculation.

1.3 Thesis Statement

The objective of my thesis is to use time resolved degenerate four-wave mixing and a single beam z-scan technique as a spectroscopic tool to investigate the nonlinear dynamics of conjugated polymer systems. The work will be divided into four parts:

[1] The determination of the relaxation of free excitons under the influence of intensity in thiophene based polymer films will be made for the first time to understand how intensity affects diffusion processes. Theoretical calculations of the bimolecular rate coefficient, diffusion coefficient, and hopping rates are reported.

[2] Using the absolute values for the third-order nonlinear optical measurements obtained from degenerate four-wave mixing in Poly[3-(6-tetrahydropyraniloxyhexyl)]-2,5-thienylene Langmuir Blodgett films, the effects of packing density on the third-order nonlinear susceptibility is

investigated.

[3] Single beam z-scan is used to determine the sign and magnitude of the nonlinear optical susceptibilities in a series of oligothiophene.

[4] The dependence of the third-order nonlinear susceptibility with respect to conjugation length is investigated in various oligothiophenes. Comparison between the absolute third-order susceptibility $|\chi^{(3)}|$ obtained from DFWM experiment and the square of the real and imaginary parts of $\chi^{(3)}$, $|(\chi^{(3)}_{R})^2 + (\chi^{(3)}_{im})^2|$ obtained from z-scan experiments are reported.

Preliminary studies on the effects of quantum confinement on the third-order susceptibility in thiophene based polymers is discussed briefly in chapter eight. The study is inconclusive because an incorrect fabrication procedure (spin coating) was used to deposit the film unto the substrate. Improvement into this research is mentioned.

The information obtained in this thesis is important to the development of photonics devices and applications. The knowledge gained may lead to new materials with enhanced nonlinearity.

1.4 Thesis Organization

This thesis is organized into eight main chapters.

The first chapter present a brief historical background on the subject of optical nonlinearity and its origin. The subject of nonlinearity as it relates to Maxwell's equation is also addressed.

The second chapter describes the experimental techniques used to investigate third-order nonlinearities. The fundamental principles of those techniques are discussed.

The third chapter is divided into two main sections. the first section describes the decay mechanism from free excitons to self-trapped excitons to polarons and finally to possible bipolarons in conjugated polymers. The second section discusses four techniques which can be used for enhancing the nonlinear optical response in conjugated polymers.

In the fourth chapter, time-resolved degenerate four-wave mixing shows that bimolecular decay via exciton-exciton annihilation dominates the temporal response at high intensities. Estimates of the singlet-singlet annihilation, exciton diffusion coefficient, and hopping rate are given.

The fifth chapter demonstrates that most of the nonlinearity $\chi^{(3)}$ is associated with the π-electron polarizability along the conjugated chain. These results were obtained from anisotropy $\chi^{(3)}$ measurements of Langmuir Blodgett thiophene

films. Different polarization components in the plane of the film were calculated.

In the sixth chapter, the sign and size of $\chi^{(3)}$ in four new oligothiophenes, dissolved in chloroform, are determined by the single beam z-scan technique. The results are in good agreement with a one dimensional semiconductor model.

The seventh chapter compares the $\chi^{(3)}$ (where $|\chi^{(3)}|^2 \approx |\chi^{(3)}{}_R|^2 + |\chi^{(3)}{}_{im}|^2$) values obtained in the previous chapter (Chap. 6) to degenerate four-wave mixing measurements presented in this chapter. DFWM only determines the absolute value of $\chi^{(3)}$.{ie. $|\chi^{(3)}|$}, where as z-scan determines the real and imaginary parts of $\chi^{(3)}$, {ie. $\chi^{(3)}{}_R$ and $\chi^{(3)}{}_{im}$}.

The eighth chapter summarizes the major conclusions of this thesis and proposes future directions.

Reference

1. P. A. Franken, A. E. Hill, C.W. Peters, and G. Weinreich. Phys. Rev. Lett. 7, 118 (1961)

2. R. Boyd " Nonlinear Optics" Academic Press Inc. 1992

3. W. K. H.Panofsky and Philips, Classical Electricity and magnetism (Addison-Wesley, Reading, MA,1962).

4. A. Yariv and P.Yeh, Optical Waves in Crystals (John Wiley & Son. New York. 1984).

5. Y. R. Shen, The Principles of Nonlinear Optics, (Wiley, New York. 1984).

Chapter 2

Experimental Methods

2.1 Introduction

In order to improve nonlinear optical materials for the development of photonic devices, certain parameters such as size, temporal response, and anisotropy of the nonlinear susceptibility have to be investigated. Additional information such as dispersion, temperature and light intensity dependence, and the contribution of both real and imaginary parts of $\chi^{(3)}$ are meaningful to the development of optical devices. Various techniques have been used to investigate the different behaviors of the third-order nonlinear optical coefficient $\chi^{(3)}$ in materials: Degenerate four-wave mixing (DFWM), which gives the magnitude and the response time of $\chi^{(3)}$; optical Kerr effect (OKE), which is sensitive to the real part of $\chi^{(3)}$, but can be modified to determine the imaginary part, Z-scan, which gives the size and the sign of the nonlinearity, third harmonic generation, which probes the purely electronic component of the nonlinearity; and electric field-induced second harmonic generation, used mainly in liquid to measure the reorientational component of the nonlinear response. Degenerate four-wave mixing (DFWM) and the single beam Z-scan technique have been used in this

thesis research to investigate the behavior $\chi^{(3)}$.

A home-made intracavity dispersion compensation dye laser was used for the DFWM experiment, while a spectra physics Ti-sapphire laser was used for the z-scan experiment.

2.2 The Laser systems

The laser system used in the DFWM set-up consist of a less than < 100 picosecond actively mode locked Coherent Nd:YAG (Neodymium:yttrium-aluminum-garnet) laser. The lasing wavelength at 1.064 μm produced pulses at 76 MHz with an average power of 26 Watts. The generated 1.064 μm pulses were then frequency doubled after passing through a Potassium Titanyl phosphate (KTP) crystal producing 4 Watts at 532 nm. One percent (180 mW) of the residual 1.064 μm was send into a home-made regenerative amplifier while the remaining ninety nine percent (99%) was dumped. The 1% seeded pulses were directed into the amplifier after reflecting off a polarizing beam-splitter (BS). The polarizing BS ensures that only p- polarization is reflected into the cavity. The beam then travels through a quarter-wave plate and Pockel's cell system. Together they work to switch the pulses in and out of the cavity. The trapped pulse was amplified after making several round trips. The amplified pulse from the regenerative amplifier (2 mJ per pulse at 1 KHz repetition rate) passed

through a second harmonic generator crystal (KTP), generating a frequency doubled beam at 532 nm. The beam was then used to pump a two and three stage dye amplifiers. The 4 Watts at 532 nm produced from the Nd:YAG was divided into two 2 Watts laser beams and used to synchronously pump a Rhodamine 6G linear and/or an intracavity-dispersion compensation dye laser. The two dye lasers provided pulses with temporal duration of 1-2 psec for the linear cavity laser and 150 fs for the dispersion compensated laser, with 250 mW and 50 mW average power, at 76 MHz respectively. The output from each dye laser was amplified after passing through separate dye amplifiers.

The linear cavity laser used a three-plate birefringent filter as a tuning element, providing pulses between 570 nm and 600 nm. The intracavity optical dye laser was basically a modification of a linear cavity laser system. The modified system made use of two pairs of AR-coated SF18 prisms separated by a distance of 6.6 cm. Two flat mirrors were used to aid in the cavity alignment. The distance between prisms (6.6 cm) was calculated based on the amount of dispersion from all other components that must be compensated for with the SF18 prism. The modified design was based on a approach attempted by Nakazawa[1], where the total phase delay through the optical compressor is constrained by:

$$\phi_{prisms}(\omega) + \phi_{cavity}(\omega) = 0. \qquad (2.2.1)$$

where $\phi_{prisms}(\omega)$ is the delay due to the two pairs of prisms and $\phi_{cavity}(\omega)$ is the phase delay due to all other components in the dye laser cavity. A schematic of the amplified dye laser system is shown in Fig. 2.2.1.

The system used for the Z-scan experiment consisted of a commercial mode-locked Titanium-doped sapphire (Ti:Sapphire) laser pumped by a continuous wave (cw) diode-pumped neodymium yttrium vanadate ($Nd:YVO_4$) laser. Laser pulses at 800 nm wavelength with 80 femtosecond pulse duration and a repetition rate 80 MHz are produced.

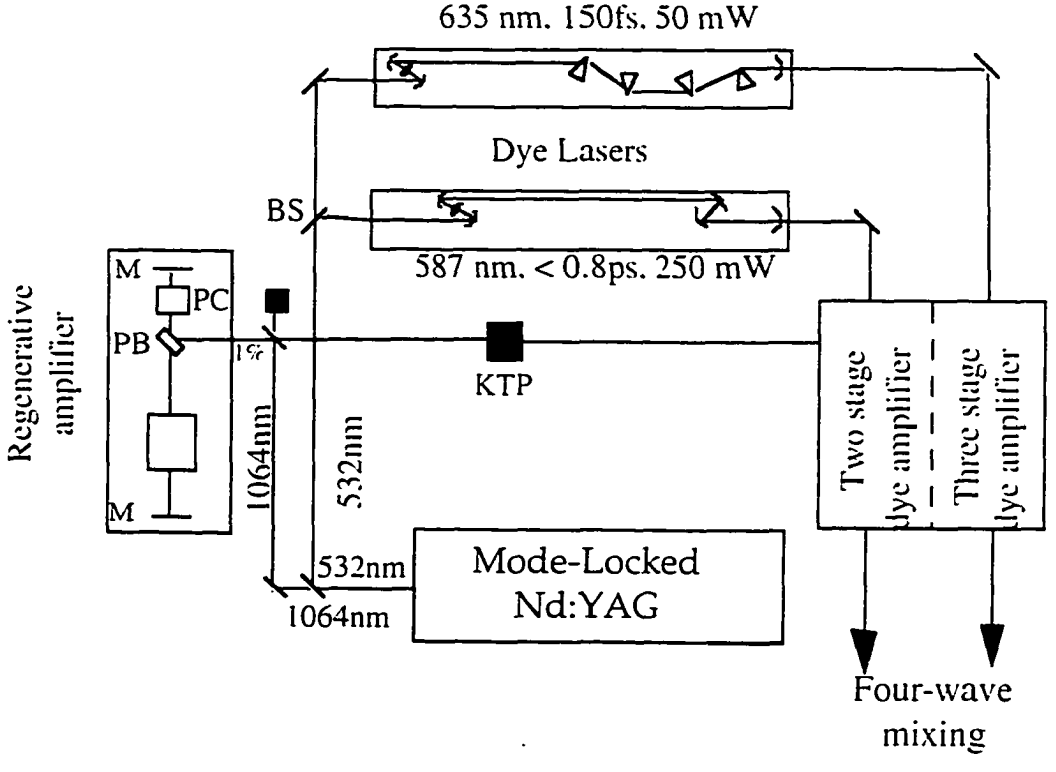

Fig. 2.2.1 Set up of the amplified laser system

2.3 Degenerate Four-wave mixing

Four wave mixing refers to a nonlinear process with four interacting electromagnetic waves. In the weak interaction limit, it is a third-order process and is governed by the third order nonlinear susceptibility $\chi^{(3)}$. Unlike second-order processes, a third-order process is allowed in all media, with or without inversion symmetry.

Four-wave mixing has many interesting applications: when more than one tunable laser is used for pumping, multiple resonances of $\chi^{(3)}$ can be excited. In the degenerate case (i.e., all four interacting waves have the same frequency) it is used for wavefront reconstruction in adaptive optics[2], it can be used as a powerful tool for material studies. Its advantages over other techniques are in the capabilities for high resolution, for elimination of strong fluorescence background, and for time-resolving measurements of ultrafast dynamic properties. In this section we will cover the fundamentals of degenerate four-wave mixing spectroscopy.

In media with inversion symmetry, $\chi^{(3)}$ is the lowest-order nonlinearity allowed under electric-dipole approximation.[3] The four-wave mixing process is directly related to the third-order nonlinear susceptibility $\chi^{(3)}$.

The theory of DFWM follows closely the general theory of optical mixing. For simplicity, we will assume a cubic or isotropic medium. Let the input beams

be: $\mathbf{E}_m(\omega_m) = \mathbf{E}_{om} \exp(i\mathbf{k}_m \cdot \mathbf{r} - i\omega_m t)$ with m = 1.2.3. The output field is (see Fig. 2.3.1) $\mathbf{E}_s(\omega_s) = \mathbf{E}_{os} \exp(i\mathbf{k}_s \cdot \mathbf{r} - i\omega_s t)$, with $\omega_s = \omega + \omega - \omega = \omega$.

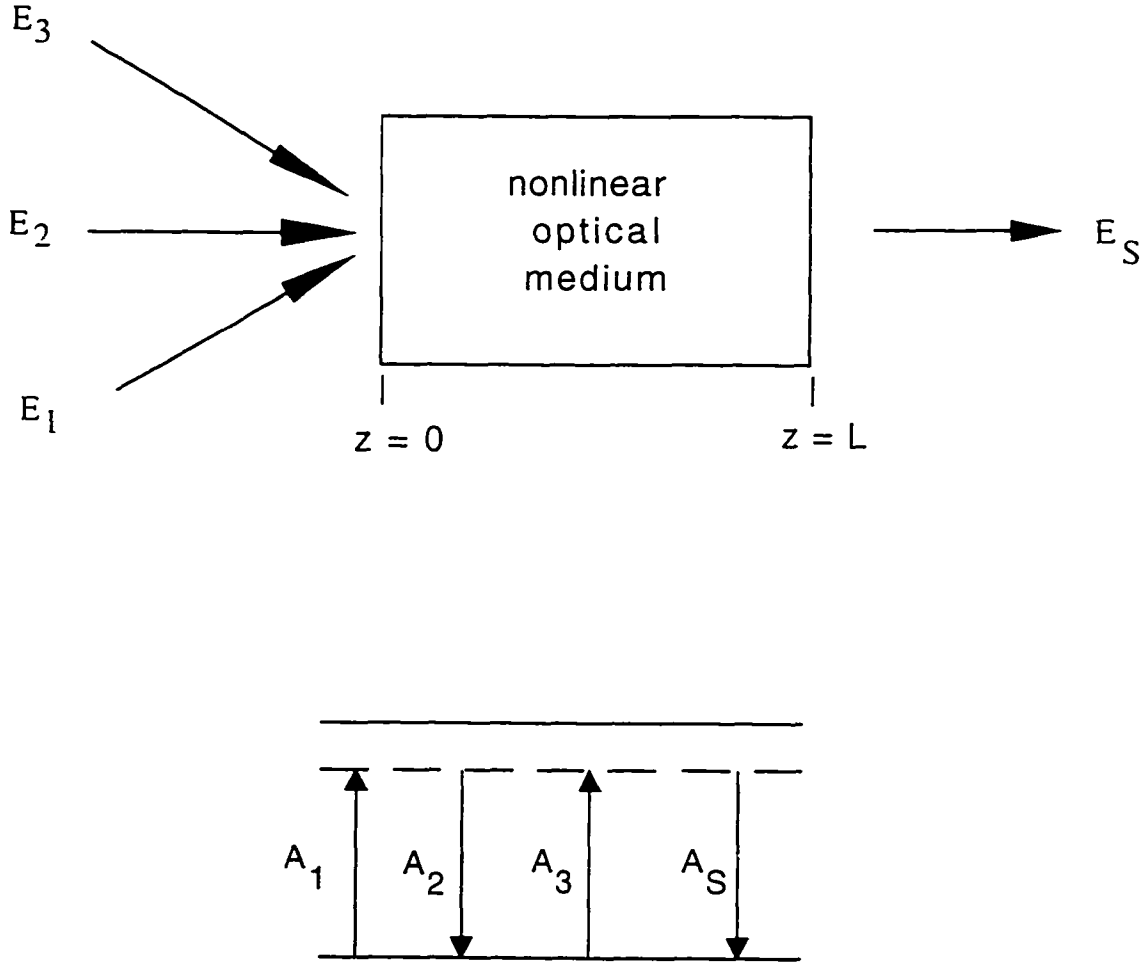

Fig. 2.3.1 shows the geometry and energy diagrams describing degenerate four-wave mixing.

Es is governed by the wave equation

$$\left[\nabla^2+\frac{\omega_S^2}{c^2}\varepsilon(\omega_s)\right]\mathbf{E}_S = -\frac{4\pi\omega_S^2}{c^2}P^{(3)}(\omega_S) \qquad (2.3.1)$$

where $\mathbf{P}^{(3)}(\mathbf{k}_s,\omega_s) = \chi^{(3)}\,(\mathbf{k}=\mathbf{k}_1\pm\mathbf{k}_2\pm\mathbf{k}_3,\ \omega=\omega\pm\omega\pm\omega)$: $\mathbf{E}(\mathbf{k}_1.\omega)\ \mathbf{E}^*(\mathbf{k}_2.\omega)$ $\mathbf{E}(\mathbf{k}_3,\omega)$. $\mathbf{E}^*(\mathbf{k}_2,\omega)$ denotes the complex conjugated of $\mathbf{E}(\mathbf{k}_2,\omega)$. With the usual slowly varying amplitude approximation,[4] negligible pump depletion, and simplifying boundary conditions; the solution of Equ. (2.3.1) yields:

$$E_{os}=-\frac{2\pi\omega_s^2}{(\Delta\mathbf{k}\cdot\mathbf{z})k_s c^2}\chi^{(3)}_{ijkl}E_{1j}E^*_{2j}E_{3l}\left(1-e^{-i\Delta\mathbf{k}\cdot\mathbf{z}}\right)e^{-\alpha_s z} \qquad (2.3.2)$$

where ijkl denote the polarization direction of the components, α is the attenuation coefficient of the waves along z, and $\Delta\mathbf{k} = \mathbf{k}_1\pm\mathbf{k}_2\pm\mathbf{k}_3\pm\mathbf{k}_4$, is the wave-vector mismatch. Enhancement in the signal output is achieved when phase matching condition is satisfied ($\Delta\mathbf{k} = 0$). By using different propagation directions of the three input beams, phase matching conditions can be achieved in a number of ways. The preferred choice however, depends on the practical situation. In this research, only the forward folded boxcar geometry will be

discussed. The set-up used to perform the FWM experiment is shown in Fig. 2.3.2. The amplified dye laser beam was subsequently split into three separate beams by two beams splitter (BS) and directed through variable and fixed delay lines toward the sample. Temporal information was obtained by delaying the arrival time of the probe beam with respect to the pump beams.

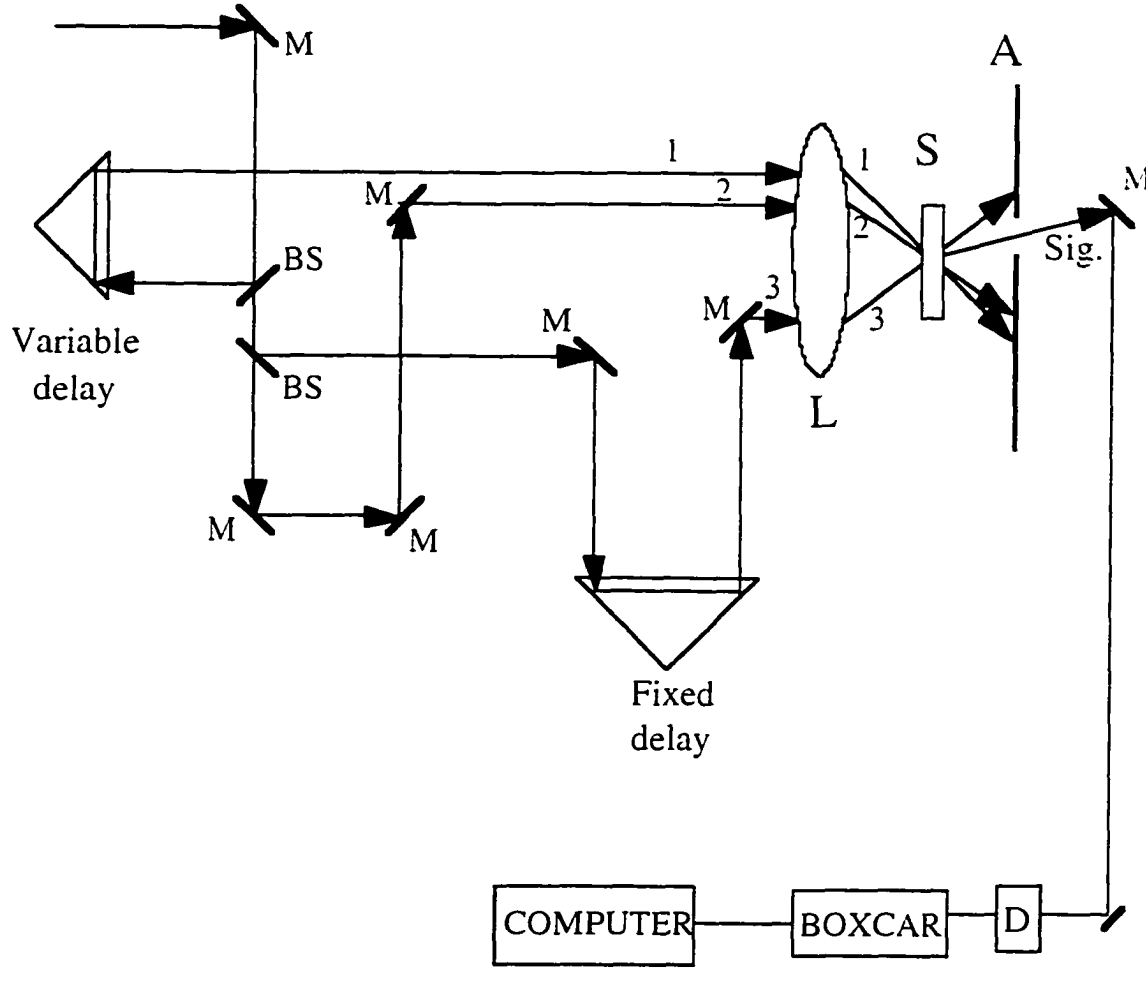

Fig. 2.3.2 Degenerate four-wave mixing set-up: M - mirror, BS - beam splitter, L - lens, S - sample, A - aperture, D - detector, Sig. - signal beam .

The folded boxcar geometry enforces a three-dimensional phase-matching geometry which enables spacial discrimination of the signal wave from the input beams. The wave-vector diagrams for the Folded Boxcar is dipicted in Fig. 2.3.3.

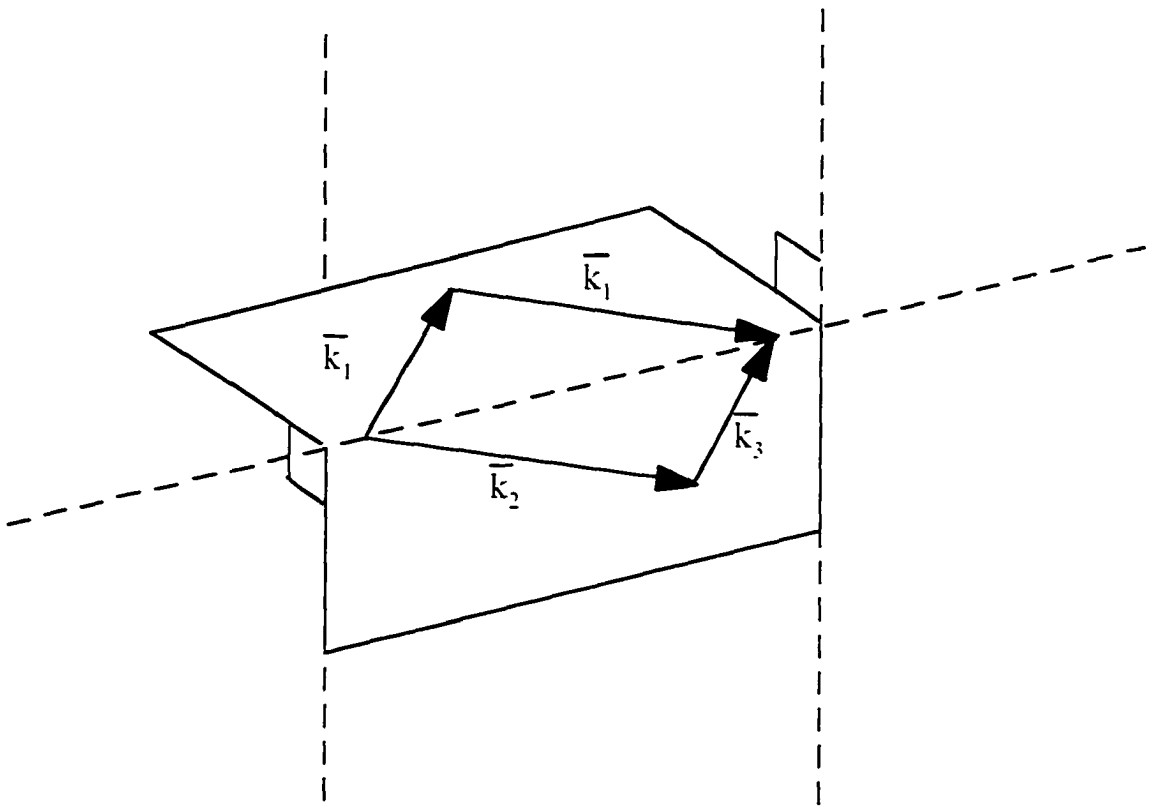

Fig. 2.3.3 **k**-vector diagram for the folded boxcar geometry.

Figure 2.3.4 shows a schematic of the beam geometry on the exiting side of the sample. The three incident beams are labeled 1, 2, and 3, with 4 being the output beam, which is generated by the input beams via $\chi^{(3)}$. Beam 2 is time delayed (T_d) or advanced relative to beams 1 and 3. This allows for the determination of the temporal response of $\chi^{(3)}$. Beams 1, 2, and 3 all coincident in time and space. Beam 4 emerging from the sample are shown to be spatially separated from the more intense incident pulses (1, 2, 3), making the detection of the signal beam free from background noise. This is important for degenerate four-wave mixing experiments because all the beams have the same frequency.

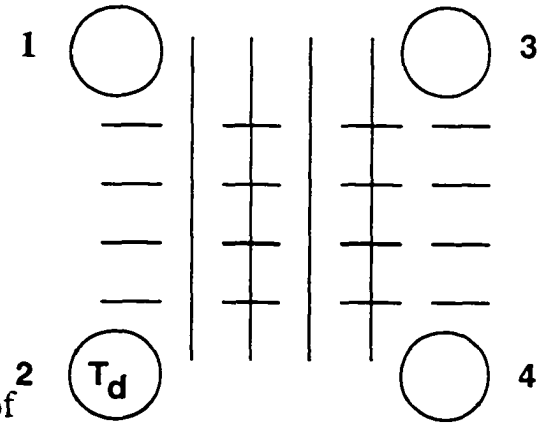

Fig. 2.3.4 Schematic of the optical beam geometry in the plane of the material for the DFWM process. The dashed and solid line represent the two population gratings produced by beams 1 and 2 and beams 1 and 3 respectively.

The total incident intensity is proportional to $|\mathbf{E}_1+ \mathbf{E}_2+ \mathbf{E}_3|^2$, and terms such as $|\mathbf{E}_1|^2$ and mixed terms such as $\mathbf{E}_2^* \mathbf{E}_3$ will appear in the intensity - dependent part of the dielectric constant. Two gratings are responsible for the combination that gives rise to the signal beam (4). They are G1 ($\mathbf{k}_2 - \mathbf{k}_1$), which is due to $\mathbf{E}_2\mathbf{E}_1^*$ and is represented by the dashed horizontal lines in Fig. 2.3.3, and G2 ($\mathbf{k}_3 - \mathbf{k}_1$), which is due to $\mathbf{E}_3\mathbf{E}_1^*$ and is represented by the solid vertical lines Fig. 2.3.3. Mixed terms such as $\mathbf{E}_2^*\mathbf{E}_1$ produce population gratings in the sample from which the other beam (in this case beam 3) can diffract: that is, the third beam sees an index and /or absorption grating that is due to the intensity - dependent part of the complex dielectric function, and the diffracted beam is therefore beam 4.

2.3.1 *Magnitude measurement*

Assuming a gaussian waist and a Sech temporal profile, the incident electric field in the sample have the following spatial and temporal dependence:

$$\mathbf{E}_m = E_{om}(\rho,t) \exp(i\mathbf{k}_m \bullet \mathbf{r} - i\omega_m t) \qquad (2.3.3a)$$

$$E_{om}(\rho,t) = A_m \exp(-\rho^2/\rho_o^2)\ \mathrm{sech}(at). \qquad (2.3.3\ b).$$

Here m = 1, 2, or 3; A_m is a constant, ρ is the transverse (cylindrical) coordinate; ρ_o is the beam waist; and a determines the pulse width of the laser. Since the generate field E_4 has the same frequency dependence as the incident fields, one can now write a general expression for E_4 in the sample for the case under consideration as follows:

$$\exp(i\mathbf{k}_4\cdot\mathbf{r})\frac{dE_4}{dz} = C\left\{\chi^{(3)}_{i123}E_1E_2E_3^*\exp\left[i(k_1+k_2-k_3)\cdot r\right]\right.$$
$$\left. + \chi^{(3)}_{j123}E_1E_2^*E_3\exp i(k_1-k_2+k_3)\cdot r + \ldots.\right\} \qquad (2.3.4)$$

To obtain the total contribution to the fourth beam leaving the sample, one must integrate Equ. 2.3.4 (with respect to z) from one surface of the sample to the other and then integrate it over the cross section of the beams. When the phase matching condition is satisfied, the following expression for $\chi^{(3)}$ can be deduced from Equ. 2.3.2 [5,6]:

$$\chi^{(3)}_{ijkl} = \frac{cn^2}{32\pi^2}\left(\frac{\lambda_0\rho_0^2}{2\alpha L}\right)\left(\frac{45}{8}\right)\frac{E_s}{E_{1j}E_{2k}E_{3l}}^{1/2}e^{-\alpha L} \qquad (2.3.5)$$

where L is the sample length, α is the absorption coefficient of the investigated sample and n the index of refraction of the sample. When equation (2.3.5) is used to determine $\chi^{(3)}$, accurate knowledge of the temporal and spatial dependence of the optical fields is required. In practice, the third order nonlinear coefficient of new materials are determined by comparing with well investigated reference material, such as carbon disulfide (CS_2). Equation 2.3.6 is used under identical excitation conditions to determine the new $\chi^{(3)}$.

$$\chi^{(3)}_{S,xxxx} = \chi^{(3)}_{CS_2,xxxx}\left(\frac{n_S}{n_{CS_2}}\right)\left(\frac{L_{CS_2}}{L_S}\right)\left(\frac{E_S}{E_{CS_2}}\right)^{1/2}\frac{e^{-\alpha_S L_S}}{e^{-\alpha_{CS_2} L_{CS_2}}} \qquad (2.3.6)$$

the subscripts S and CS_2, are the sample and reference sample.

2.3.2 *Time Resolved Measurements*

The time information of the fourth beam can be obtained by considering a simple two level system and that the pulse duration is shorter than the relaxation of the process determining $\chi^{(3)}$. The magnitude of the signal beam E_4 with the probe pulse (beam 2) delayed by T_d with respect to the excitation pump pulses is given by:

$$E_4(t)=K\left[E_3(t)\int_{-\infty}^{t} dt'\, E_2(t'+T_d)E_1(t')\, f(t,t') + E_2(t+T_d)\int_{-\infty}^{t} dt'\, E_3(t')E_1(t')\, f(t,t')\right] \qquad (2.3.7)$$

where $f(t,t') = \exp[(t'-t)/T_1]$, T_1 is the lifetime of the excited state, and K is a complex constant. Equation 2.3.7 is obtained if all three beams are polarized parallel to each other (XXXX geometry), thus giving rise to at least two temporal components. A fast component limited by the laser pulse duration and a longer decay due to the medium response. The fast component usually contribute a strong coherent peak due to the bound electronic response of the medium at zero delay. The slower component can be separated from the electronic response and allow for the investigation of the other components. When the beams are polarized parallel to each other, three gratings are formed, one grating is from the two pump beams (1 & 3) and the other two gratings are created by each one of the pump beam and the probe beam. By setting the polarizations of both the probe and signal perpendicular to the polarizations of the two pumps (XYXY geometry), only one grating is formed by the two pump beams and the probe is diffracted by this grating. The magnitude of the diffracted signal beam E_4 is then

reduced to

$$E_4(t)=E_2(t+T_d)\int_{-\infty}^{t} dt'\, E_3(t')E_1(t')\, f(t,t') \qquad (2.3.8)$$

for the experiment described here the fourth beam is detected with a photodiode that has a response time much greater than either the laser pulse duration or T_1. Thus we can approximate the signal $S_4(T_d)$ from the photodetector as the integral of $|E_4|^2$ over all time:

$$S_4(T_d)=\int_{-\infty}^{\infty} |E_4(t)|^2 dt. \qquad (2.3.9)$$

2.4 Z-Scan

The z-scan technique, shown in Fig. 2.4.1, is a simple and sensitive single beam technique for measuring the sign and magnitude of n_2. It is based on the principle of spatial beam distortion. In this method a single focused beam is used to illuminate the sample. The transmittance through an aperture placed some distance from the focal plane of the beam is monitored as the sample is scanned along the optic axis. From this measurement both the size and magnitude of n_2 can be determined.

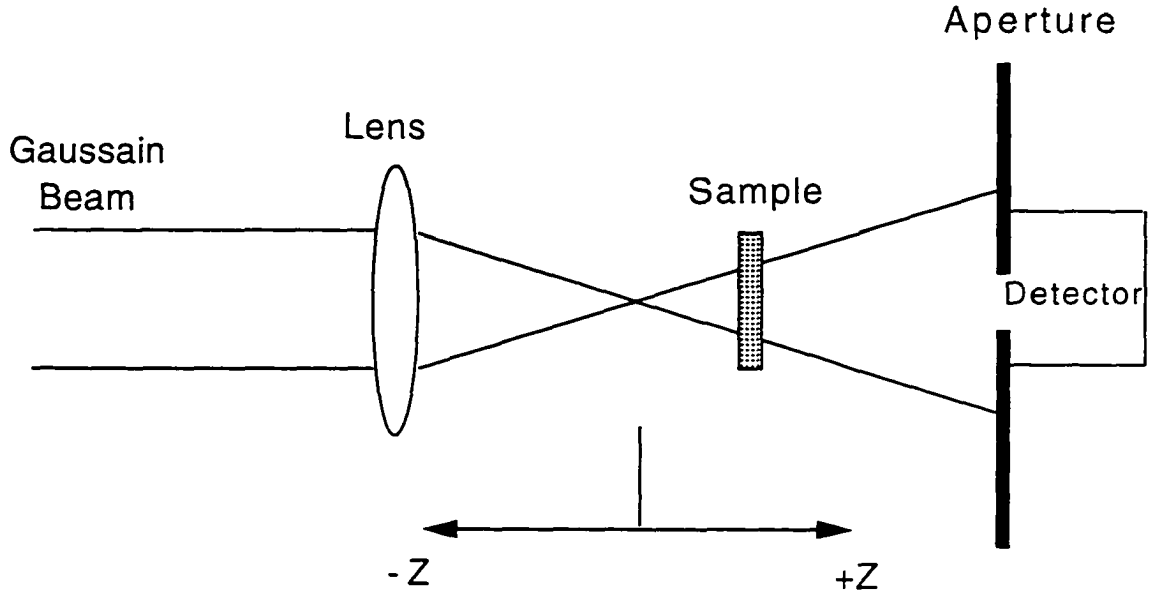

Fig. 2.4.1 Single Beam Z-scan Set-up

In general, a gaussian beam is focused into a thin nonlinear medium. The transmittance of the nonlinear medium is measured through an aperture placed in the far field as a function of the sample position z with respect to the focal plane. Assuming that the nonlinear material has a negative n_2 and very thin (thickness less than the diffraction length of the focused beam), then as the sample is translated from -z to +z its behavior will be that of a thin lens with a varying

focal length. At points well before the focal plane (-z) the irradiance will be relatively low and little nonlinear refraction will occur and the transmittance remains constant. As the sample approaches the focal plane the irradiance is increased and self-focusing occurs. A negative self-focusing action before the focal plane causes a collimation or narrowing of the beam which in turn increases the transmittance at the aperture. The same effect will result in the reduction of the transmittance when the sample is on the +z side. If the sample has a positive nonlinearity, the opposite effect, ie., lowered transmittance for sample at the -z and increases in transmittance for the sample at +z is expected. Below a theoretical analysis of the z-scan technique is given.

The index of refraction n is expressed in terms of the nonlinear indexes n_2 (esu) or γ (m^2/W) through

$$n = n_0 + \frac{n_2}{2}|E|^2 = n_0 + \gamma I = n_0 + \Delta n \qquad (2.4.1)$$

where γ is related to $\chi^{(3)}$ by

$$\chi^{(3)} = 2n_0^2 \varepsilon_0 c\, \gamma \qquad (2.4.2)$$

where n_0 is the linear index of refraction, E is the peak electric field (cgs), and I represents the irradiance (MKS) of the laser in the sample. The relationship

between n_2 and γ is n_2 (esu) = $(cn_0/40\pi)\gamma(m^2/W)$ where c (m/s) is the speed of light in vacuum. Also note that n_2 is related to $\chi^{(3)}$ by:

$$n_2=\frac{12\pi}{n_0}\chi^{(3)} \qquad (2.4.3)$$

Assuming a TEM_{00} beam with a Gaussian spatial profile (and beam waist radius of w_0) traveling in the +z direction :

$$E(z,r,t)=E_0(t)\frac{w_0}{w(z)}\exp\left(-\frac{r^2}{w^2(z)}-\frac{ikr^2}{2R(z)}\right)e^{-i\phi(z,t)} \qquad (2.4.4)$$

where $w^2(z) = w_0^2(1 + z^2 / z_0^2)$ is the beam radius, $R(z) = z(1 + z_0^2 / z^2)$ is the radius of curvature of the wavefront at z, $z_0 = kw_0^2 / 2$ is the diffraction length of the beam, $K = 2\pi / \lambda$ is the wave vector and λ is the laser wavelength in free space, E_0 is the field at the focus.

Any change in the index of refraction Δn will result in a change of the phase of the field $\Delta\phi$:

$$\frac{d\Delta\phi}{dz}=2\pi/\lambda\,\Delta n. \qquad (2.4.5)$$

The phase shift $\Delta\phi$ at the exit surface of the sample for a given position z is:

$$\Delta\phi(r,z,t)= \frac{\Delta\phi_0}{1+z^2/z_0^2} e^{-2r^2/\omega^2(z)} \qquad (2.4.6)$$

with

$$\Delta\phi_0(t)= \frac{2\pi}{\lambda}\Delta n_0(t)\frac{1-e^{-\alpha L}}{\alpha} \qquad (2.4.7)$$

where L is the sample length and $\Delta n_0(t)$ is the instantaneous on axis index change at the focus (z=0). The input beam is traced through the optical apparatus to find the normalized transmittance at the aperture (normalized Z-scan). The electric field at the exit surface of the sample at z_1 now contains the nonlinear phase distortion.

$$E'(r,z_1,t)=E(r,z_1,t)e^{-\alpha L/2}e^{i\Delta\phi(r,z_1,t)} \quad . \qquad (2.4.8)$$

Using the " Gaussian decomposition" (GD) method[7], where the complex electric field at the exit plane of the sample is decomposed into a summation of Gaussian beams via a Taylor series expansion of the nonlinear phase term.

$$e^{i\Delta\phi(z,r,t)} = \sum_{m=0}^{\infty} \frac{\left[i\Delta\phi_0(z,t)\right]^m}{m!} e^{-2mr^2/w^2(z)} \qquad (2.4.9)$$

the resultant electric field pattern at the aperture is reconstructed as

(2.4.10)

$$bE_a(r,t) = E(z,r=0,t)e^{-\alpha L/2} \sum_{m=0}^{\infty} \frac{\left[i\Delta\phi_0(z,t)\right]^m}{m!} \frac{w_{m0}}{w_m} \cdot \exp\left(-\frac{r^2}{w_m^2} - \frac{ikr^2}{2R_m} + i\theta_m\right)$$

y

propagating each Gaussian beam to the aperture plane. The propagation distance in free space from the sample to the aperture plane is defined by d and all other parameters are expressed as

$$g = 1 + d / R(z) \qquad (2.4.11)$$

$$w_{m0}^2 = \frac{w^2(z)}{2m+1} \qquad (2.4.12)$$

$$d_m = \frac{k w_{m0}^2}{2} \tag{2.4.13}$$

$$w_m^2 = w_{m0}^2 \left[g^2 + \frac{d^2}{d_m^2} \right] \tag{2.4.14}$$

$$R_m = d \left[1 - \frac{g}{g^2 + d^2/d_m^2} \right]^{-1} \tag{2.4.15}$$

and

$$\theta = \tan^{-1} \left(\frac{d/d_m}{g} \right) \tag{2.4.16}$$

Spatially integrating $E_a(r,t)$ up to the aperture radius r_a results in the transmitted power through the aperture, giving

$$P_T(\Delta\phi_0(t)) = c\varepsilon_0 n_0 \pi \int_0^{r_a} E_a(r,t)^2 r dr \tag{2.4.17}$$

where ε_0 is the permittivity in vacuum. The normalized Z-scan transmittance T(z) is calculated using

$$T(z)=\frac{\int_{-\infty}^{\infty} P_t(\Delta\phi(t))dt}{S\int_{-\infty}^{\infty} P_i(t)dt} \qquad (2.4.18)$$

where

$$P_i(t)=\pi w_0^2 I_0(t)/2 \qquad (2.4.19)$$

is the instantaneous input power in the sample and

$$S=1-\exp(-2r_a^2/w_a^2) \qquad (2.4.20)$$

is the aperture linear transmittance, with w_a as the beam radius at the aperture in the linear regime. Figure 2.4.2 is a calculated Z-scan profile which exhibits such features as the valley-peak (v-p) sequence for positive nonlinearity and a peak-valley (p-v) sequence for negative nonlinearity.

From the difference between the normalized peak and valley transmittance, defined as $\Delta T_{p-v} = T_p - T_v$, one can estimate the value of n_2 (or $\chi^{(3)}$) without performing a detailed fit to the experimental data. Within a 0.5% accuracy, for small aperture ($S \approx 0$) and for phase distortions $|\Delta\phi_0| = k\Delta n \frac{1-e^{-\alpha l}}{\alpha} \leq \pi$, the relationship of the difference between the normalized peak and valley

transmittance ΔT_{p-v} and n_2 is given by:

$$\Delta T_{p-v} \approx A|\Delta\phi_0| \approx A\left|\frac{\pi n_2}{\lambda}|E|^2\frac{(1-e^{-\alpha l})}{\alpha}\right| \qquad (2.4.21)$$

where l is the sample length, α is the absorption coefficient and A is a constant which may depend on the aperture size.

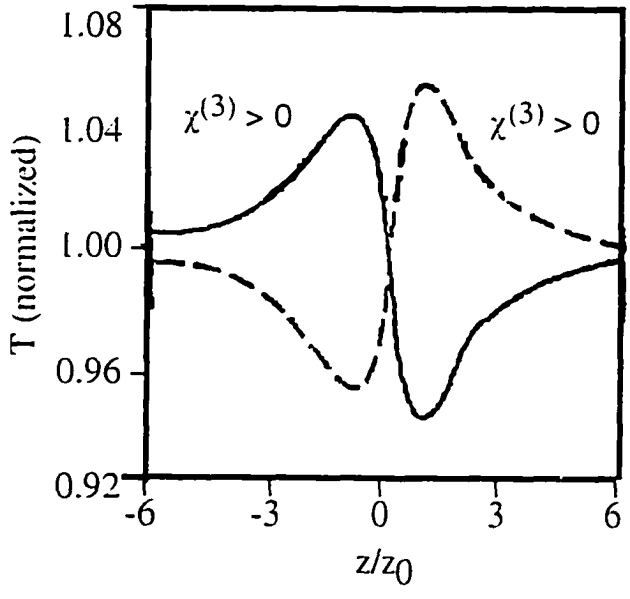

Fig.2.4.2 Calculated Z-scan transmittance for third order nonlinearity with either a negative or positive polarity and a small aperture.

When CS_2 is used as a reference under the same excitation conditions, the value of $\chi^{(3)}$ from the sample can be obtained:

$$\chi_s^{(3)} = \chi^{(3)}_{CS_2} \frac{(\Delta T_{p-v} n_0)_s}{(\Delta T_{p-v} n_0)_{CS_2}} \qquad (2.4.22)$$

where, ΔT should be obtained from the normalized transmittances for both CS_2 and the sample.

Materials with large nonlinear refractive response often times are superimposed by absorption components due to the presence of single or multiphoton resonances, saturation of the single photon absorption, or free carrier dynamic absorption. To account for any absorption component the third - order nonlinear susceptibility can be considered complex and is represented by a real $\chi^{(3)}_R$ and an imaginary part $\chi^{(3)}_i$ as follows

$$\chi^{(3)} = \chi_R^{(3)} + i\chi_i^{(3)} \quad . \qquad (2.4.23)$$

Assuming two photon absorption (TPA),the imaginary part $\chi^{(3)}_i$ is related to TPA coefficient β through

$$\chi_i^{(3)} = \frac{n_0^2 \varepsilon_0 c^2}{\omega} \beta \qquad (2.4.24)$$

and the real part is related to γ through

$$\chi_R^{(3)} = 2n_0^2 \varepsilon_0 c \gamma \qquad (2.4.25)$$

The absorption and the refractive contributions to the z-scan profile are coupled. By removing the far-field aperture (S=1) the z-scan transmittance is no longer influenced by the beam distortion (refractive component) but is only a function of the nonlinear absorption. For a temporally Gaussian pulse and $|q_0| < 1$, the open transmittance is expressed in terms of the peak irradiance as [8]

$$T(z,S=1) = \sum_{m=0}^{\infty} \frac{[-q_0(z,0)]^m}{(m+1)^{3/2}} \qquad (2.4.26)$$

where

$$q_0(z,t) = \frac{\beta I_0(t) L_{eff}}{\left(1 + \frac{z^2}{z_0^2}\right)} \qquad (2.4.27)$$

References

1. M. Nakazawa Opt. Lett. 12, 681 (1987)

2. B. I. Stepanov, E. V. Ivakin, and A. S. Rubanov, Sov. Phys. Doklady 16. 46 (1971); R. W. Hellwarth, J. Opt. Soc. Am. 67, 1 (1977)

3. R. W. Hellwarth, Prog. Quant. Electron. 5, 1, (1977).

4. Y. R. Shen, Nonlinear Optics. John Wiley & Sons. New York. 1984.

5. G.M. Carter, M.K. Tharkur, Y.J. Chen, and J.V. Hrnyniewicz, Appl.Phys. Lett. 47, 457 (1985).

6. G.M. Carter, J. Opt. Soc. Am. B6, 1018 (1987)

7. D. Weaire, B.S. Wherrett, D.A.B. Miller, and S.D. Smith. "Effect of low power nonlinear refraction on laser beam propagation in LnSb". Optics Lett., vol.4, pp. 331-333, (1974).

8. M. Shiek, A.A. Said, T.H. Wei, D.J. Hagan, and E.W. Styland, IEEE J. Quantum Electron. QE-26, 760 (1990)

Chapter 3

Dynamics and Magnitude of the Nonlinear Optical Response

3.1 Introduction

The continued motivation to develop new conjugated polymer with ultrafast responsivitivity (≤ 1 psec), enhanced nonlinearity ($> 10^{-7}$ esu), process-ability, high optical and chemical stability (months - years), makes it necessary to understand the mechanism (or mechanisms) underlying their nonlinear susceptibilities. This is essential for the design and development of new and better systems. In order for π-conjugated materials to be used in NLO based devices, the values of $\chi^{(3)}$ have to be at least two orders of magnitude larger than currently reported. Fast responses have been obtained in several systems such as polyacetylene and polythiophene[1-4], in principle any NLO processes involving virtual states are inherently ultrafast.

In this chapter we will focus on the dynamics of the NLO response of conjugated polymers.

3.2 Dynamics of the Nonlinear Optical Response in Conjugated Polymers

Various third-order nonlinear processes, such as the degenerate four-wave

mixing[5], picosecond and femtosecond pump and probe[6-7] and femtosecond absorption spectroscopy[8] have been used to focus on the ultrafast dynamics in thiophenes[9-13]. The dynamics of thiophenes are in part explained in terms of self-trapped excitons (STEs)[5]. Thiophene polymers are from one of the two classes of polymers that are distinguished in terms of their ground state, namely degenerate and nondegenerate. Because their ground state is weakly lifted (Fig. 3.2.1), these polymers are said to be nondegenerate[14]. A sketch of the molecular structure shown in Fig. 3.2.1 (upper) illustrates that the structures representing phase A and phase B are not energetically equivalent. Phases A and B are the local minimums for the energy versus distortion parameter diagram. It is well established that systems with nondegenerate ground state possess polarons and bipolarons as dominant charge species[15-18]. Fig 3.2.2 shows the structure of self-trapped exciton, polarons (P^+ and P^-) and bipolarons (BP^{++}) in polythiophene[8]. Self-trapped excitons (Fig. 3.2.2a) are sometimes call neutral bipolarons, since they are neutral in charge. Positive and negative polarons are formed from relaxation of self-trapped excitons (Fig 3.2.2b). The fusion of two positive or negative polarons during relaxation can result into a positive or negative bipolarons.

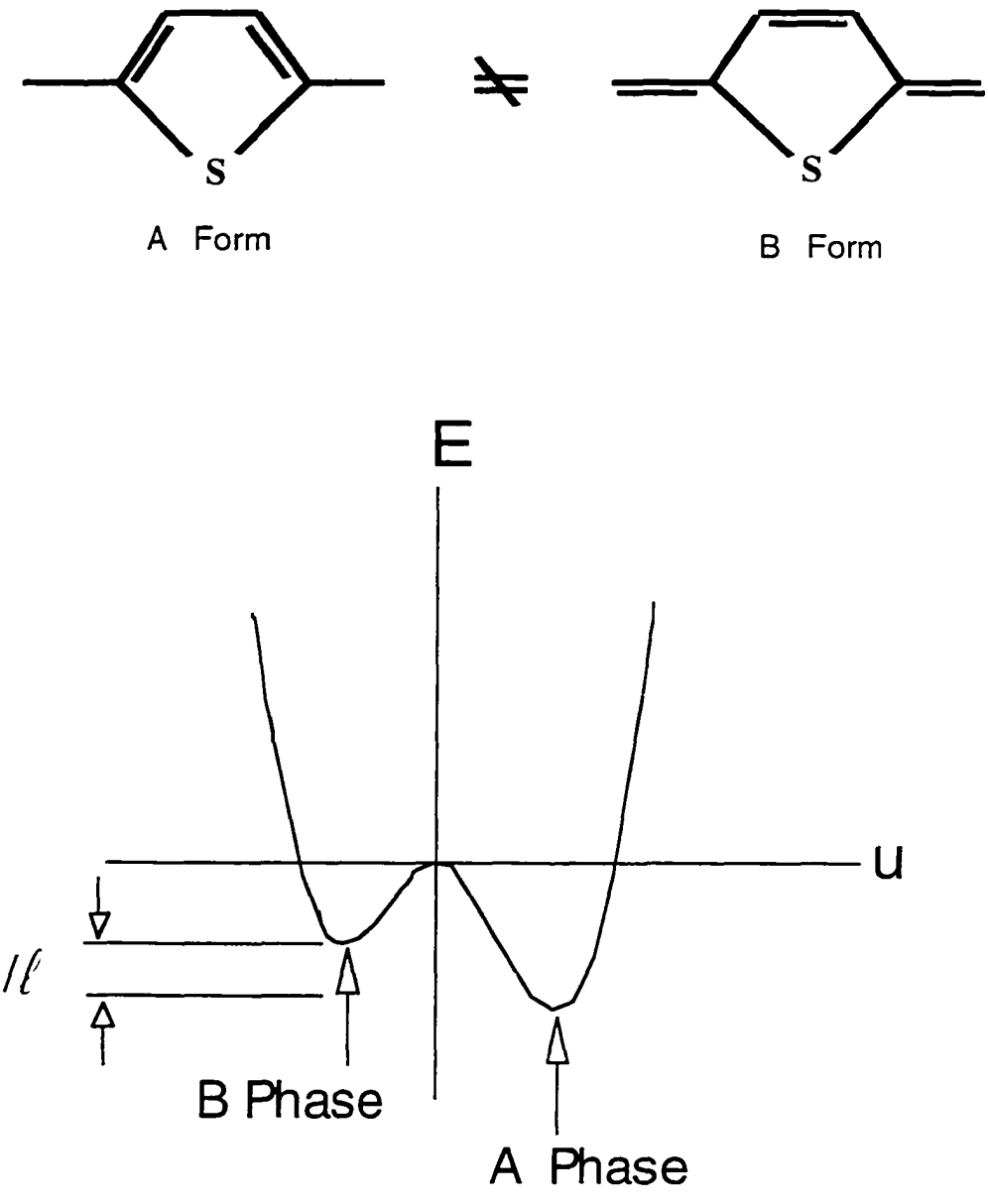

Fig. 3.2.1 The schematic diagram of polythiophene in which the ground state degeneracy is weakly lifted, energetically form A and B are not equal as shown in the diagram at the bottom of the figure where a plot of the energy versus the distortion parameter u.

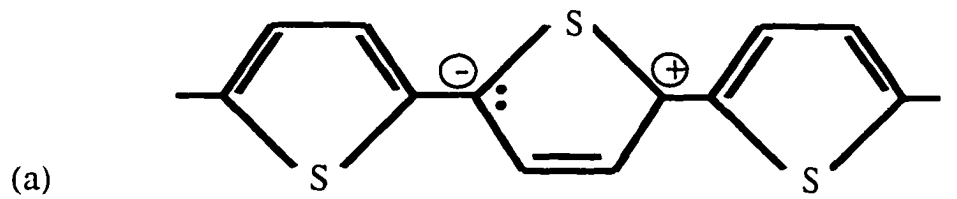

(a) STE

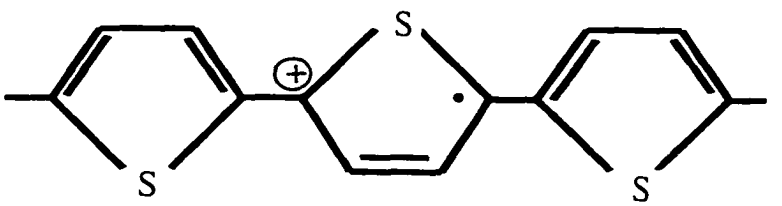

(b) P^+

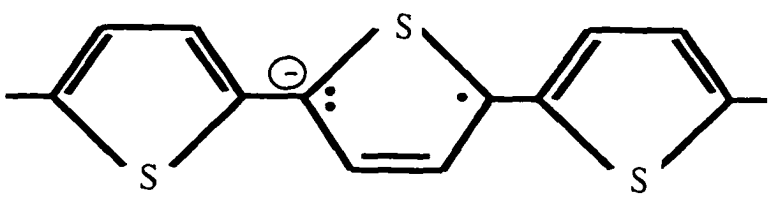

(c) P^-

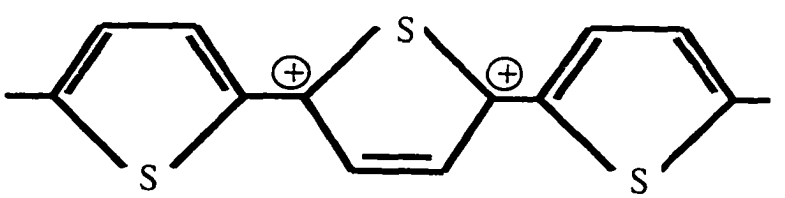

(d) BP^{++}

Figure 3.2.2 shows the molecular structure of self-trapped exciton, polaron (P^+ and P^-) and bipolaron (BP^{++}) in polythiophene. ⊖ and ⊕, represent an electron - hole pair, double dots "∶" represents a lone pair, and single dot "•" represents a unpair electron.

3.2.1 Relaxation of Self-Trapped Excitons in Conjugated Polymers

Self-trapped excitons are basically free excitons that are relaxed by the emission of lattice phonons. The mechanism behind self-trapping, is one in which the binding energy becomes the kinetic energy of the lattice oscillation. The formation time of STE depends on the energy redistribution from the strongly coupled phonons to other phonon modes[8]. The formation and decay time constants of ST excitons in several polymers are listed in Table 3.2.1. The transition of energies from free exciton to ST exciton was noticed by Kobayashi et al. as a shift in the absorption spectra to lower energy.

The dynamics of one dimensional systems such as polythiophene (PT) can be explained by using the model proposed by Kobayashi et al. {Ref 8}. The relaxation kinetics and adiabatic potential surface for this model is shown in Fig. 3.2.3. The potential curves of the ST exciton starts from the minimum of the free exciton. The curve then become substantially lower in energy than that of free exciton potential because of electron - phonon coupling. As a result, the potential curves of the ST exciton and the ground state intercept at a point that is elevated only slightly above the minimum of the ST exciton potential curve. From the model shown in Fig. 3.2.3, it can be seen that excitons after tunneling through or crossing over a barrier between potential minima of the free exciton and ST exciton, the excitons relax to a lower energy state. The radius of

curvature (Fig. 3.2.3) of the potential of STE is larger than those of G and FE states in order to take into account the reaction coordinate [19].

In one dimensional systems the formation of the relaxed excitons is expected to take place within the period of the coupled phonon cycle[20]. Self-trapped exciton can relax to the ground state by either (1) tunnelling through the barrier between the STEs and ground-state potential, or (2) relaxing to long-lived species such as polarons and bipolarons as previously mentioned. These polarons and bipolaron are known to give rise to localized vibrational modes that are connected with the local structure distortions and the appearance of symmetric gap states [21,22,23]. In chapter 4, we will investigate diffusion processes of free excitons and self-trapped excitons using time resolved relaxation measurements.

Table 3.2.1

The formation time τ_f (fs) and decay τ_d (ps) of Self-Trapped (ST) Excitons.

Polymer	Formation time τ_f (fs)	Decay Time τ_d (ps)
PDA-3BCMU	150 ± 50	2.0 ± 0.2
PDA-4BCMU	< 200	3.0
P3MT	70 ± 50	0.8 ± 0.07
P3DT	100 ± 50	0.45

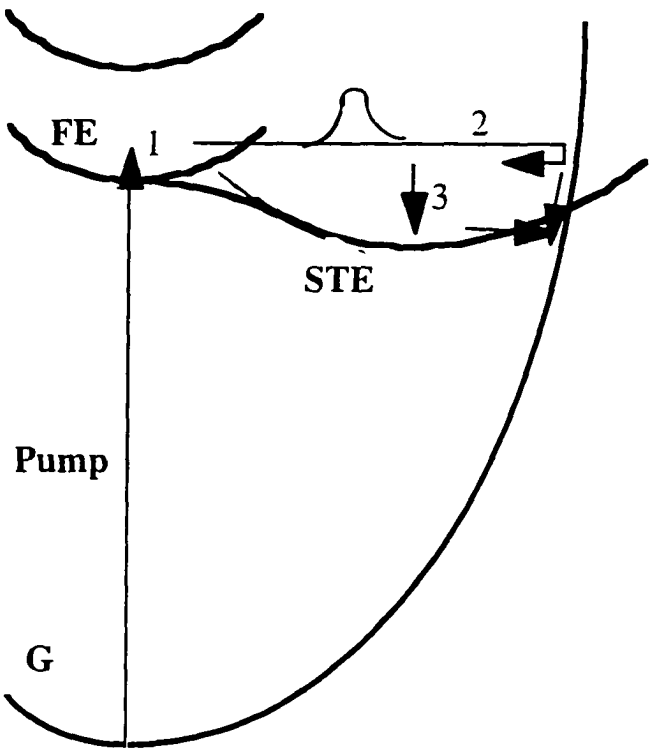

Fig. 3.2.3 Model of the relaxation kinetics and adiabatic potential surface of excitons in polythiophene. Numbers 1, 2, and 3 indicates FE, and STE before the emission of phonons, and STE after the phonon emission. G - ground state , FE - free exciton , STE - and self-trapped exciton.

3.3 Magnitude of the Nonlinear Optical Response

In this section, we address the enhancement of the nonlinear optical properties of conjugated polymers. Typically four techniques can be used to enhance the nonlinear optical response: packing, confinement, conjugation length and phonon resonance.

3.3.1. *Packing*

First we will discuss packing, by packing we mean the fabrication of compact monomolecular films, where film pinholes are eliminated, as shown by dielectric measurements (Barraud and Rosilio, 1970). This process can be achieved through the Langmuir Blodgett technique. Thus, providing highly ordered molecules with alignment in a single direction (dipping or drawn direction). Liming Wang et al. [24] have shown that control of the packing density using LB techniques, enhances the nonresonant third-order nonlinear optical properties of poly(p-phenylene benzobisthiazole) film, and that the $\chi^{(3)}_{xxxx}$ value increases dramatically with fabrication surface pressure. In chapter 5, we will show that the nonlinear optical response of a LB film (packed film) is enhanced by one order of magnitude when compared to a 1 μm thick polythiophene film measured simultaneously under the same conditions.

Nonlinear optical responses are expressed through the relationship of the

polarization $P(t)$ of a nonlinear medium in an intense optical field $E(t)$:

$$P(t) = \chi^{(1)}E(t) + \chi^{(2)}E^2(t) + \chi^{(3)}E^3(t) + \ldots \quad (3.3.1)$$

Each term in the macroscopic polarization of Equ. 3.3.1 can be expressed as a microscopic nonlinear optical response

$$P(t) = \alpha E(t) + \beta E^2(t) + \gamma E^3(t) + \ldots \quad (3.3.2)$$

where α is the linear polarizability, and β and γ are the second and third order nonlinear electronic susceptibility, respectively. Considering the third-order terms from equation 3.3.1 and 3.3.2, the nonlinear polarization P^{NL},

$$p^{NL} = \chi^{(3)}_{ijkl} E^{\omega}_j E^{\omega}_k E^{\omega}_l, \quad (3.3.3)$$

originates from the microscopic third-order polarization p^{NL} of individual molecules. The individual molecules are driven by local field E^{ω}_{loc}, thus p^{NL} is given by

$$p^{NL} = \gamma_{i'j'k'l'} \left(E^{\omega}_{loc}\right)_{j'} \left(E^{\omega}_{loc}\right)_{k'} \left(E^{\omega}_{loc}\right)_{l'}. \quad (3.3.4)$$

The local field can be related to the macroscopic field by the local-field correction tensor f^{ω}_s,

$$\left(E^{\omega}_{s,loc}\right)_{i'} = \left(f^{\omega}_s\right)_{i'j'} E^{\omega}_{j'}. \quad (3.3.5)$$

In the Lorentz-Lorentz model, f^{ω} is a scalar given by

$$f^{\omega}=\frac{2+\left(n^{\omega}\right)^{2}}{3} \qquad (3.3.6)$$

where n^{ω} is the refractive index at frequency ω.

The macroscopic polarization P^{NL} is a sum over microscopic polarization, taking into account the local field at frequency ω.

$$P_i^{3\omega}=\sum_{s=1}^{N} R_{ii'}^{S}\left(f_S^{3\omega}\right)_{i'j'}\left(p_S^{3\omega}\right)_{j'} \qquad (3.3.7)$$

where the summation is over all N molecules within a unit volume. R^S is the rotation matrix transforming the molecular frame to the laboratory frame. Combining Equ. 3.3.4 and 3.3.5, and Comparing like terms of $(E_j^{\omega}E_k^{\omega}E_l^{\omega})$ with Equ. 3.3.3. The third order macroscopic nonlinear susceptibility $\chi^{(3)}$ can be related to the corresponding microscopic susceptibility γ by considering an ensemble average over the orientational distribution and local field correction factors

$$\chi^{(3)}_{ijkl} = N \cdot \left\langle R_{im'} R_{jn'} R_{ko'} R_{lp'} \cdot f_m^{\omega_4} \cdot \gamma_{i'j'k'l'} \cdot f_j^{\omega_1} f_k^{\omega_2} f_l^{\omega_3} \right\rangle \quad 50$$

$$\chi^{(3)}_{ijkl} = N \cdot \left\langle R_{im'} R_{jn'} R_{ko'} R_{lp'} \cdot f_m^{\omega_4} \cdot \gamma_{i'j'k'l'} \cdot f_j^{\omega_1} f_k^{\omega_2} f_l^{\omega_3} \right\rangle. \quad (3.3.8)$$

where N, the number density of molecules, $< >$ represents an average over the orientational distribution of molecules. Equation 3.3.8 shows the relation between $\chi^{(3)}$ and N. The LB technique allows for the enhancement of $\chi^{(3)}$ by controlling the packing density through the surface pressure during fabrication.

3.3.2. *Quantum Confinement in one dimensional systems*

A strong effect on the nonlinear optical susceptibility is expected as a results of quantum confinement when the microcrystalline size is close or below the exciton diameter. A semiconductor superlattice is a periodic structure[21,22], $(-A_xB_y-)_m$, consisting of alternating layers (x and y) of two semiconductor with unit cells A and B and different bandgaps E_g^A and E_g^B ($E_g^A > E_g^B$). In such a periodic structure, the small gap semiconductor (B) forms a series of potential wells and the large gap semiconductor (A) form a series of potential barriers in the direction of periodicity. The height of the potential wells form depend primarily on the magnitude of the gap difference, $\Delta Eg = E_g^A - E_g^B$. In a superlattice (SL) structure the barrier thickness (d_A) is small enough for charge

carriers in adjacent wells of width (d_B) to interact; otherwise, the periodic structure is a multiple quantum well (QW). In polymers the required SL or QW structure, $(-A_xB_y-)_m$, is a multiblock conjugated copolymer containing sufficiently long blocks ($x > 1$ and $y > 1$) of repeating unit cells A and B of the conjugated homopolymers $(-A-)_m$ and $(-B-)_m$, with energy gaps E_g^A and E_g^B.

Samson A. Jenekhe et al[27]. have discussed theoretically the relationship between semiconductor superlattices and quantum wells in organic polymers and nonlinear optics. The important property of semiconductor superlattices and quantum wells is the phenomenon of quantum size effect. This phenomenon arises from the spatial confinement of charge carriers in semiconductor structures of small sizes. Based on the predicted quantum size effects: (1) the effective superlattice bandgap E_g^s ($E_g^A > E_g^s \geq E_g^B$) will decrease as the well width (d_B or y) increase or alternatively, the λ_{max} of the lowest energy absorption band will increase with increasing y, ie. a progressive spectra red shift as the copolymer block length y increases. (2) new structures will appear in the electronic absorption spectrum due to excitonic excitations or discrete quantum states in the valence and conduction bands.

In block copolymers with barrier thickness ($d_A \sim 3 - 4$Å) that is too small

to confine charges to a potential well that is equally too thin (d_B ~ 3- 4Å), have resulted in the formation of block segment band gaps E_{gb}^{A} and E_{gb}^{B} as the copolymer block length increases. Note that E_{gb}^{A} and E_{gb}^{B} are not necessarily identical to the homopolymer bandgaps E_g^{A} and E_g^{B}. Absorption bands due to these two characteristic energies of block conjugated copolymers. E_{gb}^{A} and E_{gb}^{B}. are expected to appear in the electronic spectra provided that the block length is large enough. In addition to the two-band structure due to E_{gb}^{A} and E_{gb}^{B}. quantization of the conduction and valence bands due to the potential barrier $\Delta E_g = E_{gb}^{A} - E_{gb}^{B}$ should lead to additional absorption bands with energies between the two block segment bandgaps. The formation of additional absorption bands with energies between the two block segment bandgaps have shown to exhibit very large cubic optical nonlinearities [26,27].

3.3.3 *Length dependence in conjugated systems*

Earlier theoretical studies show the dependence of π-electron contribution to the nonlinear polarizabilities of conjugated chains[30]. Using a simple free-electron model, the respective influence of chain length on optical nonlinearities

were analyzed. Consider a degenerate electron gas with 2N electrons confined in a one-dimensional box ($-L \leq r \geq L$) of length $2L$ by infinite barriers. In order to calculated γ for this system, the fourth-order perturbation energy $E^{(4)}$, induced by the electric-dipole interaction $H^{(1)} = -eEr$, where E is the electric field component along the chain must be evaluated. In the usual Rayleigh-Schrödinger perturbation theory one has to do infinite sums over intermediate states to obtain perturbation energies in orders higher than one. However, in simple systems such as a one dimension box

$$H\psi = \varepsilon\psi \tag{3.3.9}$$

where the wavefunction $\psi_n(r)$ is the solution to equ. (3.3.9). Neglecting potential energy, $H = p^2/2m$, and p is the momentum. From quantum theory p may be represented by $-i\hbar\, d/dr$ so that

$$H^0 = -\left(\frac{\hbar^2}{2m}\right)\left(\frac{d^2}{dr^2}\right), \quad \psi(\pm L) = 0, \tag{3.3.10}$$

It is simpler to solve the inhomogeneous differential equation

$$(H^{(0)} - E^{(0)})\,\psi^{(n)} = E^{(n)}\psi^{(0)} + E^{(n-1)}\,\psi^{(1)} + \ldots\ldots + (E^{(1)} - H^{(1)})\,\psi^{(n-1)}, \quad (3.3.11)$$

to obtain eigenstates in successively higher orders, than to do an infinite sum over intermediate states.

If one chooses the phases of $\psi^{(n)}$ such that

$$\langle \psi^{(n)} | \psi^{(0)} \rangle = \delta_{n,0}$$

it can be shown that

$$\left\langle \psi^{(s)} | H^{(1)} | \psi^{(r)} \right\rangle = \sum_{q=0}^{s} \sum_{p=0}^{r} E^{(p+q+1)} \left\langle \psi^{(s-q)} | \psi^{(r-p)} \right\rangle. \quad (3.3.12)$$

Due to the parity rule $E^{(1)} = 0$, equation 3.3.11 can be solved for n=1 knowing $\psi^{(1)}$, $E^{(2)}$ and $E^{(3)}$ can be obtained from Equ. (3.3.12). $\psi^{(2)}$ is found next by solving equ. (3.3.11) for n = 2. Finally $E^{(4)}$ is evaluated using Equ. (3.3.12). The method can be continued to successively higher orders. However γ can be expressed as [28]

$$\gamma = -2 \sum_{n=1}^{N} \frac{1}{6} \frac{d^4 E_n^{(4)}}{dE^4}$$

$$= \frac{128L^{10}}{a_0^3 e^2} \sum_{n=1}^{N} \left(\frac{-2}{9\pi^6 n^6} + \frac{140}{3\pi^8 n^8} - \frac{440}{\pi^{10} n^{10}} \right), \qquad (3.3.13)$$

where $a_0 = \hbar^2 / me^2$ is the atomic Bohr radius.

The summations for large N to the lowest order in (1/N), result in

$$\gamma = \frac{256L^{10}}{45a_0^3 e^2 \pi^6 N^5} \qquad (3.3.14)$$

Equation 3.3.14 shows that γ for a free electron like system increases significantly with the L (length of the one dimensional box).

3.3.4. *Phonon resonance*

Due to nonlinear quantum lattice fluctuations stimulated by vibrational resonance, nonlinear response is expected to be greatly enhanced by the photoexcitations that produces lattice distortions around photogenerated carriers.

The idea behind resonance enhancement of the nonlinear optical susceptibility is shown schematically in Fig 3.3.1 for the case of non-degenerate four-wave mixing.

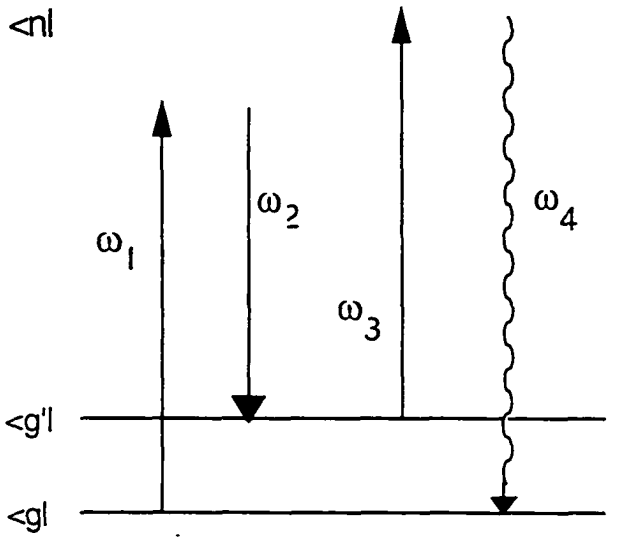

Fig. 3.3.1 Schematic showing a four-wave mixing process with $\omega_1 - \omega_2$ at resonance.

The derivation of the nonlinear optical susceptibility is based on quantum-mechanical perturbation theory of the atomic wave function [30]. The atomic wave function $\psi(r,t)$ is assumed to describe all properties of the atomic system and is the solution to the time-dependent Schrödinger equation

$$i\hbar\frac{\partial\psi}{\partial t}=\hat{H}\psi \qquad (3.3.15)$$

Here $\hat{H}$ is the Hamiltonian operator.

The third-order susceptibility $\chi^{(3)}$ can be derived from the perturbation calculation using the Feynman diagrams[31]. In general, $\chi^{(3)}$ consists of 48 terms. While $\chi^{(3)}$ is governed by the symmetric properties of the materials, each term follows the selection rules on its matrix element. Near resonances, only a few terms of $\chi^{(3)}$ are resonantly enhanced through the resonant denominators. Assume three input pump frequencies ω_1, ω_2, and ω_3 (Fig. 3.3.1). Single resonance of $\chi^{(3)}$ occurs when any of the frequencies or their algebraic sums approach a transition frequency of the medium. From Fig. 3.3.1, $\chi^{(3)}_R$ is singly resonant at $\omega_1 - \omega_2 = w_v$ and can be written in the form[30]

$$\chi_R^{(3)} = \frac{a}{\left(\omega_1 - \omega_2 - \omega_v\right) + i\Gamma_{g'g}}$$

where $a = -N\left(M^a_{g'g}\right)^*\left(M^s_{g'g}\right)\left(\rho_g - \rho_{g'}\right)/\hbar$ is independent of ω_1 and ω_2 and $\omega_1 - \omega_2$. Here N is the density of molecules, and Γ is the characteristic relaxation time between the states $<g|$ and $<g'|$.

M^s and M^a are Raman matrix elements,

$$\left(M^{s}_{g'g}\right)_{kl} = \sum_{n}\left[\frac{\langle g'|er_k|n\rangle\langle n|er_l|g\rangle}{\hbar\left(\omega_1-\omega_{ng}\right)} - \frac{\langle g'|er_l|n\rangle\langle n|er_k|g\rangle}{\hbar\left(\omega_2+\omega_{ng}\right)}\right]$$

$$\left(M^{a}_{g'g}\right)_{ij} = \sum_{n}\left[\frac{\langle g|er_j|n\rangle\langle n|er_i|g\rangle}{\hbar\left(\omega_a-\omega_{ng}\right)} - \frac{\langle g'|er_i|n\rangle\langle n|er_j|g\rangle}{\hbar\left(\omega_3+\omega_{ng}\right)}\right]$$

In my thesis, I will report on and discuss the effects of packing and conjugation length as they affect the nonlinear optical susceptibility. Quantum confinement and phonon resonance will be addressed as part of future direction in the final chapter.

Reference

1. W. S. Fann, S. Benson, J. M. J. Madey, S. Etemad, G. L. Baker and F. Kajzar,Phys. Rev. Lett. 62 1492 (1989)

2. M. Sinclair, D. Moses, K.Akagi and A. J. Heeger, Phys. Rev. B 38 10724 (1988).

3. R. Worland, S. D. Philips, W. C. Walker and A. J. Heeger. Synth.Met. 28. D663 (1989).

4. L. Yang, R. Dorsinville, Q. Z. Wang, W. K. Zou, P. P. Ho, N.L. Yang, R. R. Alfano, R. Zamboni, R. Danieli, G. Ruani and C.Taliani. J. Opt. Soc. Am. B 6 753 (1989).

5. D. Harris, R. Dorsinville, and T. Mukai Appl. Phys. Lett. 70. 1216 (1997).

6. G. S. Kanner, X. Wei, B. C. Hess, L. R. Chen, Z. V. Vardeny

7. M.T. Zhoa, B.P. Singh, and P.N. Prasad, J. Chem. Phys. 89, 5535 (1988)

8. T. Kobayashi, M. Yoshizawa, U. Stamn, M. Taiji, and M. Hasegawa, J. Opt. Soc. Am. B 7,1558 (1990).

9. M. Yoshizawa, M. Taiji, and T. Kobayashi, IEEE J. Quantum Electron. QE-25 2532 (1989).

10. U. Stamm, M. Taiji, M.Yoshizawa,T. Kobayashi, and K. Yoshino, Mol. Cryst. Liq.Cryst. 182A, 147 (1990).

11. D. McBranch, A . Heys, M. Sinclair, D. Moses, and A.J. Heeger, Phys. Rev. B42, 3011 (1990).

12. Z. V. Vardeny, H.T. Grahn, W.J. Heeger, and F. Wudl . Synth. Metals 28. C299 (1989).

13. I.D.W. Samuel, K.E. Meyer, R.H.friend, J. Ruhe, and G. Wegner, Proceedings of ICSM preprint(1990).

14. T.C. Chung, J. H. Kaufman, A. J. Heeger and F. Wudl Phys. Rev. B. 30. 702 (1984).

15. A. Brazovskii and N.N. Kirova, Pis'ma Zh. Eksp. Teor. Fiz. 33, 6 (1981) [JETP Lett. 33, 4 (1981)].

16. K. Fresser, A.R. Bishop, and D.K. Campbell, Phys. Rev. B. 27, 4804 (1983).

17. A.J. Heeger, Comments Solid State Phys. 10, 53 (1981)

18. J.L. Bredas, R.R. Chance, and R. Silbey, J. Phys. Mol. Cryst. Liq. Cryst. 77, 319 (1981).

19. H. Sumi, M. Georgier, and A. Sumi, Rev. Solid State Science 4, 209 (1990).

20. E. I. Rashba, "Self-trapping of excitons," in Excitons (selected chapter), E. I. Rashba, and M. D.Struge, eds. (North-Holland, Amsterdam, 1987), pp. 273-332.

21. A.J. Heeger, S. Kivelson, J. R. Schrieffer, and W.P. Su, " Solitons in conducting polymers," Rev. Modern Phys. 60, 781 (1988)

22. Z. Vardeny, E. Ehrenfreund, O. Brafman, M. Nowak, H. Schaffer, A.J. Heeter, and F. Wudl "Photogeneration of confined soliton pairs (bipolarons) in polythiophene" Phys. Rev.Lett. 56, 671-674 (1986).

23. K. Kaneto, S. Hayashi and K. Yoshino, " Kinetics of photoluminescent excitons in polythiphene films during electrochamical doping," J. Phys. Soc. Jpn. 57, 1119-1126 (1988).

24. L.Wang, T. Wada, T. Yuba, M. Kakimoto, Y. Imai and H. Sasabe J. Appl. Phys. 79 (12) 9321 1996.

25. S.A. Jenekhe and W. Chen Mat. Res. Soc. Symp. Proc. Vol.173 (1990)

26. S.A. Jenekhe, W. Chen , S.K. Lo and S.R. Flom, Appl. Phys. Lett.

27. S.A. Jenaekhe, S.K. Lo, and S.R. Flom, Appl. Phys. Lett., 54, 2524 (1989)

28. C. Sauteret, J. P. Hermann, R. Frey, F. Pradere, J. Ducuing, R.H. Baughman and R. R. Chance. Phys. Rev. Lett. 36, 956 (1976)

29. K. C. Rustagi and J. Ducuing, Optics Comm. 10. 259 (1974)

30. R. Boyd " Nonlinear Optics" Academic Press Inc. 1992

31. Y. R. Shen, "The principle of Nonlinear Optics, (John Wiley & Sons. Inc. 1984 Chapter 14 and 15

Chapter 4

Excited-State Dynamics of Thiophene Thin Films Studied by Time - Resolved Degenerate Four-Wave Mixing

4.1 Introduction

A continuing problem has been to develop new conjugated polymers with enhanced nonlinearity and stability[1]. Polythiophenes belong to a relatively new class of π-electron conjugated polymers that show large and fast electronic $\chi^{(3)}$, comparable with those of polydiacetylenes[2-5]. Like polyacetylenes and polydiacetylenes they also possess the C_{2h} point group symmetry. The π electrons are delocalized along the main chain, providing high electronic nonlinearity.

In this chapter, thin films of polydithieno(3,2-b; 2',3'-d)thiophene (PDTT) were used. The structural model for PDTT consists of a typical ribbon-like polymer chain, packed together at a distance d≈(3-4)Å[6]. The molecular structure of PDTT is shown in Fig. 4.1. The magnitude and sign of the nonlinear optical coefficient of this and other thiophene based thin films have extensively been studied by Dorsinville et al.[7,8]. The dynamics of the excited states of similar

thiophene based polymers have also been studied by Z. Vardeny[9]. Prasad[10] and Kobayashi[11] using picosecond and femtosecond pump and probe techniques. It has been suggested[11] that in similarly electrochemically prepared films of poly(3-methylthiophene) {P3MT}, free excitons (FE) relaxed to self-trapped excitons (STE) with a time constant of 70 ± 50 fsec and the self-trapped exciton relaxed at (800 ± 100) fsec. After the 800-fsec relaxation, a long decay component of a few tens of a picosecond was observed and attributed to polaron and bipolaron dynamics. Vardeny et al.[9] have measured in polythiophene films a single 300 fs fast component (attributed to self trapping) followed by a long (~3 ns) slow component. However, the pump intensity dependence of the excited state dynamics of polythiophenes has never been addressed. In this chapter, we report on direct measurements of the effect of fluence on the dynamics of the nonlinear optical response of a thiophene based polymer.

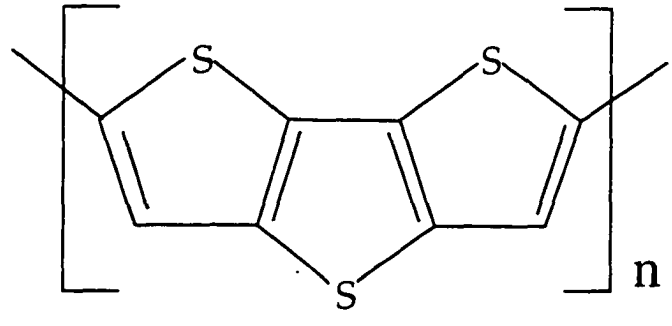

Fig. 4.1 Molecular stucture of Polydithieno(3,2-b;2',3'-d)thiophene (PDTT).

4.2 Experimental Set-up

The second harmonic of a continuous wave (cw) mode-locked Nd:YAG was used to synchronously pump a Rhodamine 6G home made intracavity-dispersion compensation dye laser. The output of the dye laser was synchronously amplified to 10 microjoules per pulse at 1 KHz repetition rate through a multiple stage amplifier dye chain that is pumped by the second harmonic of a regenerative Nd:YAG amplifier. The amplified beam was subsequently split with beam splitters and directed through variable delay lines toward the sample. The DFWM experiments were performed using a folded boxcar geometry which has been discussed in detail elsewhere[12]. The temporal response is measured by delaying the arrival time of the probe beam with respect to the pump beams. The signal wavelength was selected by a spectrometer and detected with a cooled PMT via fiber coupling. The intensity of the input beam was varied by the use of calibrated neutral density filters at the wavelength under study.

The sample used in this experiment was made by electrochemical polymerization on an indium tin oxide (ITO) glass substrate. The thickness of the sample was ~ 2mm. Details of the sample preparation process have been well established elsewhere[13-15].

4.3 Results and Discussion

Figure (4.2) shows the DFWM signal at 635 nm as a function of delay in the case of copolarized (||) beams and in the cross polarized ($\perp$) case. By simply using the XYXY configuration (probe beam cross with respect to the two pump beams) we were able to reduce the electronic response at the zero delay and allow for the investigation of other components of the DFWM signal. PDTT showed no significant change in the DFWM signal when rotated, indicating that the film is isotropic. A semi-log plot (fig. {4.2} insert) of the XYXY configuration reveals two distinct slopes in the decay curve. One can extract an acceptable approximation of the longer live component if the decay curve is fitted to a double exponential. This results in a fast time of (9 $\pm$ 1) ps and a slow time of more than 40 ps at pumping energy less than 0.1 μJ (1.3 X 10^9 W/cm^2), the fast component reduces by a factor of four (to about 2 ps) as the intensity increases by one order of magnitude. According to the model proposed by Kobayashi et. al.[11] for (P3MT), after excitation free excitons are first created which decay into STE then to longer lived species (in a few ten of picoseconds, also conforming to a nonexponential decay kinetics) probably polarons and/or bipolarons, with possible contributions from triplet excitons generated through two photon absorption. Our earlier measurement of the DFWM results at 635nm seems to fit this model quite well since we observe a fast component followed by a long

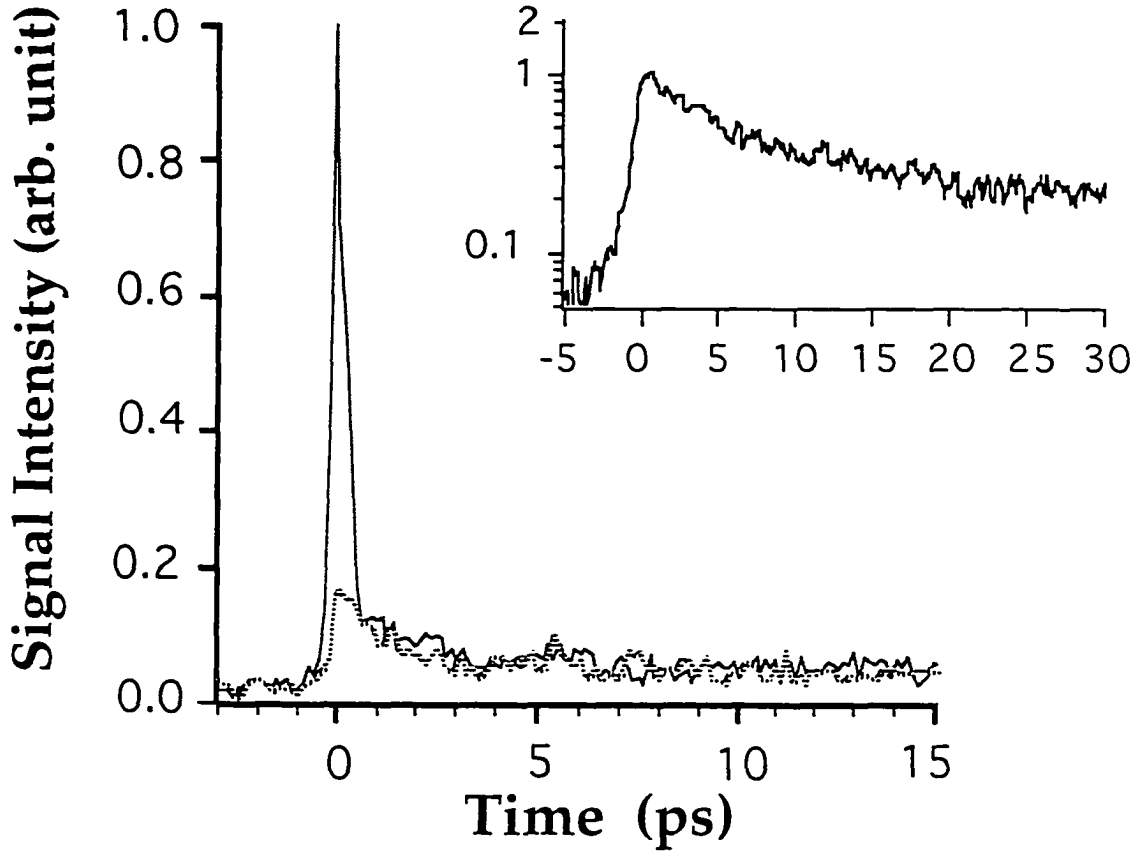

Fig. 4.2 Time dependence of the DFWM in PDTT thin films are plotted with a XXXX (solid) and (XYXY (broken) configuration. The inset shows a semi-log plot of the XYXY configuration with (9±1) ps and 40 ps.

lasting tail[16]. However, the measured time constant for the fast component is about one order of magnitude slower than the ST exciton lifetime measured by Kobayashi. It is important to note that this discrepancy could be due to the fact that our excitation fluence might be two order of magnitude lower than Kobayashi et. al [11], Prasad et. al.[17] and Z. Vardeny et. al.[9] as inferred from the energy values given in their papers (0.2 - 0.3 μJ). Our results are consistent with previous work when intensity dependence effcts is taken into account.

In order to further understand the decay mechanisms. we have measured the decay as a function of excitation intensity. Figure (4.3). shows the early temporal response of the DFWM signal observed for PDTT as a function of time for different pumping intensities at 635nm. The dynamics of the resonant third-order response shows two components, the first (fast) component being intensity dependent and the second (slow) component being almost intensity independent. When the intensity of the excitation light pulse is increased. the signal decay becomes faster and has a pronounced deviation from a single exponential decay. The possibility of heating effects was studied by Kobayashi[10] at 295K and 10K. and no significant difference was found between the decay kinetics. In our experiment, the kinetics was strongly fluence dependent, and the fastest component measured seems to be limited by our experimental laser intensity. Such fluence dependence is typical to diffusion controlled processes such as

bimolecular singlet exciton annihilation.

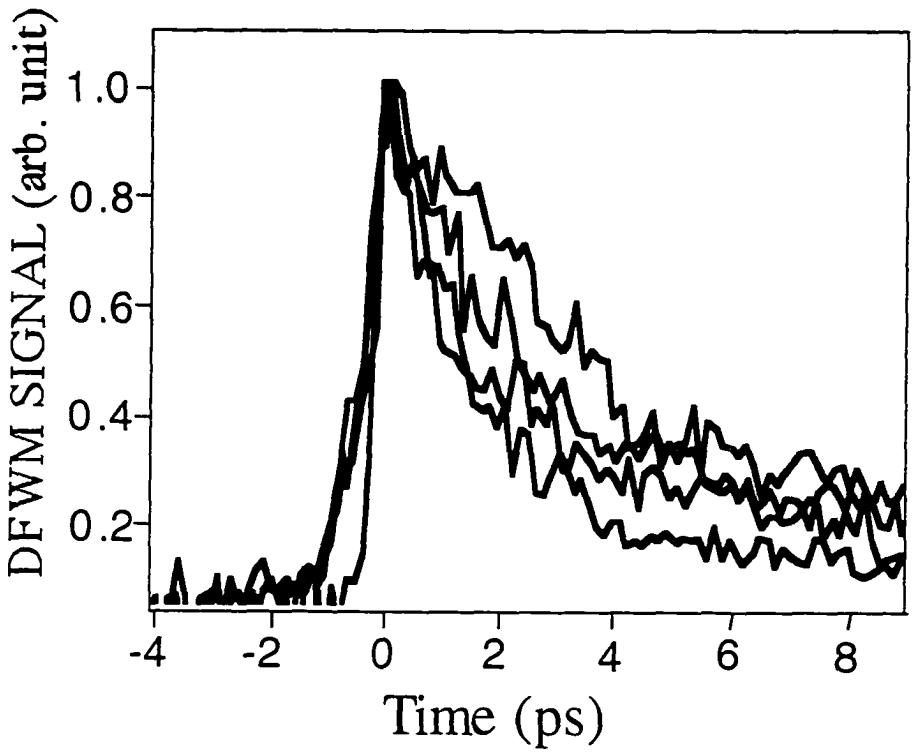

Fig. 4.3 The fluence dependence of the early temporal response of the NLO signal of PDTT at 635nm. The following laser fluences were used (top to bottom) 0.51, 1.34, 2.74, and 5.54 mJ/cm^2 .

Exciton - exciton annihilation plays a very important role in the dynamics of molecular solids, especially in the high density limit. In this high density limit, exciton-exciton interaction is dominant due to the close proximity of excitons to each other. Therefore, the exciton decay could be governed by a combination of exciton-exciton annihilation and exciton-phonon interaction leading to ST excitons and/or polarons and bipolarons.

If the decay of the excitons is governed by the two processes, exciton - exciton annihilation (bimolecular) and exciton - phonon coupling (self - trapping), then the kinetic equation for the concentration of singlet molecular excitons [S1] is

$$\frac{dS_1}{dt} = \alpha I(t) - (k_r + k_{nr})[S_1] - f\gamma_{ss}[S_1]^2 \qquad (4.1)$$

where α is the absorption coefficient, I is the intensity of the excitation, k_r and k_{nr} are radiative and nonradiative rates of the monomolecular decay of singlet excitons, γ_{ss} is the rate constant for bimolecular recombination, and is a parameter which takes into account losses due to auto-ionization and direct

nonradiative relaxation to the ground state S_0 from states above the singlet exciton state. For simplicity let $k_1 = k_r + k_{nr}$, where k_1 correspond to exciton - phonon interaction (monomolecular) and $k_2 = f\gamma_{ss}$, where k_2 correspond to exciton - exciton annihilation.

Equation (4.1) was used to fit our experimental data[18] Fig (4.4).

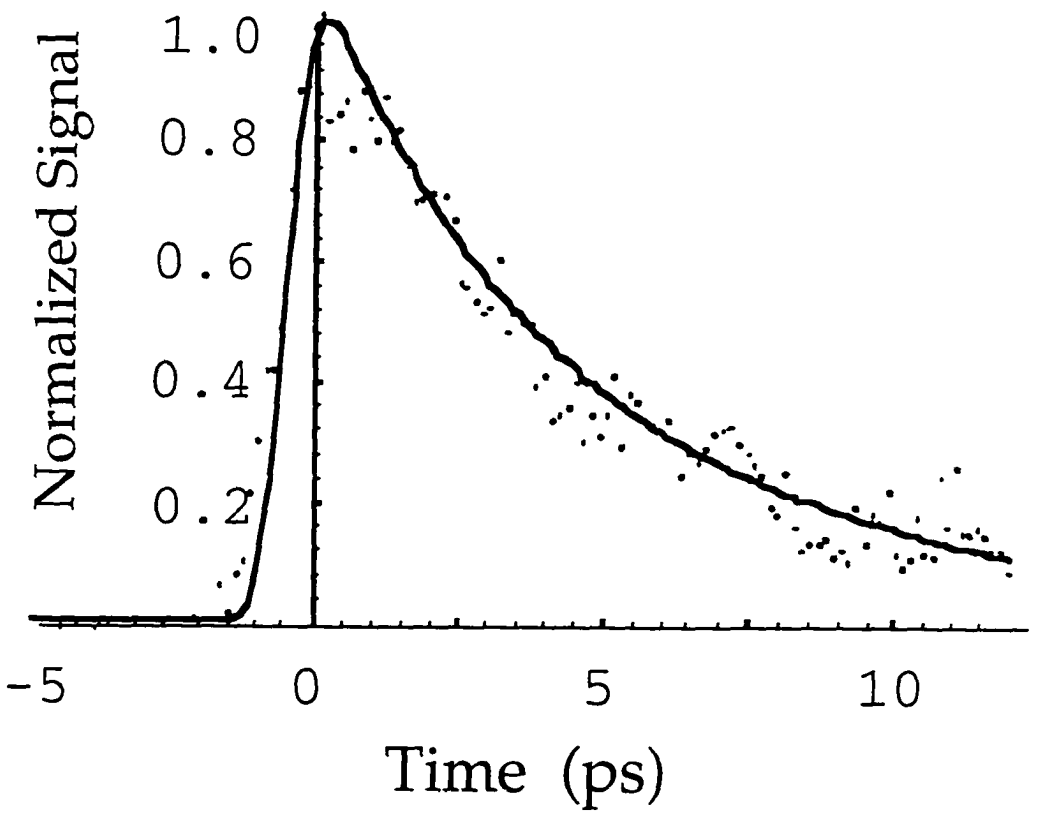

Fig.4.4 Temporal resolution of the bimolecular reaction (solid) fitted to the experimential data (data), pulse energy of 1.7mJ.

We modeled Equ. 4.1 to extract the bimolecular coefficient (k_2) of PDTT at the various excitation intensities. The unimolecular lifetime $1/k_1$ of singlet excitons was assumed to be equal to the long component of the decay dynamics (>40) ps { $k_1 = 2.5 \times 10^{10}\ s^{-1}$}, in agreement with our previous measurements[16]. The value of k_2 was determined to be $7.5 \times 10^{-9}\ cm^3/s$. The maximum error in the determination of the bimolecular coefficient due to the parameter *f* is a factor of 2.

The bimolecular recombination process can be represented by the model shown in Figure 4.5. After excitation, free excitons decays quickly (~ 70 fsec) to self-trapped excitons by the emission of phonons. The diffusion path of self-trapped exciton to the ground state depends on the excitation intensity. At low intensity, STE decays within 10 picoseconds to possible polarons then to the ground state within 45 picoseconds. At high intensity, exciton - exciton interaction dominates due to the close proximity of the excitons to each other. A new and higher state S^2 is created which quickly decays back to the S^1 state by the emission of phonons. The decay process continues within 10 picoseconds to polaron states and finally within 45 picoseconds to the ground state.

The bimolecular rate constant k_2 for a diffusion controlled process depends on the rate of encounter of two excitons and their subsequent annihilation. We

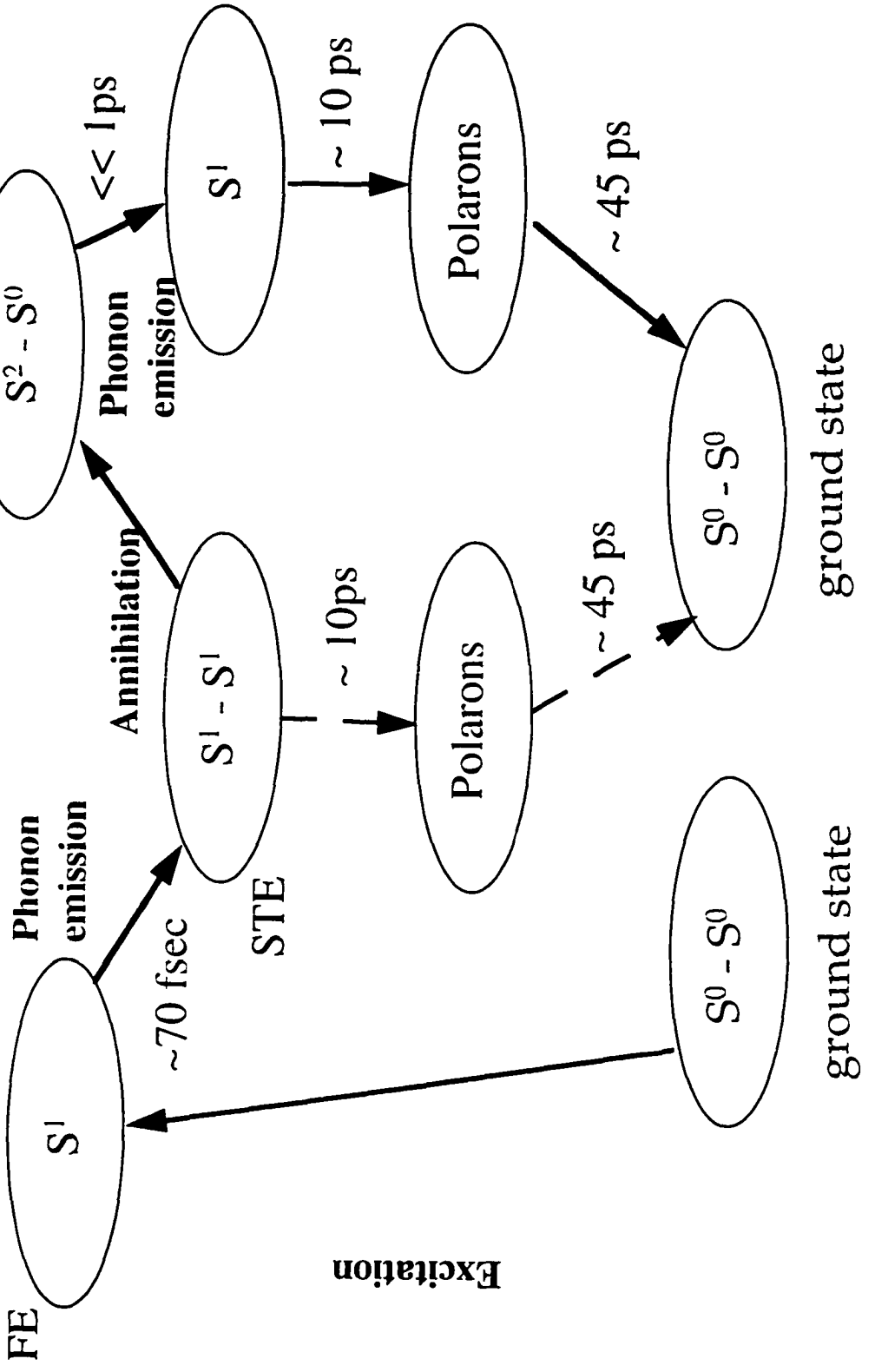

Fig. 4.5 A model of the diffusion processes in polydithieno(3,2-b; 2'3'-d)-thiophene thin films. Free excitons (FE), self-trapped excitons (STE), S^0, S^1 and S^2 are energy levels.

will assume that annihilation occurs "immediately" following the exciton-exciton encounter within a given spherical reaction volume[21]. For isotropic, three dimensional diffusion, where both reaction partners are mobile, the maximum bimolecular rate constant k_2 can be written as[22]

$$k_2 = 8\pi D_s R(1 + R/\Lambda) \qquad (3)$$

R is the spherical reaction radius, D_s the diffusion constant and $\Lambda = (6D_s/k_1)^{1/2}$ is the diffusion length.

Assuming R = 10 Å, and $R/\Lambda << 1$, from Equ. (3)

$$D_s = 3.0 \pm 1 \text{ X } 10^{-3} \text{ cm}^2\text{s}^{-1}$$

and

$$\Lambda \approx 85 \text{ Å}.$$

We assumed that k_2 is time independent , this is valid as long as the average separation distance between excitons, l_o, is small compared to the exciton diffusion length, Λ , and large compared to R [23], i.e.,

$$L > l_o > R, \quad (4)$$

Where: $\Lambda = (D_s\tau)^{1/2}$ and $\tau = 1/k_1$ $l_o = (4\pi n_0/3)^{-1/3}$ where n_0 is the initial excited state density.

Condition 4 is satisfied (l_o= 20Å) for the excitation level used in our experiments.

Within the framework of the random walk model, where the exciton step size is on the order of the nearest neighbor distance l_{SS}, the exciton diffusion coefficient can be expressed in terms of l_{SS} and the hopping rate ω using the relation[24,25].

$$D = 1/6 \, (l^2_{SS} \, \omega) \quad (5)$$

Assuming l_{SS} = 3Å[5] for PDTT and using this value in equation 5, we obtain a hopping time $\tau_h = 1/\omega$ between nearest neighbors of about (250 ± 50) fs for PDTT.

Our measurements show that intensity plays a significant role in determining the decay components. If we assume the intensity used by others [9-11], we approach values that are consistent with their findings, and it becomes

evident that bimolecular exciton-exciton annihilation occurs simultaneously with self-trapping.

4.4 Conclusion

We have shown that the decay kinetic of thiophene based polymers are intensity dependent. The fast decay component is dominated by exciton - exciton annihilation at high intensity. The shortest decay component measured in our experiments was 2 ps. However, with higher intensity we could probably approach values within close proximity of the 0.8 ps measured in 11. We have determined the time - independent bimolecular rate coefficients for PDTT. and have obtained an estimate of the diffusion coefficient and hopping time for singlet excitons from the measured bimolecular recombination rate constant.

Reference

1 P. N. Prasad and D. J. Williams, Introduction to Nonlinear Optical Effects in Molecules & Polymers (Wiley, New York, 1991).

2 R. Dorsinville, L. Yang, and R. R. Alfano, R. Tubino, and S. Destri Sol. State Com. vol. 68, 875, (1988)

3 F. Kajzar, J. Messier, C. Sentein, R. L. Elsenbaumer, and G. G. Miller. Proc. Soc. Photo-Opt. Instrum. Eng. 1147, 36 (1989).

4 D. Neher, A. Wolf, M. Leclerc, A. Kaltbeitzel, C. Bubeck, and G. Wegner. Synth. Metals 37, 249 (1990).

5 T. Sugiyama, T. Wada, and H. Sasabe, Synth. Metals 28, 323 (1989).

6 C. Taliani, R. Danieli, R. Zamboni, P. Ostoja and W. Porzio, Synth. Meth. 18, 177 (1987).

7 R. Dorsinville, L. Yang, R. R. Alfano, R. Zamboni, R. Danieli, G. Ruani, and C. Taliani, Optics Letters. 14, 1321 (1989).

8 L. Yang, R. Dorsinville, Q. Z. Wang, P. X. Ye, and R. R. Alfano Opt.Let. V 17, 325 (1992) .

9 G. S. Kanner, X. Wei, B. C. Hess, L. R. Chen, and Z. V. Vardeny in press

10 M. T. Zhao, Bhanu P. Singh, Paras N. Prasad, J. Chem. Phys. 89 5535 (1988).

11 T. Kobayashi, M. Yoshizawa, U. Stamm, M. Taiji, and M. Hasegawa. J. Opt. Soc. Am. B. / Vol. 7, 1558-1577, (1990).

12 A. Khyzniak, V. Kondilenko, Y. Kucherov, S. Lesnik, S. Odoulov, and M. Soskin J. Opt. Soc. Am. A V. 1, 169 (1984).

13 L. Yang, R. Dorsinville, Q. Z. Wang, W. K. Zou, P. P. Ho, N. L. Yang, R.R. Alfano, R. Zamboni , R. Danieli, G. Ruani and C. Talini J. Opt. Soc. Am. B. 6753 (1989).

14 R. Dorsinville, L. Yang, R.R. Alfano, R. Zamboni , and C. Talini Opt.

Lett. 14, 1321 (1989).

15 R. Worland, S.D. Philips, W.C. Walker and A. J. Heeger, Synth. Met. 28. D663 (1989).

16 D. Harris, E. Royer, R. Dorsinville, NASA Conf. Pub. 3314. Pg. 21. (1995).

17 P. N. Prasad Mat. Res. Soc. Symp. Vol. 109. 271 (1988).

18 I. Sokolik, R. Priestley, A. Walser. R. Dorsinville. Appl. Phys. Lett. Vol. 69, 27 (1996).

19 M. Pope and C. E. Swenberg, Electronic processes in organic crystals. (Oxford University Press, New York. 1982). p.158.

20 C. E. Swenberg and N. E. Geacintov in: Organic molecular photophysics, Vol. 1, ed. J. B. Birks (Wiley-Interscience. London. (1973), p.495.

21 A. Bergman, M. Levine, and J. Jortner, Phys. Rev. Lett. 18. 593 (1967).

22 U. Gösele. Chem. Phys. Lett. 43. 61 (1976): 46. 196(E) (1977).

23 T. Kobayashi, S. Nagakura. Mole. Phy. 24 695 (1972).

24 S. Chandrasekhar. Rev. Mod. Phys. 15, 1 (1943).

25 R. C. Powell and Z. G. Soos, J. Lumin. 11 1 (1975).

Chapter 5

Nonlinear Optical Anisotropy and Molecular Orientational Distribution in Poly[3-(6-tetrahydropyraniloxyhexyl)]-2,5-thienylene Langmuir Blodgett Films

5.1 INTRODUCTION

Langmuir Blodgett technique possesses the ability to construct well defined molecular structures of organic materials with various kinds of functionality[1]. Controlled thickness and uniformity are some of its most noted functionalities. However recent attention focused on the development of polymer Langmuir Blodgett (LB) films, by which controlling the chain conformation, molecular orientation and packing density in π-conjugated polymer structures allow for the enhancement of optical nonlinearity[2]. The optical nonlinearity originates from the interaction of the delocalized π-electrons along the linear chains with an electromagnetic field. Polythiophene[3], polydiacetylene[4] and polydibutylstannane[5] have received considerable attention as some of the third-order nonlinear optical materials because of its large and ultrafast third-order NLO response. However, the size of the nonlinearity attained as of today in organic polymers are still

below the value needed for device applications. Recently, the introduction of oxygen atoms in different functional groups on the side chain of poly(3-alkylthiophene) {PAT} has improves PAT adhesion with water, making possible the fabrication of LB structures[6]. Using this technique, the PAT LB films tend to form extended chain conformation showing good orientation of the main chain in the dipping direction along with condensed packing.

In this chapter, we present femtosecond degenerate four-wave mixing (DFWM) measurements that probe the magnitude and temporal response of the third order nonlinear optical susceptibility of a new PAT LB film. We also successfully measured the anisotropic $\chi^{(3)}$ behavior of poly[3-(6-tetrahydropyraniloxyhexyl)]-2,5-thienylene (PTHT) oriented thin films which demonstrates that most of the nonlinearity is associated with the π-electron polarizability along the conjugated chain. We describe the physical properties and theoretical treatment of the molecular orientation distribution and the packing behaviors of the polymer chains concerning the deposition and process of the films. The magnitude of the NLO susceptibility is directly compared with results obtained from electrochemically prepared polythiophene (PT), measured simultaneously under similar conditions.

5.2 Sample

The molecular structure of poly[3-(6-tetrahydropyraniloxyhexyl)]-2.5-thienylene (PTHT) is shown in Fig. 5.2.1. The polymer was synthesized according to the M^{c}Coullough procedure as reported in reference 6. The molecular structure of PTHT can be broken into three main groups: non-polar thiophene rings, flexible side chain (or spacer), polar ether group (or end group). The thiophene rings are hydrophobic and are each stabilized by a sulfur atom that is known to interact only weakly with the π-electron system of the backbone[7]. The six H-C-H {$(CH_2)6$} group acts as a flexible side chain and spacer between the non-polar and polar groups. The two oxygen atoms at the end of the side chain made the ends hydrophilic. This is important in order to improve the stability of the monolayers on the water surface for the preparation of LB films[8]. Therefore, the structure shown in figure 5.2.1 represent a poly(3-alkylthiophene) with a polar group at the end of the side chain. This made possible the preparation of thiophene LB films in water with cannot be achieved with long chain fatty acid used by other authors[9].

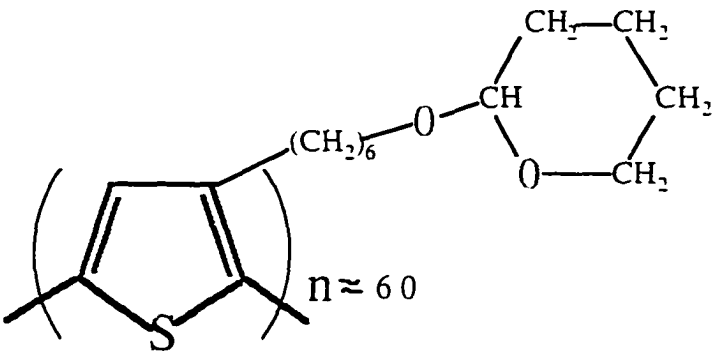

Fig. 5.2.1. Molecular structure of PTHT LB film

5.3 Experimental Techniques

A Y-type multilayered transfer (Fig. 5.3.1) was observed on slightly hydrophobic glass slides which were prepared by immersion of a precleaned glass into a chloroform solution of $(CH_3)_2SiCl_2$ (5% V)[10]. The polymer was precipitated in methanol and dried under reduced pressure. Details on the Lauda Filwaage computer controlled unit used to prepares these LB films are reported in reference 8. The regioregularity of the polymer was found to be 95% as detected by ^{1}H-NMR spectroscopy and its molecular weight ($\overline{M}_w$) is around 11,000. This means that on the average there are sixty monomers for each macromolecular chain. The LB films consisted of 8 monolayers per side for a

total estimated thickness of ≈130 Å.

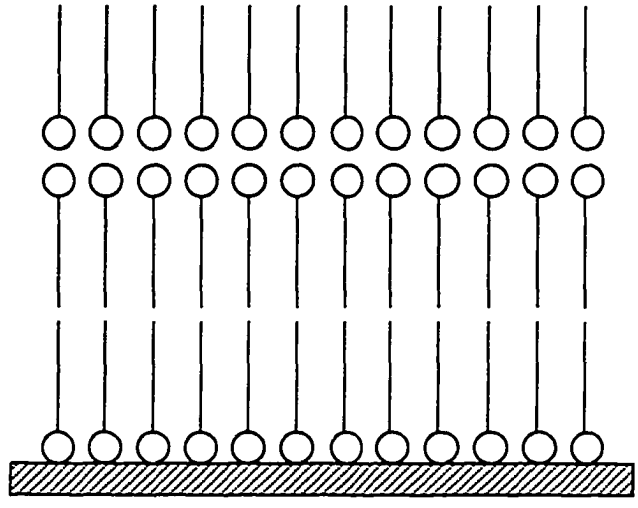

Fig. 5.3.1 A Y-type multilayer film (centrosymmetric) where stacking of the layers is head to head or tail to tail.

The absorption spectra were measured on a PTHT LB film at different angle of light polarization with respect to the dipping direction using a Cary 2400 Spectrometer. Note that a large dichroism appears as shown in Fig.5.3.2. A dichroic ratio up to 3 was observed. The order parameter describing the degree of orientation of the chains with regard to the dipping direction was determined to be about 0.4. (calculated as $Abs_{//} - Abs_{\perp}/Abs_{//} + Abs_{\perp})^{[1]}$.

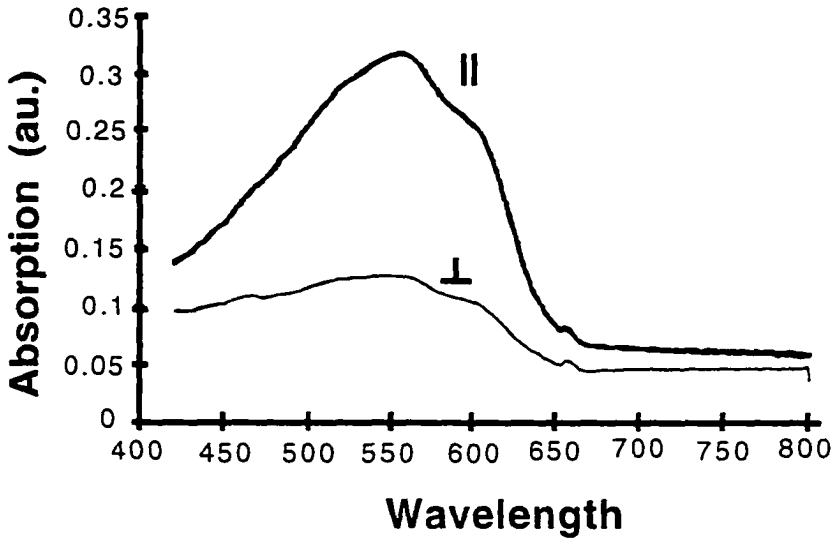

Fig.5.3.2. UV-Visible spectra of 8 layers of PTHT LB film measured with light polarization parallel with (||) and perpendicular to (⊥) the dipping direction.

Degenerate four-wave mixing experiments were performed using the folded boxcar geometry with 500 fsec pulses at 635 nm. Details on the experimental set-up is introduced and discussed in chapter 2. The film is mounted on a precision rotational stage so that it can be rotated while maintaining the spot position and that the orientational anisotropy of $\chi^{(3)}$ can be measured. Isotropic films of polythiophene used as our reference were reported to have a

$\chi^{(3)}$ value of 0.7 x 10^{-9} esu obtained with picosecond pulses at 635 nm[12].

The samples were also thermally treated in order to investigate its thermal stability. Fig. 5.3.3 shows a plot of the ratio between $A_{//}$ and $A_{\perp}$ versus temperature. The chains maintained their orientation up to 40 degree. However, by increasing the temperature a reduction of the $A_{//}$ is observed while the $A_{\perp}$ increases. This indicated a progressive isotropization of the chain orientation. As the temperature approached 50 degree celsius the highly oriented sample loose its orientational order due to the increased mobility of the polymeric structure. Moreover an observed blue shift of the absorption maxima for $A_{//}$ indicates that the conjugation length of the chain decreases[7].

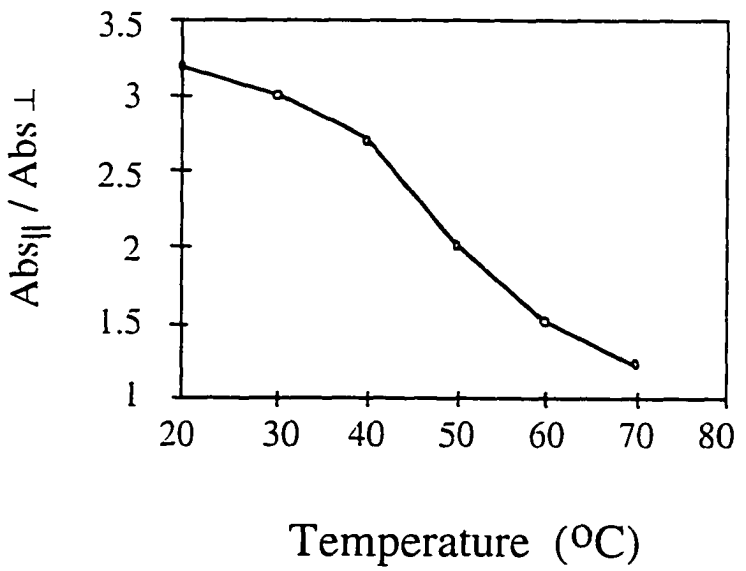

Fig. 5.3.3. Fig. 5.3.3 shows a plot of the ratio between $A_{//}$ and $A_{\perp}$ versus temperature.

5.4 Results and Discussion

5.4.1 Third-order nonlinear optical responses

The degenerate four-wave mixing signal as a function of time delay with the electric vectors of all the waves parallel to the draw direction is shown in Figure 5.4.1. The rise time and decay of the signal is clearly very fast and is limited by the laser pulse. However, as shown in previous chapters a weaker and slower contribution from polarons and bipolarons is probably present.Thus, the third-order nonlinearity of PTHT was determined to have a sub-picosecond response time of less than 500 femtosecond.

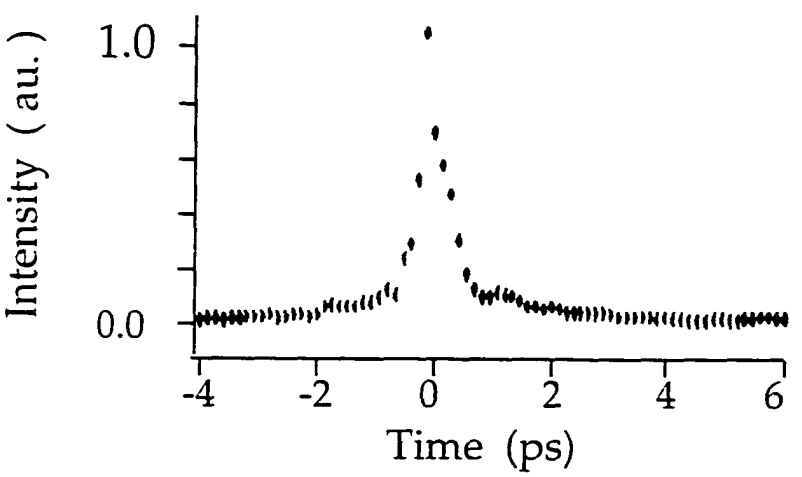

Fig. 5.4.1. Shows the observed DFWM signal as a function of time delay, and with the electric vectors of all the waves parallel to the draw direction. Pulse limited subpicosecond (<500 fsec) time response is measured.

The magnitude of $\chi^{(3)}$ was obtained by using the following equation with PT used as the reference (under same excitation condition),

$$\chi_S^{(3)} = \chi_{PT}^{(3)} \frac{n_{0LB}^{\ 2}}{n_{0PT}^{\ 2}} \frac{L_{eff.PT}}{L_{eff.LB}} \left(\frac{I_{LB}}{I_{PT}}\right)^{1/2} \frac{e^{-\alpha_{LB}L_{LB}}}{e^{-\alpha_{PT}L_{PT}}} \qquad (5.4.1)$$

where L_{eff} is the effective sample length, I is the intensity of the signal intensity of the fourth beam, signal beam. Equ. 5.4.1 has been corrected for absorption losses. The calculation of $\chi^{(3)}$ value for PTHT LB film along the draw direction from Equ. 5.4.1 yielded ~ 10^{-8} esu at 635 nm.

The change in $\chi^{(3)}$ value (actually the square root of the DFWM signal) as a function of the film rotation with respect to the incident electric field vector yields the plot shown in Fig. 5.4.2. The highest value of $\chi^{(3)}$ is obtained when the electric field vectors of all four wave are parallel to the draw direction. The minimum value of $\chi^{(3)}$ is for the orientation when all the electric vectors are perpendicular to the draw direction. The ratio of the $\chi_{eff}^{(3)}$ (ie. $\chi^{(3)}$ parallel to $\chi^{(3)}$ perpendicular) is about 4. The in-plane anisotropy is attributed to the flow alignment of polymer chains along the dipping direction. The movement of the substrate through the floating monolayer during the film transfer process makes the long chain axes tend to lie parallel in the film surface plane with an extended

chain conformation Fig. 5.4.3. By maintaining good surface pressure. films of good homogeneity and condensed packing are fabricated. Our result then provides confirmation that the largest component of $\chi^{(3)}$ (and hence microscopic nonlinearity γ) tensor is along the chain direction as is expected from any theoretical calculation of in a π- conjugated polymeric structures.

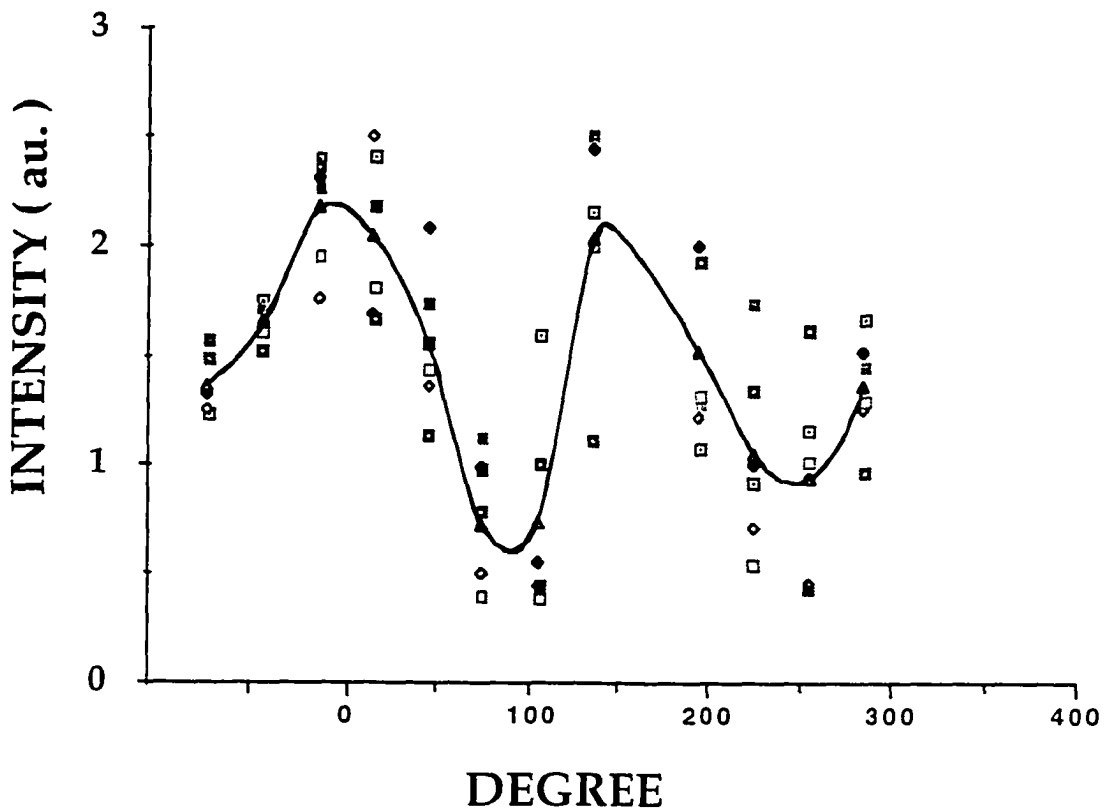

Fig. 5.4.2 Shows a plot of $\chi^{(3)}$, the square root of the DFMW signal intensity as a function of the film rotation with respect to the incident electric field vector. The dots represent the number of data scans. the solid line represent the average of all scan.

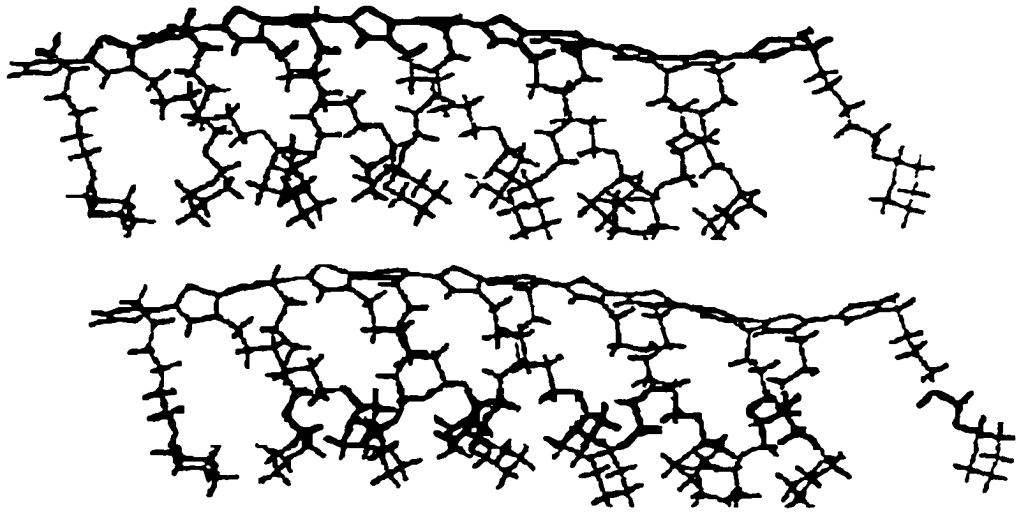

Fig. 5.4.3. A stereoscopical view of the molecular structure after the transfer process.

To explain the observed plot Fig. 5.4.2, we use a simple transformation of the fourth rank tensor $\chi^{(3)}$ from the film-based co-ordinate to the laboratory-based coordinate system. The third order optical susceptibility tensor $\chi^{(3)}$ in the laboratory framework (defined by the polarization vectors of the laser beam) is related to the film based $\chi^{(3)}$ as follows:

$$\chi^{(3)}_{ijkl} = \sum A_{im} A_{jn} A_{kp} A_{lq} \chi^{(3)}_{mnpq} \qquad (5.4.2)$$

where the As are the elements of the transformation matrix. For a orthorhombic in-plane symmetry one obtains the effective third-order susceptibility $\chi^{(3)}_{eff}$.

$$\chi^{(3)}_{eff.L} = \chi^{(3)}_{yyyy.F}\cos^4\Phi + \left\{\chi^{(3)}_{yyxx.F} + \chi^{(3)}_{yxxy.F} + \chi^{(3)}_{xxyy.F} + \chi^{(3)}_{xyxx.F} + \chi^{(3)}_{yxyx.F} + \ldots .\right\}\cos^2\Phi\,\mathrm{Sin}^2\Phi + \chi^{(3)}_{xxxx.F}\sin^4\Phi \qquad (5.4.3)$$

In equation 5.4.3, $\chi^{(3)}_{eff.L}$ is the $\chi^{(3)}$ of the film in the laboratory co-ordinate, when the beams are polarized parallel and vertical to each others. $\chi^{(3)}_{yyyy.F}$ and $\chi^{(3)}_{xxxx.F}$ are the components parallel and perpendicular to the draw directions. The other components $\chi^{(3)}_{off.F}$ are therefore the in-plane off-diagonal terms. Noted that the tensor components $\chi^{(3)}_{yyyy.F}$, $\chi^{(3)}_{xxxx.F}$, and $\chi^{(3)}_{off.F}$ are determined from the coordinate plane of the film. Whereas the $\chi^{(3)}{}_{eff}$ value is measured as a function of relative direction to the coordinate of the laboratory.

To extract information about the orientational distribution of the film, Equ. 5.4.3 was fitted to the experimental data (Fig. 5.4.4). The dotted line indicates the (normalized) average of all measurements. The solid line represents a theoretical fit.

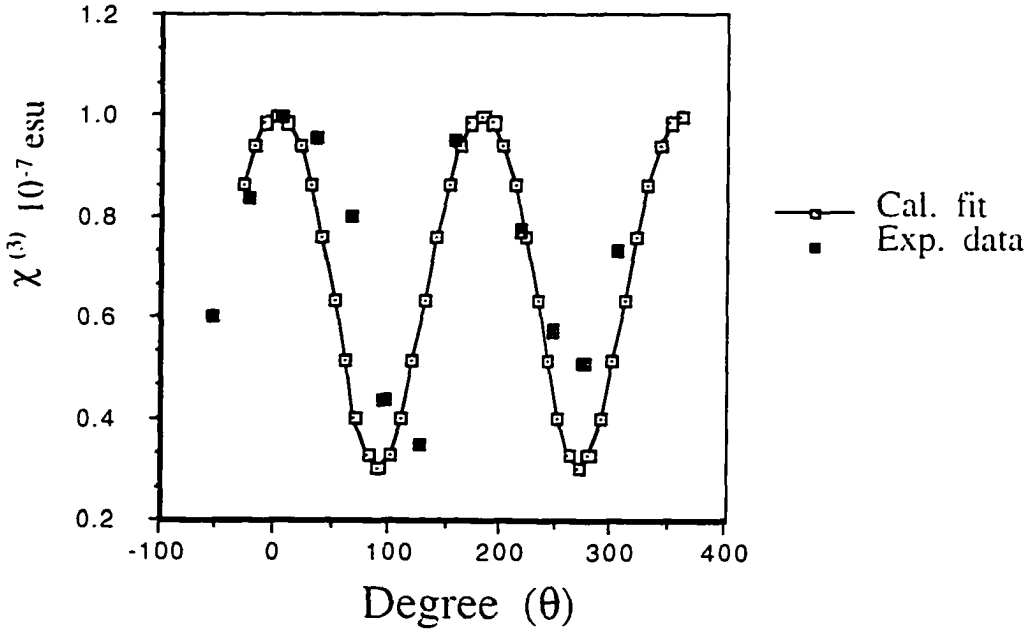

Fig. 5.4.4. The polarization dependence of the D4WM signal generated from an aligned sample. An error bar of ~0.2 x 10^{-8} esu was obtained base on the repeatability of the results from measurement to measurement.

The $\chi^{(3)}_{eff}$ values with the polarization parallel ($\Phi = 0^0$), perpendicular ($\Phi = 90^0$) and off diagonal to the dipping direction are ~1.1 ± 0.2 x 10^{-8}esu. and 2.5 ± 0.2 x 10^{-9} esu, and 0.75 x 10^{-8}esu respectively.

5.4.2 Anisotropy and packing effects:

The anisotropy of the third-order NLO susceptibility originates from the second-order hyperpolarizability of individual molecules and the packing geometry. For isotropic cases, $\chi^{(3)}$ can be related to the molecular parameter γ^* by,

$$\chi^{(3)}_{ijkl} = N\left\langle R_{ii'}\, R_{jj'}\, R_{kk'}\, R_{ll'}\, \gamma^*_{i'j'k'l'}\right\rangle \qquad (5.4.4)$$

where N is the number density of the molecules, R is the rotation matrix transforming the molecular frame to the laboratory frame, and γ^* is a "dressed" molecular susceptibility which has the same principle axes as the "bare" susceptibility γ and is defined by,

$$\gamma^*_{i'j'k'l'} = f^{3\omega}_{i'i'} f^{\omega}_{j'j'} f^{\omega}_{k'k'} f^{\omega}_{l'l'} \gamma_{i'j'l'k'}$$

where $f^{(\omega)}$ is a local field factor that provides the correction of the incident field. This field factor simply describes the interaction of a molecule with the vibrating dipoles of its neighbors. The '<>' represents an average over the

orientational distribution of the molecules. Based on the assumption that the orientational distribution of the polymer chains follows a Gaussian function, the nonzero $\chi^{(3)}$ tensor components can be expressed as equ. 5.4.5[2]

$$\chi^{(3)}_{xxxx} = \frac{N}{C}\gamma^{*}_{yyyy}\int_{0}^{\pi} d\theta \sin\theta \cos^{4}\theta \exp\left[-\left\{\frac{\theta}{\theta_0}\right\}^{2}\right] \qquad (5.4.5\ a)$$

$$\chi^{(3)}_{yyyy} = \frac{3N}{8C}\gamma^{*}_{yyyy}\int_{0}^{\pi} d\theta \sin^{5}\theta \exp\left[-\left\{\frac{\theta}{\theta_0}\right\}^{2}\right] \qquad (5.4.5\ b)$$

$$\chi^{(3)}_{off} = \frac{N}{2C}\gamma^{*}_{yyyy}\int_{0}^{\pi} d\theta \sin^{3}\theta \cos^{2}\theta \exp\left[-\left\{\frac{\theta}{\theta_0}\right\}^{2}\right] \qquad (5.4.5\ c)$$

where θ is the angle of the individual polymer chain with respect to the dipping direction and the parameter θ_0 indicated statistically the orientational degree of the polymer chains and is related to the standard deviation as $\sigma = \theta_0/\sqrt{2}$. C is a normalization constant, and $N\gamma^{*}_{yyyy}$ determines the packing density of the molecules.

For two extreme cases

(a) Polymer chains perfectly aligned, then

$$\chi^{(3)}_{eff} = N\gamma^{*}_{yyyy}\cos^{4}\Phi. \quad \text{and}$$

(b) Polymer chain randomly oriented, then

$$\chi^{(3)}_{eff} = \frac{1}{5}N\gamma^{*}_{yyyy} \qquad \text{can be derived}^{2}.$$

From our results it appears that some amount of distortion may have occurred between the adjacent chains, thus resulting in the low dichroic ratio observed in Fig. 5.4.2. Larger $\chi^{(3)}_{eff}$ ratio can be obtained if the chains are perfectly aligned. The $\chi^{(3)}$ value with the polarization parallel ($\Phi = 0$) to the chain alignment of the thiophene LB films was found to be approximately one order of magnitude larger than that of the similarly randomly oriented electrochemically prepared thiophene polymer films (PT). Although the $\chi^{(3)}$ value obtained when the polarization is perpendicular ($\Phi = 90$) to the chain alignment was 4 times smaller than when its parallel, its value was at least twice larger than the reference sample (PT). It is therefore clear from our results that the enhancement of the third order nonlinear coefficient is largely due to the packing density of the polymer molecules. The anisotropic behavior can also be explained from the orientational distribution of the polymer chains. Studies have shown

that by increasing the surface pressure during fabrication (ie. increasing the packing density ($N\gamma^*_{yyyy}$)), the third order nonlinear coefficient increases dramatically[2].

5.5 CONCLUSION

The orientational distribution and density of polymer chains packed anisotropically in thin films is investigated using degenerate four wave mixing technique. We obtained a large $\chi^{(3)}$ (~10^{-8} esu) value with subpicosecond response for a Langmuir Blodgett film of PTHT. Significant values of the orientational anisotropy in $\chi^{(3)}$ values is determined. The largest $\chi^{(3)}$ value however was obtained in the draw direction along which the polymeric chains are oriented. The fourth rank tensor property of $\chi^{(3)}$ was used to extract all the tensor component relative to the $\chi^{(3)}$ value in the coordinate of the laboratory. The anisotropy of the DFWM for PTHT demonstrates that the nonlinearity is entirely associated with the nonlinear polarizability of the π-electrons in the conjugated polymer backbone. The magnitude and anisotropy were directly compared with results obtained from electrochemical prepared polythiophene measured in the same apparatus. Upon heating to 50^0C the orientation order is lost because of thermal motion of the polymer.

References

1. V. K. Agarwal, Physics Today, pg. 40, June 1988

2. L. Wang, T. Wada, T. Yuba, M. Kakimoto, Y. Imai, and H. Sasabe, J.Appl. Phys. 79 (12) 9321 1996

3. R. Dorsinville, L. Yang, R.R. Alfano, R. Zamboni, R. Danieli, G. Ruani, and C. Taliani, Opt. Lett. 14, 1321, 1989

4. T. Kobayashi, M. Yoshizawa, U. Stamm, M. Taiji, M. Hasegawa J. Opt. Soc. Am. B 7, 1558 (1990)

5. R. Priestly, A.D. Walser, R. Dorsinville, W.K. Zou, D.Y. Xu, and N.L. Yang Optics Comm. 131, 347 (1996)

6. A. Bolognesi, G. Bajo, Z. Geng, W. Porzio, and F.S. Speroni, Thin Solid Films 243 (1994) 683

7. T.C. Chung, J. H. Kaufman, A. J. Heeger, and F. Wudl, "Charge storage in doped polythiophene: optical and electrochemical studies," Phys. Rev. B 30, 702-710 (1984).

8. A. Bolognesi, G. Bajo, and D. Villa, LB7 Conference, Numana (Ancona) Italy, September 10-15 1995,p 46 Abstract Book

9. A.T. Royappa, M.F. Rubner, and Langmuir. 8 (1992) 3168; C.L. Callender, C. A. Carere, G. Daoust, and M. Leclerc, Thin Solid Films 204 (1991) 451

10. A. Bolognesi, F. Bertini, G. Bajo, A. Provasoli, D. Villa, and O. Ahumada to be published in Thin Solid Films

11. A. Wu, T. Akagi, M. Jikei, M. Kakimoto, Y. Imai in Thin Solid Films as proceeding of LB7 Conference, Numana (Ancona) Italy, September 10-15 1995

12. R. Dorsinville, L. Yang, R.R. Alfano, R. Zamboni, R. Danieli, G. Ruani, and C. Taliani Opt. Lett. 14, 1321, 1989

Chapter 6

Nonlinear Optical Analysis of a Series of Oligothiophenes: Length Dependence of the Third-Order Nonlinear Susceptibility in Conjugated Organic Molecules

6.1 INTRODUCTION

Systemic studies of the influence of the chain length and nature of the conjugated unit underlying the optimization of the third-order nonlinear optical susceptibility of polyenes have been demonstrated[1] and measured[2]. It has been observed in linear conjugated molecules that the third-order polarizability γ increases dramatically with the molecular dimension, a property attributed to the highly delocalized π electrons along the chain direction[2]. Earlier work on the third-order susceptibility $\chi^{(3)}$ in polydiacetylene polymer crystal shows that under certain conditions, $\chi^{(3)}$ may take values which exceed those generally obtained in inorganic semiconductors[3]. This was largely due to the one dimensionality of the π-electron system. However, studies on oligothiophenes have shown that about 6-7 monomer repeated units resulted in the same nonlinear properties as those obtained with their corresponding high molecular weight. These features can be

related to a saturation of the effective conjugation length[4].

In this chapter we report on the characterization of the third-order nonlinear optical susceptibility of new polyesters derived from oligothiophene . and compared our experimental data with theoretical calculations of relatively long conjugated systems and infinite one dimensional semiconductor models.

A single-beam Z-scan technique was used at 800-nm with femtosecond pulses. The different polymers studied in this chapter consists of polyester with two (bithiophene), three (terthiophene), four (quaterthiophene) and five (pentathiophene) thiophene units: *4,4'-Didecyl-2,2'-bithiophene-5,5'-dicarbonly dichloride* (**P B C 1 0**), *3,4'-dihexyl2,2':5',2''-terthiophene-5,5''-dicarbonly dichloride* (**PTC10**), *3',4''-didecyl-2,2';5',2'';5''2'''-quaterthiophene-5,5'''-dicarbonly dichloride* (**PQC10**) and *3'',4''-dihexyl-2,2';5',2'';5'',2''';5'''2''''-pentathiophene -5,5''''-dicarbonly dichloride* (**PPC10**) respectively. The samples used here were a solution in the solvent chloroform ($CHCl_3$).

6.2 SAMPLE

The molecular structures for PBC10, PTC10, PQC10 and PPC10 are shown in Fig. 6.2.1. The conjugation backbone of the polymer is stabilized by a sulfur atom and a flexible spacer $HO-(CH_2)_{10}-OH$ is used after each different set of conjugation length. The oligothiophenes were synthesized through chemical polymerization between oligothiophene-dicarbonyl dichlorides and various aliphatic diols. The synthesis as well the preparation of the oligothiophenes is described by Anne Donat-Bouillud et al. in Ref. 4. All four polyesters exhibited a difference in optical and electrical properties[4].

The single photon absorption and photoluminescence spectra recorded on a Perkin-Elmer λ19 UV-Vis spectrophotometer and Spex Fluorolog-2 spectrometer respectively, using a 1-mm quartz cells from polymer solutions (1×10^{-3} M) in chloroform are shown in Fig 6.2.2. Despite the different electronic structures the overall spectral features of the four polymers are very similar to each other. The absorption, emission maxima, optical band-gap and quantum yield are reported in table 6.2.1.

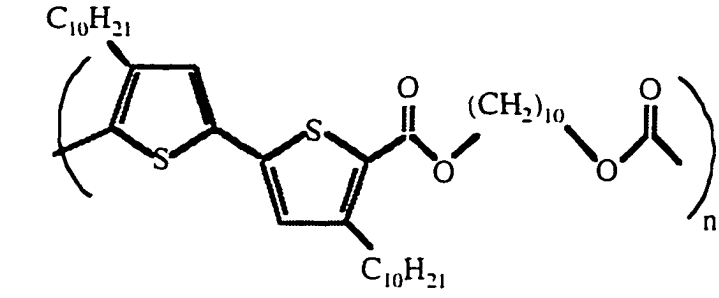

PBC10

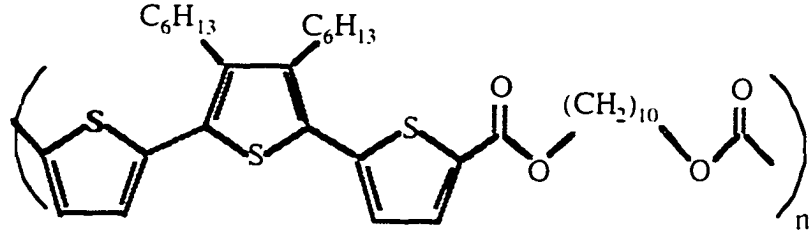

PTC10

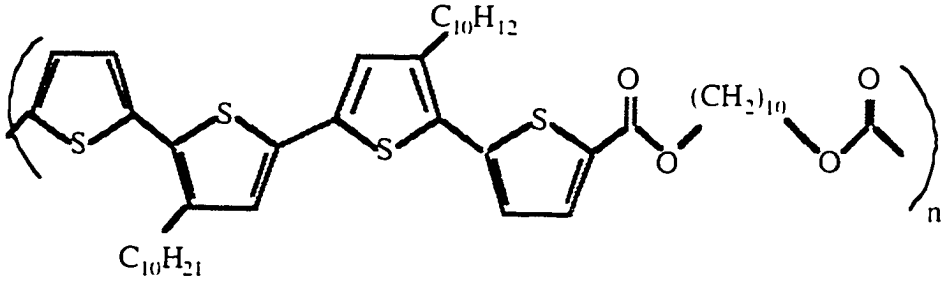

PQC10

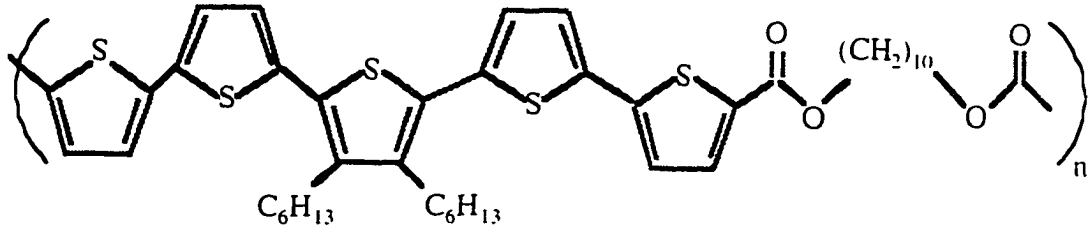

PPC1C

Fig. 6.2.1 Molecular structure of PBC10, PTC10, PQC10, PPC10

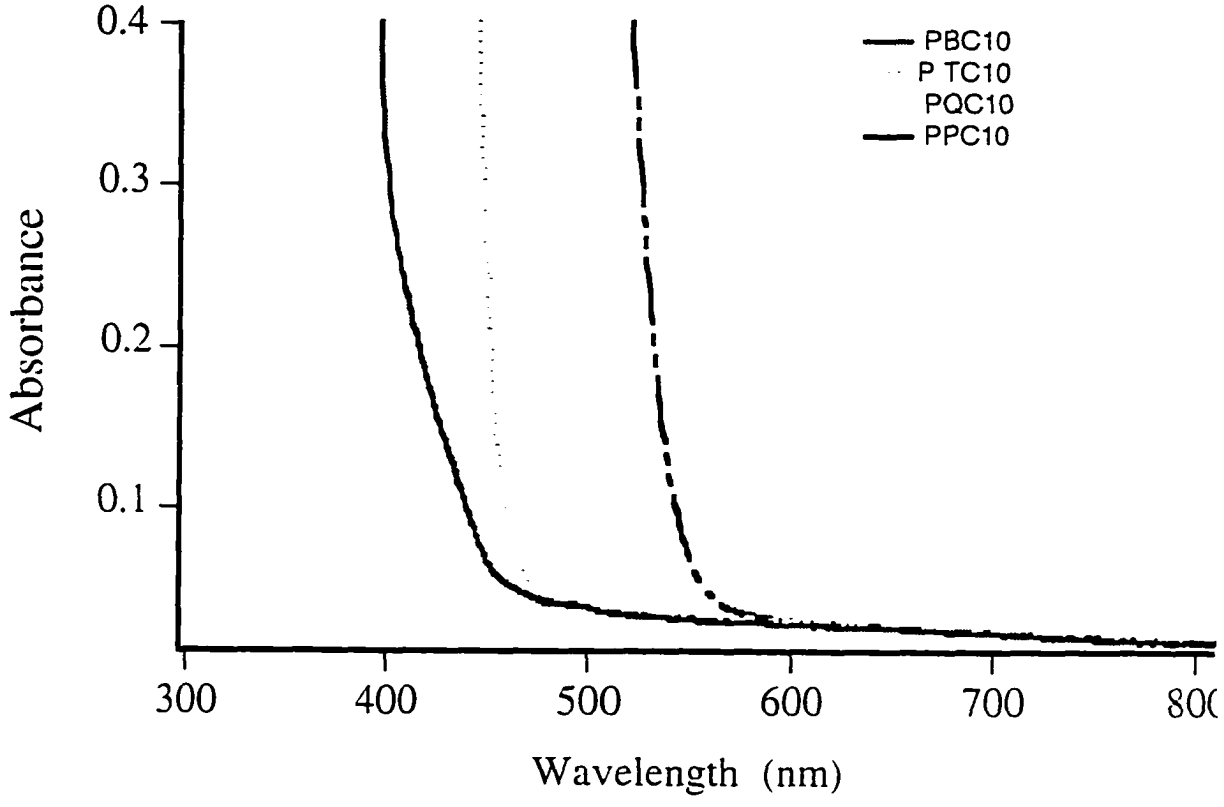

Fig. 6.2.2 Absorption spectra of PBC10, PTC10, PQC10, and PPC10.

Figure 6.2.2 shows that at 800-nm the oligothiophenes are transparent with an absorbance at less than 0.05. A red shift with increasing number of thiophene repeated units is observed, this is as a result of the average increase in the π-electron conjugation. Longer conjugation give rise to lower energy absorption.

Table 6.2.1. Photophysical properties of PBC10, PTC10, PQC10, and PPC10

Polymer	Absorption Maximum (eV)/(nm)	Fluorescence Maximum (eV)/(nm)	Optical bandgap (eV)/(nm)	Quantum Yield
PBC10	3.63 (342)	3.02 (411)	2.64 (470)	0.07
PTC10	3.28 (378)	2.60 (478)	2.60 (480)	0.07
PQC10	3.03 (410)	2.36 (525)	2.41 (515)	0.11
PPC10	2.90 (428)	2.23 (557)	2.20 (565)	0.10

6.3 EXPERIMENTAL SET-UP

The single beam Z-scan technique based on the principle of spatial beam distortion was introduced and discussed in Chapter 2. In this method a single

Gaussian beam is tightly focused into the sample. The transmission through an aperture placed some distance from the focal plane of the lens is monitored as the sample is scanned along the optic axis. The sign and magnitude can be determined from these measurements. Nonlinear materials possessing negative n_2 will display a valley followed by a peak in the transmittance curves. Likewise, positive n_2 will result in a peak - valley sequence as the sample is translated from -z side to +z side, thus making the sign of the nonlinearity easy to determine. Also the size of n_2 can be determined from the difference in peak to valley in transmittance.

A Mode-Locked Titanium-doped sapphire (Ti:Sapphire) laser pumped by a continuous wave (cw) diode-pumped, neodymium yttrium vanadate ($Nd:YVO_4$) laser provided laser pulses with 80 femtosecond duration at 800 nm and 80 MHz repetition rate. The laser beam was tightly focused to a spot size ω_0 of ~100-μm. The 2 mm diameter aperture (far field) was placed from the focus point of the lens a distance of 4 times the focal length . The transmitted beam through the far field aperture was detected and recorded by a Lockin amplifier and Unidex stepping motor with the aid of a Labview program. Both the oligothiophene solutions and the reference, carbon disulfide (CS_2), was contained in a 2 mm quartz cell.

6.4 RESULTS

A close aperture z-scan was performed on CS_2 and Chloroform ($CHCl_3$) at $I_0 = 6.25\ GW/cm^2$. The normalized z-scan through the far field aperture as a function of z from CS_2 and $CHCl_3$ are shown in Fig. 6.4.1. The peak to valley configuration as the sample moves from -z to +z in Fig. 6.4.1 for CS_2 and $CHCl_3$ indicates that both CS_2 and $CHCl_3$ have a positive nonlinearity ($n_2 > 0$) at 800-nm. The samples used in this chapter were a solution in the solvent chloroform ($CHCl_3$). Figure 6.4.2 displays the normalization transmittance from PBC10 at 800-nm. The peak - valley sequence in Fig. 6.4.2 shows a positive nonlinearity at 800-nm. Z-scan transmittances measurements were made for all four polymers at 800-nm and they all displayed a positive nonlinearity. Fig. 6.4.2 only displays the transmittance for PBC10.

In the absence of nonlinear absorption, Sheik-Bahae et al Ref 5. showed that the difference in transmittance between the peak and the valley, $\Delta T_{p\text{-}v}$ in a Z-scan measurement, is related to the on-axis phase change at focus, $\Delta\Phi_0$, through the following equation;

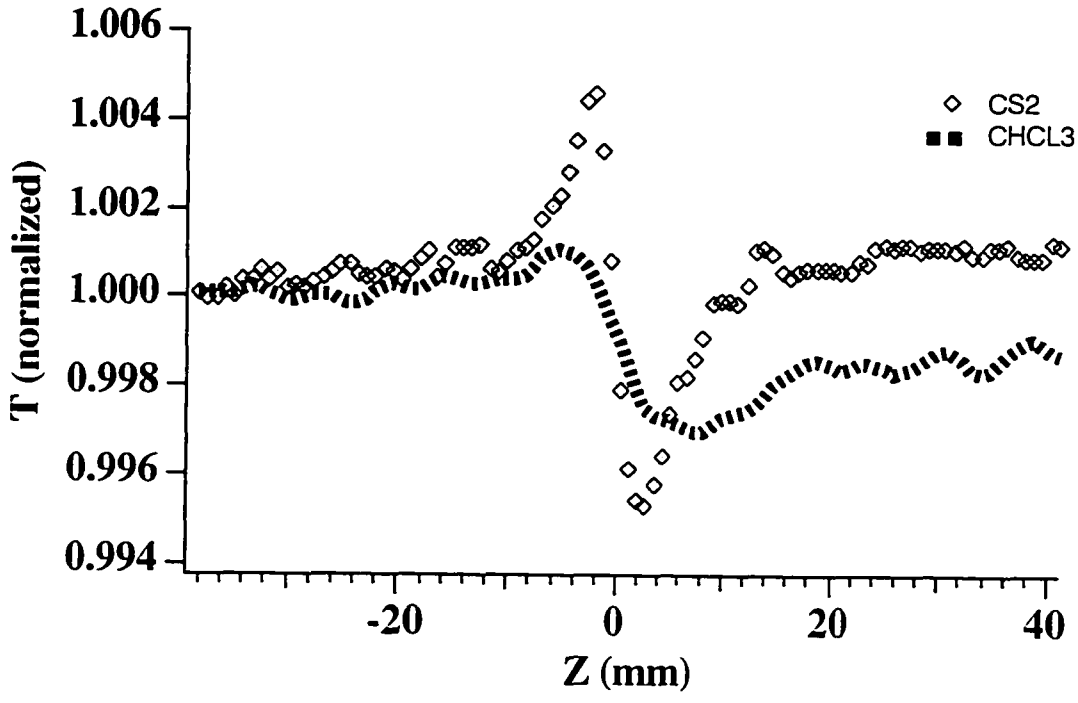

Fig. 6.4.1 Normalized transmittance of Z - scan measurements from $CHCl_3$ and CS_2 at 800-nm.

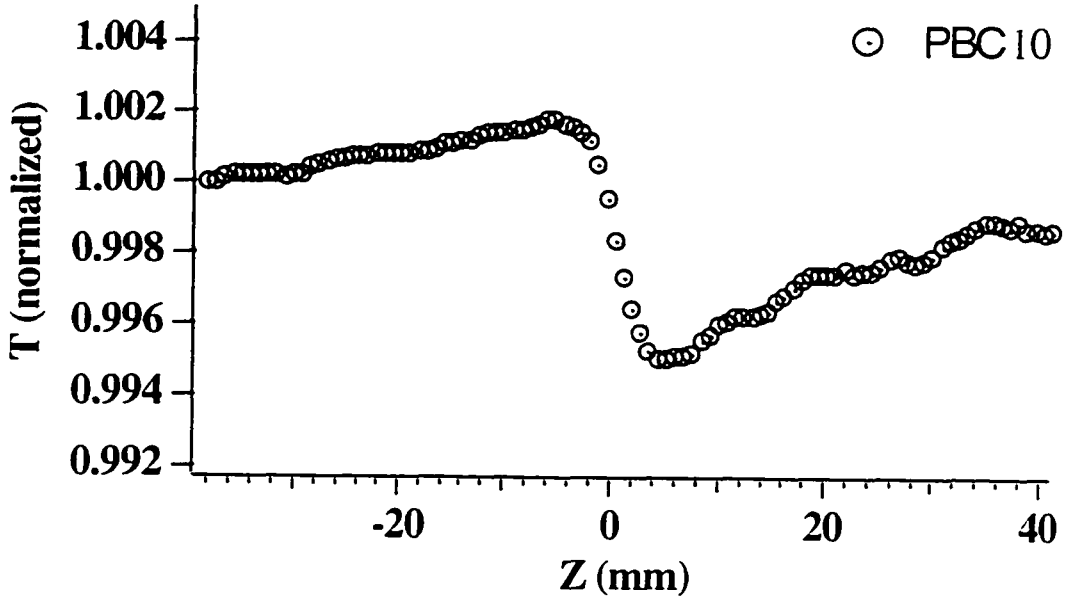

Fig. 6.4.2 Normalized transmittance of Z-scan measurements from PBC10 at 800-nm, with I_0= 6.25 GW/cm^2.

$$\Delta T_{p-v} \approx A\left|\Delta\Phi_0\right| \approx A\left|\frac{\pi n_2}{\lambda}\,|E|^2 L_{eff}\right|, \qquad (6.4.1)$$

where $L_{eff} = \frac{1-e^{-\alpha l}}{\alpha}$ is the effective sample length and A is a constant that may depend on the aperture size.

When CS_2 is used as a reference with the assumption that the measurements for CS_2 have been performed under the same condition as for PBC10, PTC10, PQC10 and PPC10, the $\chi^{(3)}$ value of samples is obtained from:

$$\chi^{(3)}_{PBC10} = \chi^{(3)}_{CS_2}\,\frac{\left(\Delta T_{p-v} n_0\right)_{PBC10}\left(L_{eff} E_{exci}\right)_{CS_2}}{\left(\Delta T_{p-v} n_0\right)_{CS_2}\left(L_{eff} E_{exci}\right)_{PBC10}} \qquad (6.4.2)$$

where L_{eff} for CS_2 and all four samples are equal to the cell length L, since neither absorbed at 800 nm, and E_{exci} is the excitation energy. A Kerr type nonlinear response is well know to be responsible for the positive nonlinearity in

CS_2 with a magnitude of ($\chi^{(3)} = 6.8 \times 10^{-13}$ esu). All the experimental irradiance were maintained at the same value (ie. ~ 6.25 GW/cm^2). Both CS_2 and the samples were studied in a 2 mm quartz cell. The values of the linear indices of refraction for CS_2 and $CHCl_3$ were CS_2 = 1.627 and $n_{CHCl_3} = n_{PBC10} = n_{PTC10} = n_{PQC10} = n_{PPC10}$ = 1.44 respectively.

Using equation (2) and the data obtained from the transmittance curves, the calculated values of $\chi^{(3)}$ for all the samples are listed in Table 6.4.2 along with their concentrations. The $\chi^{(3)}$ values of the samples were obtained after the substraction of the solvent contribution. This was done by calculating the actual $\chi^{(3)}$ value of chloroform and subtracting its values from the values of all four samples.

Table 6.4.2 listed the concentrations and calculated values of $\chi^{(3)}$

Samples	Wavelength (nm)	Concentration (M)	$\chi^{(3)}$ (10^{-13} esu)
PBC10	800	1.01 x 10^{-3}	0.17
PTC10	800	0.965 x 10^{-3}	0.6
PQC10	800	0.95 x 10^{-3}	5.0
PPC10	800	0.96 x 10^{-3}	6.2

Two-photon absorption (TPA) process in all four samples were also investigated by measuring the transmittance without the far field aperture. In this case, the transmittance is only a function of the nonlinear absorption. The normalized transmittance without an aperture is[5],

$$T(z) = \sum_{m=0}^{\infty} \frac{\left| \frac{-\beta I_0 L_{eff}}{1+z^2/z_0^2} \right|}{(m+1)^{3/2}} \qquad (6.4.3)$$

where I_0 is the incident laser intensity at the focus point and β is the TPA coefficient. The open aperture transmittance with I_0 = 6.25 GW/cm^2 at 800-nm was basically flat with little features. This indicated the absence of nonlinear absorption, such as two-photon absorption or saturation. The open aperture result is a strong indication of a small imaginary component (γ^{im}~0).

6.5. DISCUSSION

The values of $\chi^{(3)}$ obtained from the various solution given in Table 6.4.2 with a corresponding density in solution of N_{sol} = 5.05 x 10^{-6}gcm^{-3} and using the density of polythiophene as 1.4 gcm^{-3}, an extrapolation to a solid film can be found from equation (6.5.4).

$$\chi^3_{film} \approx \frac{N}{N_{sol}} \chi^3_{sol} \qquad (6.5.4)$$

where N is the assumed density of the polythiophene solid. The extrapolated values in the solid film were found to be 4 x 10^{-11} esu for PBC10, 1.75 x 10^{-10} esu for PTC10, 1.4 x 10^{-9} esu for PQC10, and 1.8 x 10^{-9} esu for PPC10. These values are in good agreement with the value ~1.0 x 10^{-9} esu, obtained from DFWM measurements in polydithieno(3,2-b:2'3'-d)thiophene at 635-nm[6]. Our results are therefore consistent with previous studies on oligothiophenes that revealed that about 6-7 repeated units are necessary to get similar optical (linear and nonlinear) properties as those obtained with their corresponding high molecular weight[4]. An increase of two orders of magnitude in the nonlinear optical susceptibility is evident when the number of thiophene repeated units is increased from two to five monomer units. Because of saturation of the conjugation length at 6 - 7 repeated units, the largest $\chi^{(3)}$ value can be expected to reach values of ~ 10^{-8} esu. Figure 6.5.3(a) shows a plot of the nonlinear coefficient versus the number of thiophene repeated units. It is obvious from the graph that as the number of repeated units is increase beyond five, the rate of increase of the nonlinear coefficient decreases, thus approaching the limit (6-7) to the number of repeated units for saturation of the conjugation length. Such

saturation is expected for conjugated systems exhibiting a strong intramolecular charge transfer through the π-electron linkage, thus the ability of the double-single bonds to communicate break down because the connecting conjugation pathway are too far away from each other to establish the charge transfer connection.

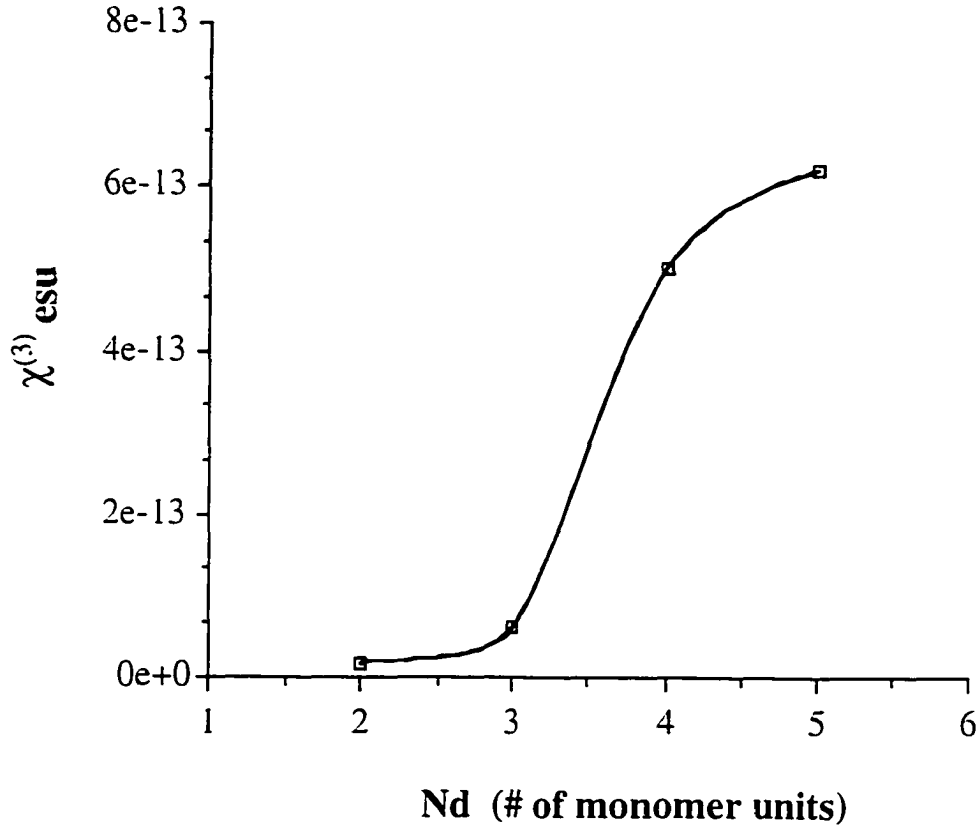

Fig. 6.5.3(a). Third order nonlinear optical coefficient versus delocalization parameter N_d. The squares represents the $\chi^{(3)}$ values from each oligomers, and the solid line is a best fit line.

This tendency has been rationalized in the case of cubic properties of conjugated polymers by the introduction of the electron delocalization length defined as the quadratic mean deviation of the electron position in a one-electron model as derived from the chain bond alternation[7]: extension of the chain length beyond the delocalization length, which is found to be of the order of hundreds of repeat units will not increase the oligomer susceptibility owing to such saturation effects. Further the chains are never infinitely long since they are interrupted by impurities and other defects along the chain.

In one-dimensional system the contribution of increasing the oligomers can be relatively large. The contribution due to the increasing length of the oligothiophene can be estimated by plotting the measured nonlinear optical coefficient as a function of repeated units. Fig. 6.5.3(b) shows a semi-log plot. The nonlinear response is found to be proportional to the fourth power of N_d. { $\chi^{3} \sim (N_d)^4$ }, resulting in a slope of the curve Ln $\chi^{(3)} = f$(Ln N_d) of about 4.2. Our results are within range of the slopes of 2.3, 3.4 and 4.6 observed by Zyss et al[8] on various polyenic derivatives, and the slope of 4.05 reported by P. Prasad in thiophene monomer and oligomers (N = 2 - 6) in THF solutions[9].

Generally, one dimensional (1D) systems are characterized by highly anisotropic optical, dielectric, conducting and mechanical properties. The optical index of refraction and optical nonlinear coefficients having their origin in the

valence electrons are expected to be highly anisotropic and reflect strongly the effect of the electron delocalization.

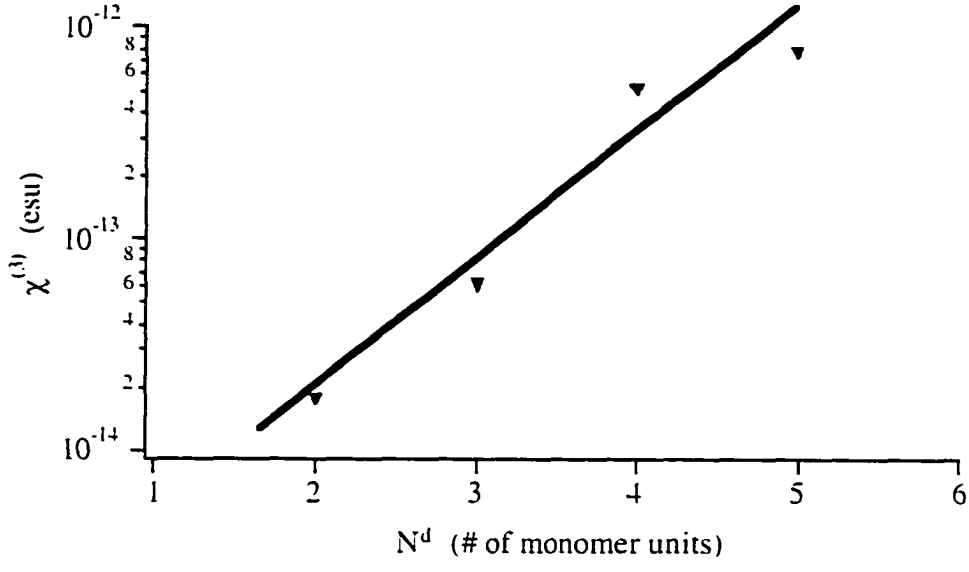

Fig. 6.5 .3 (b) Semi-log plot of $\chi^{(3)}$ versus N_d for PBC10, PTC10, PQC10 and PPC10. The solid line is a theoretical fit for $\chi^{3} \sim (N_d)^4$

A simple model in which the π electrons move in a 1D semiconductor was used in Ref 7 to predict the hyperpolarizabilies of polyenes. This model can be

extended[10]. to describe infinite polymeric chains.

In Ref. 11, the Bloch wave functions, energies and the dipole transition matrix elements obtained within the tight-binding approximation by linear combination of atomic orbitals (Hückel approximation)[12] were used to calculate the nonlinear optical susceptibilities, the expression of the lattice were obtained by the Genkin-Medinis approach[13] [given in Appendix A]. It was found that the behavior of the nonlinear susceptibilities can be expressed in terms of the optical delocalization parameter N_d as,

$$\chi^{(3)}_{xxxx} = \frac{16}{45}\pi^{-1}\,\chi^{(3)}_{0}\;N_d^6 \qquad (6.5.6)$$

where N_d is a measure of the π- electron delocalization length (number of repeated unit over which the π-electrons are delocalized), thus $\chi^{(3)}_{xxxx}$ strongly reflects π- electron delocalization effects. Electron delocalization depends upon orbital overlap between π-orbitals on adjacent atoms. The sixth power dependence of $\chi^{(3)}_{xxxx}$ on N_d is characteristic of 1D systems. This expression is valid in the low-frequency range, away from resonances.

Although our results show a fourth power dependence of $\chi^{(3)}_{xxxx}$ on N_d

which agree with similar finding from Zyss and Huijts, earlier theoretical model from Agrawal et al. within a one-electron theory using the tight-binding approximation shows a sixth power dependency. The discrepancy between the theoretical calculations and our experimental data maybe due to the following general assumptions; theoretical results were derived for the homoatomic bond alternated chains of an organic 1D semiconductor (much simpler system), the delocalization parameter N_d was large N_d ($\gg 1$) even for heteroatomic chains, a highly anisotropic semiconductor material. The oligothiophene studied in this chapter can be assumed as a 1D semiconductor because the valence electrons responsible for these properties are forced to move along linear chains of atoms or molecules with distance which are small enough to allow the formation of energy states more or less delocalized in one direction while a similar delocalization in the other two directions is hindered by a surrounding sea of stable saturated bonds which keeps the chains well apart[14]. However, these oligothiophene are not highly oriented and this will therefore contribute to the discrepancy mentioned. It has been shown that in amorphous structures such as PBC10, PTC10, PQC10 and PPC10 the size of the nonlinearity is reduced by more than one order of magnitude as compared to Langmuir Blodgett (LB) films[15].

6.6 CONCLUSION

From the single z-scan measurements, the third order nonlinearity has been shown to be positive and mostly real at 800-nm for PBC10, PTC10, PQC10 and PPC10, with $\chi^{(3)}$ =1.74 x 10^{-14} esu, 6.0 x 10^{-14} esu, 5.0 x 10^{-13} esu, and 6.2 x 10^{-13} esu respectively. Extrapolated values to a solid film was estimated to be ~10^{-8} esu.

We have shown a strong dependence of the $\chi^{(3)}$ on N_d at 800-nm, $\chi^{(3)} \sim N_d^4$. The discrepancy between our results and the theoretical value of the sixth power is probably due to the samples not highly anisotropic, furthermore the theoretical calculation were made based on the assumption that $N_d \gg 1$.

Our results are in good agreement with the theoretical consideration if these assumptions are taken into consideration.

References

1. J. P. Hermann, D.Richard, and J. Ducuing, Appl. Phys. Lett. 23, 178 (1973)

2. K.C. Rustagi, and J. Ducuing, Opt. Commun. 10. 258 (1974)

3. J. J. Wynne, Phys. Rev. 178.1295 (1969)

4. Anne Donat-Bouillud, Louise Mazerolle, Paul Gagnon, Leonid Goldenberg, Micheal C. Petty, and Mario Leclerc submitted for publication

5. M. Sheik-Bahae, A. A. Said, T. H. Wei. D. J. Hagan, and E. W. Van Stryland, IEEE J. Quantum Electron. 26, 760 (1990)

6. R. Dorsinville, L. Yang, R. R. Alfano, R. Zamboni, R. Danieli, G. Ruani, and C. Taliani, Opt. Letts 23.1321. 1989

7. G.P. Agrawal, C. Cojan, and C. Flytzanis. Phys. Rev. B 17, 776 (1978)

8. J. Zyss, I. Ledoux, J. Nicoud "Molecular Nonlinear Optics" Academic Press 1994

9. J. Messier, F. Kajzar, P. Prasad and D. Uldich "Nonlinear Optical Effects in Organic Polymers. 375-378. 1989 Kluwer Academic Publishers.

10. J. Ducuing, in Nonlinear Spectroscopy, Proceedings of the International School of Physics "Enrico Fermi," Course LXIV, edited by N. Bloembergen (Academic, New York, 1974)

11. C. Cojan, G. P. Agrawal and C. Flytzanis Phys. Rev. B 15. 909 (1977)

12. L. Salem, Molecular orbital theory of conjugated systems (Benjamin. New York, 1966).

13. Y.N. Genkin and P.M. Mednis, Zh. Eksperim. I Teor. Fiz. 54 (1968) 1137 English Transl. Soviet Phys. JETP 27 (1968) 609

14. H.J. Keller, ed., Low-dimensional cooperative phenomena (Plenum Press.

New York, 1974); I.F. Shchegolev, Phys. Stat. Sol. 12A (1972) 9

15. D.Harris, R. Dorsinville, T. Mukai to be published

Chapter 7

Time-resolved Degenerate Four-wave Mixing in Solution of Oligothiophenes

7.1 Introduction

In the previous chapter, the magnitude and sign of the third order nonlinear optical susceptibility $\chi^{(3)}$ of the oligothiophenes were determined by Z-scan measurements. However, their temporal resolutions could not be determined using the z-scan technique. In this chapter, the time response and magnitude of $\chi^{(3)}$ have been determined using degenerate four-wave mixing (DFWM) technique. Comparison between the magnitude of $\chi^{(3)}$ obtained from the z-scan technique and that of the DFWM are made. Information about the sign of the nonlinearity can not be obtained from DFWM since the DFWM is only sensitive to the square of $\chi^{(3)}$.

The molecular structures of these oligothiophenes were shown in the previous chapter. A detailed analysis of the optical structural and electrical analysis of these polymers is reported elsewhere[1].

7.2 Degenerate four-wave mixing experimental results

A forward folded boxcar degenerate transient grating technique was used for the measurements. The details of the experimental set-up are illustrated in chapter II. A homemade intracavity dispersion compensated dye laser pumped by a frequency double Nd:YAG regenerative amplifier beam was used to produce pulse at 635-nm and 1 KHz repetition rate. The 1 psec output pulse duration was then amplified by a three stage dye amplifier producing pulses with energy of 1μJ.

The degenerate four-wave mixing signal as a function of the delay time is measured for the different samples. The following typical setup considered. where at $t = 0$ two short excitation pulses crossed with an angle θ. interfered in the sample and created an excitonic grating. The decay of the grating as a result of the dephasing and population relaxation is monitored by applying a probe pulse at $t = \tau$. The observable $R(\tau)$ is the time integrated intensity of the nonlinear (diffracted) signal as a function of the pump-probe delay τ.

Where $R(t) = \exp(-2\gamma\tau)$, where γ represent the population relaxation rate.

In figure 7.2.1 the time evolution of the degenerate four-wave mixing signal is shown for two of the oligothiophenes dissolved in chloroform. The other two

samples had similar profiles. A time response of ~1.1 psec. of the third order nonlinearity was determined. For PBC10, PTC10, PQC10 and PPC10, the initial DFWM temporal behavior closely matches that of the solvent $CHCl_3$ (< 1.0 psec).

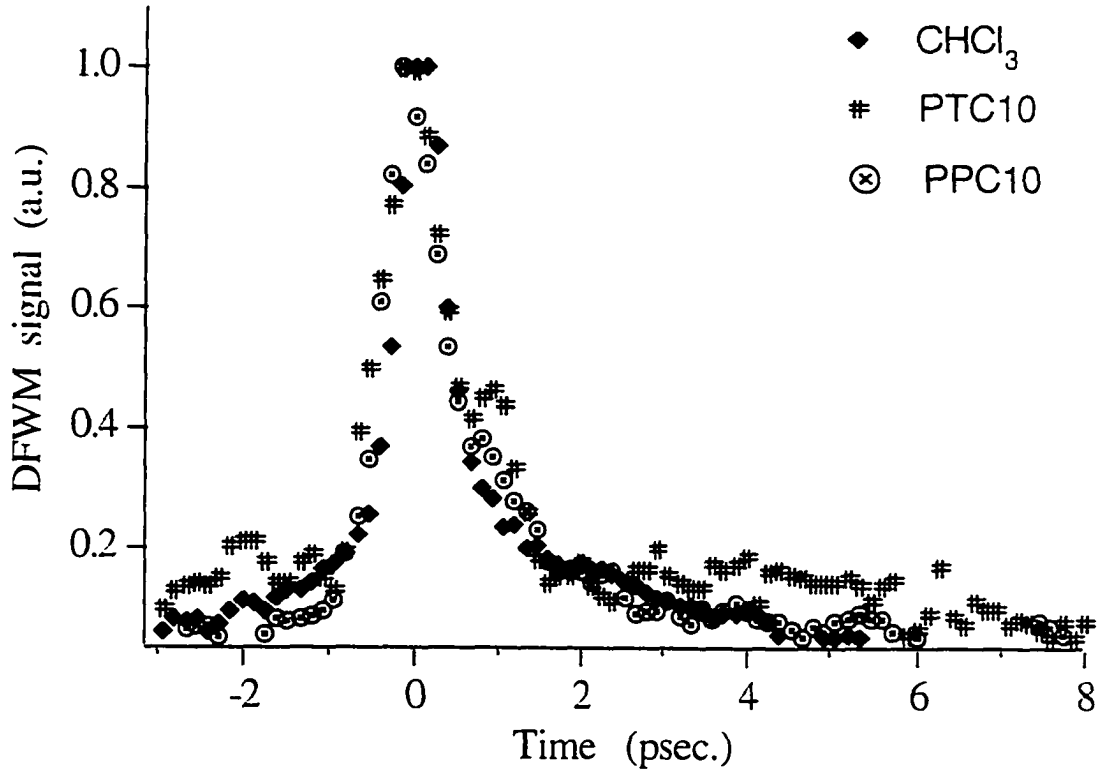

Fig. 7.2.1 The degenerate four-wave mixing signal as a function of delay time for oligothiophenes in a solution of chloroform.

From the measurements of the DFWM signal, the third order nonlinearity in an absorbing medium can be obtained from [2],

$$\chi^3 = A\frac{n^2}{\omega L}\left(\frac{I_s}{I_1 I_2 I_3}\right)^{1/2}\left\{\frac{\alpha L}{(1-\exp(-\alpha L))}\right\}\exp(\alpha L). \qquad (7.2.1)$$

where α is the absorption coefficient of the investigated sample, n is the index of refraction of the sample, I_s is the four-wave mixing signal intensity. I_1, I_2, and I_3 are the intensities of the three interacting beams, and A is a constant that depends on the pulse duration and the geometry of the experiment. Experimentally, a more straight forward approach is applied to determine the $\chi^{(3)}$ value of all four oligothiophenes. The effective $\chi^{(3)}$ value was measured by comparing the strength of the conjugated signal with that of CS_2 and was corrected for the absorption losses according to the following relationship:

$$\frac{\chi_s^{(3)}}{\chi_{cs}^{(3)}} = \left(\frac{n_s}{n_{cs}}\right)^2 \frac{l_s}{l_{cs}} \left(\frac{I_s}{I_{cs}}\right)^{1/2} \frac{\alpha l_s}{\exp(-\alpha l_s/2)\left[1-\exp(-\alpha l_s)\right]} \qquad (7.2.2)$$

The subscripts s and cs refer to the sample and CS_2 respectively. The CS_2 is non-absorbing at the wavelength used in our experiment. We took $\chi^{(3)} = 6.8 \times 10\text{-}13$ esu as the reference value for CS_2 [3] and index of refraction n to be 1.9.

The measured effective $\chi^{(3)}$ values for PBC10, PTC10, PQC10 and PPC10 are $1 \times 10^{-13} \pm 0.5$ esu, $1.8 \times 10^{-13} \pm 0.5$ esu, $3 \times 10^{-13} \pm 0.5$ esu and $5 \times 10^{-13} \pm 0.5$ esu, respectively at 635 nm wavelength. By extrapolating these values to that of a solid film, we were able to obtain values ranging from $\sim 3.0 \times 10^{-10}$ esu to $\sim 1.6 \times 10^{-9}$ esu. These values can be compared with $\sim 4 \times 10^{-9}$ esu reported by Prasad et al. [4], for polythiophene at 602 nm, and $\sim 4 \times 10^{-11}$ esu determined by Singh et al.[5] with poly(3-dodecylthiophene) at 705 nm. For all these measurements, the interacting beams are polarized parallel with respect to each other. Under these conditions the observed four-wave mixing signal was generated by the $\chi^{(3)}_{yyyy}$ component of the optical nonlinear susceptibility.

The values for $\chi^{(3)}$ as a function of N_d (delocalization parameter: number of repeated units over which the π-electrons are delocalized) for DFWM is given in Table 7.2.1. Table 7.2.1 compares the results of our DFWM experimental studies with previous z-scan data. The illustrated calculated values of $\chi^{(3)}$ for

PQC10 and PPC10 are shown to agrees quite well, but that of PBC10 and PTC10 do not agree as well. The discrepancy observed in bithiophene and terthiophene are probably due to the computational complexity arising from the contribution of the solvent to that of the solution. The computation was made even more difficult with the instability of the laser source, thus reducing the signal to noise ratio.

Table 7.2.1 Nonlinear Coefficient $\chi^{(3)}$ versus delocalization length.

Polymer	Thiophene repeated units	DFWM $\chi^{(3)}$ (x 10^{-13} esu.)	Z-scan $\chi^{(3)}$ (x 10^{-13} esu.)
PBC10	2	1	0.2
PTC10	3	1.8	0.6
PQC10	4	3	5
PPC10	5	5	6

A third order nonlinear refractive index (n_2) can be obtained from equation 7.2.3, which relates n_2 in units of cm^2/W with that of $\chi^{(3)}$ (esu);

$$n_2 = \frac{0.0395}{n_0^2} \chi^3_{solution} \qquad (7.2.3)$$

Using the value of $\chi^{(3)}$ for PPC10 solution, we calculated n_2 to be of the order of 10^{-14} cm^2/W, assuming a linear index of refraction value (n_0) of 1.45. With the excitation intensity of about 5 GW/cm^2 at the sample, $\Delta n = 5 \times 10^{-5}$. Equ. 7.2.4 is used to calculated the Stegeman[6] optical figure of merit,W, for optical devices.

$$W = \frac{\Delta n}{\alpha \lambda} \qquad (7.2.4)$$

The low absorption coefficient ($\alpha = 10^2$ cm^{-1}) for these materials lead to an optical figure of merit of $\sim 10^{-2}$ at 635-nm. Material requirements of figure of

merit for optical devices is on the order of 10^5. Thus making this values about six order of magnitude less than that needed for optical device[7].

7.3 Conclusion

Using DFWM technique, we have measured the magnitude and response time of the third order optical nonlinear coefficient in four thiophene based polymers and compared their magnitude with those obtained from z-scan measurements. A time response of less 1 psec was observed in all four polymers. A increase in $\chi^{(3)}$ was observed with increasing delocalization length, which indicates that the nonlinearity is entirely associated with the nonlinear polarizability of the π - electrons in the conjugated polymer backbone.

References

1. Anne Donat-Bouillud, Louise Mazerolle, Paul Gagnon, Leonid Goldenberg, Micheal C. Petty, and Mario Leclerc submitted for publication

2. G. M. Carter, M. K. Thakur, Y. J. Chen, and J. V. Hryniewicz, Appl. Phys. Lett. 47, 457 (1985)

3. N. P. Xuan, J. L. Ferrier, J. Gazengel, and G. Rivoire, Opt. Commun. 51, 433, (1984)

4. P.N. Prasad, J. Swiatkiewicz, and J. Pfleger, Mol. Cryst. Liq. Cryst. 160, 53, (1988)

5. B. P. Singh, M. Samoc, H. S. Nalwa, P. Prasad J. Chem. Phys., Vol. 92, No. 5 (1990)

6. G. I. Stegeman, R.H. Stolen, J. Opt. Soc. Am. B 6 (1989) 652

7. J. Messier, F. Kajzar, P. Prasad and D. Uldich "Nonlinear Optical Effects in Organic Polymers, 375-378, 1989 Kluwer Academic Publishers.

Chapter 8

Summary and Future Directions

8.1 Summary

In summary, this thesis contributes to the knowledge of nonlinear optical response in conjugated π-electron systems for the development of photonic device applications. The π-electron conjugated systems studied were thiophene based compound. We have shown that the decay kinetic of thiophene based polymers are intensity dependent. The fast decay component is dominated by exciton - exciton annihilation at high intensity and the slower component is controlled by exciton-phonon interactions. The relaxation process starts from free excitons to self-trapped excitons then polarons and/or bipolarons. Estimations of the time-independent bimolecular rate coefficients, diffusion coefficient and hopping time were made.

Large $\chi^{(3)}$ ($\sim 10^{-7}$ esu) value with subpicosecond response for Langmuir Blodgett film of PTHT was investigated using DFWM technique. The largest $\chi^{(3)}$ value was obtained in the drawn direction. The fourth rank tensor property of $\chi^{(3)}$ was used to extract all the tensor component relative to the $\chi^{(3)}$ value in the coordinate of the laboratory.

The magnitude and response time of the third order optical nonlinear

coefficient in PBC10, PTC10, PQC10 and PPC10 have been determined using DFWM and Z-scan techniques. The third order nonlinearity has been shown to be positive and real at 800 nm for all four polymers, with $\chi^{(3)}$ = 1.74 x 10^{-14} esu for PBC10, 6.0 x 10^{-14} esu for PTC10, 5.0 x 10^{-13} esu for PQC10, and 6.2 x 10^{-13} esu for PPC10. A strong dependence of $\chi^{(3)}$ on the delocalization length was observed. Extrapolated values to a solid film was estimated to be ~ 10^{-18} esu.

8.2 Future Directions

One of the goals of the current third order polymer research is to design multi-functional polymers having unique combinations of semiconductor, NLO and structural properties. Considerable improvement to the understanding of structure - property relationship is needed to project structural requirements for enhanced third-order optical nonlinearity. The experiment proposed below describes how enhanced third-order nonlinear optical responses can be achieved.

8.2.1 Enhancement of the third-order nonlinear susceptibility in thiophene based block conjugated copolymers.

Our studies on thin films of thiophene based block conjugated copolymers (T_6B_2

and T_8B_2) showed no significant changes in the third-order nonlinear optical susceptibility when investigated using degenerate four-wave mixing technique. Thin films T_6B_2 and T_8B_2 with multiple quantum well (MQW) structure (Fig. 8.1) were obtained by spin coating unto glass substrates. The band gap of the thyenilenic chains and the benzenic chains are 2.0 eV and 3.1 eV respectively. Each triblock copolymer chain thus contains a single quantum well with a potential barrier of $\Delta E_g = E_g^A - E_g^B = 1.1$ eV. Because of their linear chain structures and the dominant role of electronic delocalization along the chain on their electronic and optical properties, π-conjugated or semiconducting polymers have generally been thought to be quasi one dimensional (1-D) materials[1]. However, they are best regarded as three dimensional (3-D) bulk materials due to chain aggregation and strong interchain interactions[2,3].

We believe the reason our experiment was not successful to enhance the third-order nonlinear susceptibility $\chi^{(3)}$, had to do with the fact that the films were not quantum confined heterostructures. This effect is in part due to interchain interactions and chain aggregation[4]. It is worth noting that the theoretical calulations which predict quantum confinement effects in heterostructured semiconducting polymers have been made on isolated single polymer chains[5,6].

We proposed that by repeating the experiment with block copolymer films prepared using the Langmuir Blodgett technique, where the separation between chains are controlled and interchain interaction and chain aggregation are not factors then large enhancement is expected. We expect that the LB films will have strong 2-D lateral confinment and no confinement along the chain.

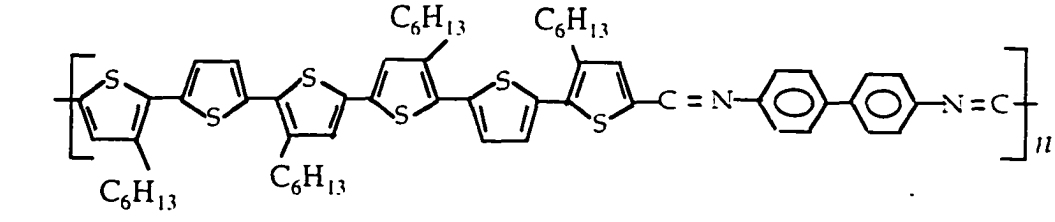

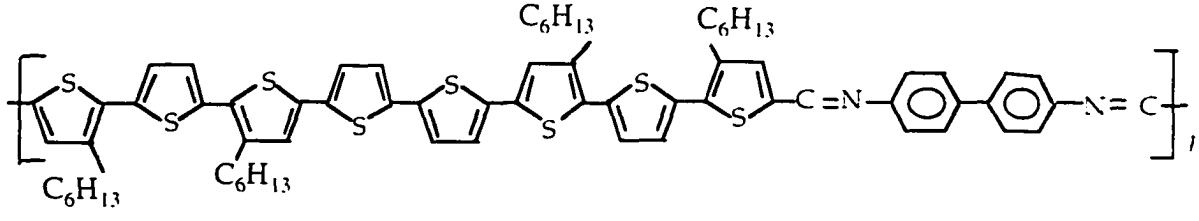

Fig.8.1 Molecular structure of (a) T_6B_2 and (b) T_8B_2, T stands for thyenilenic rings, and B stands for benzenic rings.

References

1. Conjugated Polymeric Materials: Opportunities in Electronics, Optoelectronics, and Molecular Electronics, edited by J.L. Brédas and R.R. Chance (Kluwer Academic Publishers, Dordrecht, The Netherlands, 1990).

2. J. A. Jenekhe and J. A. Osaheni, Science 265, 765 (1994)

3. D.A.B. Miller, J.S. Weiner, and D.S. Chemla, IEEE J. Quantum Electron. QE-22, 1816 (1986).

4. X. L. Chen and S.A. Jenekhe Appl. Phys. Lett. Submitted.

5. R. Ruckh, E. Sigmund, C. Kollmar, and H. Sixl, J. Chem. Phys. 85, 2797 (1986).

6. M. Seel, C. M. Liegener, W. Forner, and J. Ladik, Phys. Rev. B 37.956 (1988).

Appendix

The Genkin-Mednis Approach

In this approach the solution of the Schrödinger equation

$$i\hbar\frac{d\psi}{dt} = H\psi \tag{A1}$$

with $H = (1/2m)[\vec{p}+(e/c)\vec{A}(t)]^2 + V(\vec{r})$

is $\psi = \sum_{n\vec{k}} \psi_{n\vec{k}} c_n(\vec{k}t)$ (A2)

where,

$\vec{k} = \vec{k} + (e/\hbar c)\vec{A}(t)$ and $\psi_{n\vec{k}} = e^{i\vec{k}\cdot\vec{r}} u_{n\vec{k}}(\vec{r})$ are the Bloch states of the unperturbed Hamiltonian $H_0 = p^2/2m + V(r)$ and $\vec{A}$ is the vector potential.

Substituting (A2) into (A1) and taking into account that the $\psi_{n\vec{k}}$ constitute an orthonormal basis, one obtain

$$i\hbar\frac{dc_n(\vec{k}t)}{dt} = \sum_{n'} [\varepsilon_n(\vec{k})\delta_{nn'} + ie\,\vec{\Omega}_{nn'}(\vec{k})\,\vec{E}(t)]c_{n'}(\vec{k}t) \tag{A3}$$

where $E(t) = (1/c)(dA(t)/dt)$ and $\vec{\Omega}_{nn'}(k)$ is the dipole transition strength

$$\Omega_{nn'} = \int_{uc} u^{*}_{ik}(du_{jk}/dk)dr \qquad (A4)$$

where $u_{jk}(r) = e^{-ikr}\,\psi_j(k)$ is the cell-periodic part of the bloch function and the (A2), and has been properly normalized. The integration in (A4) is over a basic unit of length a, (uc) unit-cell [1].

Equation (A3) can also be written in the matrix form

$$i\hbar\frac{dc(\vec{k}t)}{dt} = [H_0(\vec{k}) + H(\vec{k}t)]c(\vec{k}t) \qquad (A5)$$

The solution of (A5) in powers of $\vec{E}$ is obtained by carrying out a unitary transformation $S(\vec{k}t)$ on the c's

$$c_n(\vec{k}t) = \sum_{n'} S_{nn'}(kt)\,\bar{c}_{n'}(\vec{k}t)$$

such that

$$H'(\mathbf{k}t) = S^{\dagger}(\vec{\mathbf{k}}t)\,[H_0(\vec{\mathbf{k}}) + H(\vec{\mathbf{k}}t)]S(\vec{\mathbf{k}}t) + ieS^{\dagger}(\vec{\mathbf{k}}t)\,\vec{\nabla}_{\vec{\mathbf{k}}}\,S(\vec{\mathbf{k}}t)\,\vec{E}(t) - i\,\bar{h}\,S^{\dagger}(\vec{\mathbf{k}}t)\frac{dS(\vec{\mathbf{k}}t)}{dt} \tag{A6}$$

has only diagonal terms, or

$$H'_{nn'}(\bar{\mathbf{k}}t) = 0 \text{ for } n \neq n';$$

one obtains

$$i\hbar\frac{d\bar{c}_n(\vec{\mathbf{k}}t)}{dt} = H'_{nn'}(\vec{\mathbf{k}}t)\,\bar{c}_n(\vec{\mathbf{k}}t) \tag{A7}$$

The perturbation solution of (A7) is obtained by putting

$$S(\bar{\mathbf{k}}t) = 1 + \sum_n S^{(n)}(\bar{\mathbf{k}}t) \tag{A8}$$

in (A6) where $S^{(n)}$ is of order n in the field intensity. This only determines the nondiagonal elements of S; the diagonal ones are determined by the additional conditional $S_{nn} = S^{\dagger}{}_{nn}$.

The polarization is then determined by

$$\vec{P}=e\sum_{el}\langle\vec{r}\rangle=-\frac{ie}{V}\sum_{n,n',n''}\sum_{\vec{k}}f_n(\vec{k})\,S^{T}_{nn'}(\vec{k}t)[\vec{\Omega}_{n'n''}(\vec{k}) + \delta_{n'n''}\,\overline{\nabla}_{\vec{k}}]S_{n''n}(\vec{k}t) \tag{A9}$$

where $f_n(\vec{k})$ is the distribution function over the band states. By inserting (A8) in (A9) one obtains the polarization in powers of the electric field.

$$\vec{P}=\vec{P}^{(0)}+\sum_{n=1}^{\infty}\vec{P}^{(n)} \tag{A10}$$

and hence the expressions of the susceptibilities.

The expressions for the linear and second-order susceptibilites is defined in Ref 2. The expression of the third-order susceptibility is quite involved for a system with an arbitrary number of bands and different frequencies. In the present work we are mainly interested in the nonlinear optical properties of one-dimensional semi-conductors with an effectively two-band structure. Neglecting the frequency dispersion of $\chi^{(3)}_{xxxx}$

$$\chi^{(3)}_{xxxx}=\frac{8e^4}{Vh^3}\int_{B.Z}\frac{1}{\omega_{cv}}\frac{dS_{cv}}{dk}\frac{dS_{vc}}{dk}-\Omega_{vc}S_{cv}S_{vc}S_{cv}\;dk \tag{A11}$$

where $\hbar\omega_{cv} = \varepsilon_c - \varepsilon_v$, Ω_{vc} is the transition dipole moment matrix element between the highest valence (v) and the lowest conduction (c) bands, $S_{vc} = \Omega_{vc} / \omega_{vc}$, and ε_v and ε_c are the band energies for the v- and c-band, respectively. $V = L/\sigma$ where V is the normalization volume, L = Na is the length of the chain and σ is the density of such chains per unit cross-area. It is also assumed that the system possess an inversion symmetry so that in particular $\chi^{(2)} \approx 0$. As can be seen from (A11), the magnitude and the sign of the nonlinear optical susceptibilities $\chi^{(n)}$ is determined by the competition of two terms an intraband term, the first term in the integral in (A11), that arises from field mixing of Bloch band states within a band, and an interband term, the second term in the integrand in (A11) that arises from mixing of states across the gap with wave vector conservation. It is quite evident that the intraband term will be dominant whenever the band vary strongly with k (wide bands) which willbe the case for very delocalized systems or strong overlap between wave functions of neighboring units in the periodic structure; on the other hand this contribution will be negligeablefor highly localized systems (very narrow bands) and the interband term becomes then dominant. Accordingly the sign of $\chi^{(3)}$ gives a crucial indication of the degree of electron delocalization[3].

The two contributions to $\chi^{(3)}_{xxxx}$ are evaluated in terms of the hypergeometric functions F and

$$\chi^{(3)}_{\text{inter}} = -\chi^{(3)}_0 (1-p)^2 \; F(11/2, 1/2, 1; p) \tag{A12}$$

$$\chi^{(3)}_{\text{intra}} = 9\,\chi^{(3)}_0 p\,(1-p)\,F\,(11/2,\ 3/2,\ 3;\ p) \tag{A13}$$

where $\chi^{(3)}_0 = \gamma_0 / v$ and $\gamma_0 = 2e^4 a^4 / (8\beta_2)^3$ and $p = 4v/(1+v)^2$.

Expanding the resulting expression in terms of the delocalization parameter $N_d = (1 + v)/(1 + v) = 4\Omega_{cv}(\theta = \pi)/a$ and retaining the highest power of N_d it is shown that

$$\chi^{(3)}_{xxxx} = \frac{16}{45}\,\pi^{-1}\,\chi^{(3)}_0 \left| \frac{\beta_2 + \beta_1}{\beta_2 - \beta_1} \right|^6 = \frac{16}{45}\,\pi^{-1}\,\chi^{(3)}_0\,N_d^6. \tag{A14}$$

where the notations $E_g = 2(\beta_2 - \beta_1)$ and $2E_F = 2(\beta_1 + \beta_2)$.

References

1. G. P. Agrawal, and C. Flytzanis Chem. Phys. Letters. 44 (1976) 366

2. C. Cojan, G. P. Agrawal, and C. Flytzanis Phys. Rev. B 15 (1977) 909

3. J. Messier, F. Kajzar, P. Prasad and D. Ulrich "Nonlinear Optical Effects in Organic Polymers" Kluwer Academic Publishers pg. 1-12. 1989.

Bibliography

Agrawal, G.P., C. Cojan, and C. Flytzanis, Phys. Rev. B 17, 776 (1978)

Agrawal, G. P., and C. Flytzanis Chem. Phys. Letters. 44 (1976) 366

Agarwal, V. K., Physics Today, pg. 40, June 1988

Anne Donat-Bouillud, Louise Mazerolle, Paul Gagnon, Leonid Goldenberg, Micheal C. Petty, and Mario Leclerc submitted for publication

Bergman, A., M. Levine, and J. Jortner, Phys. Rev. Lett. 18, 593 (1967).

Bolognesi, A., F. Bertini, G. Bajo, A. Provasoli, D. Villa, and O. Ahumada to be published in Thin Solid Films

Bolognesi, A., G. Bajo, Z. Geng, W. Porzio, and F.S. Speroni, Thin Solid Films 243 (1994) 683

Bolognesi, A., G. Bajo, and D. Villa, LB7 Conference, Numana (Ancona) Italy, September 10-15 1995,p 46 Abstract Book

Boyd, R., " Nonlinear Optics" Academic Press Inc. 1992

Brazovskii, A., and N.N. Kirova, Pis'ma Zh. Eksp. Teor. Fiz. 33, 6 (1981) [JETP Lett. 33, 4 (1981)].

Bredas, J.L., R.R. Chance, and R. Silbey, J. Phys. Mol. Cryst. Liq. Cryst. 77, 319 (1981).

Brédas, J.L., "Conjugated Polymeric Materials: Opportunities in Electronics, Optoelectronics, and Molecular Electronics", edited by and R.R. Chance (Kluwer Academic Publishers, Dordrecht, The Netherlands, 1990).

Carter, G., M. M.K. Tharkur, Y.J. Chen, and J.V. Hrnyniewicz, Appl.Phys. Lett. 47, 457 (1985).

Carter, G.M., J. Opt. Soc. Am. B6, 1018 (1987)

Chandrasekhar, S., Rev. Mod. Phys. 15, 1 (1943).

Chen X. L., and S.A. Jenekhe Appl. Phys. Lett. Submitted.

Chung, T.C., J. H. Kaufman, A. J. Heeger and F. Wudl Phys. Rev. B. 30, 702 (1984).

Cojan, C., G. P. Agrawal, and C. Flytzanis Phys. Rev. B 15 (1977) 909

Dorsinville, R., L. Yang, R. R. Alfano, R. Zamboni, R. Danieli, G. Ruani, and C. Taliani, Optics Letters. 14, 1321 (1989).

Dorsinville, R., L. Yang, and R. R. Alfano, R. Tubino, and S. Destri Sol. State Com. vol. 68, 875, (1988)

Ducuing, J., in Nonlinear Spectroscopy, Proceedings of the International School of Physics "Enrico Fermi," Course LXIV, edited by N. Bloembergen (Academic, New York, 1974)

Fann, W. S., S. Benson, J. M. J. Madey, S. Etemad, G. L. Baker and F. Kajzar,Phys. Rev. Lett. 62 1492 (1989)

Franken, P. A., A. E. Hill, C.W. Peters, and G. Weinreich, Phys. Rev. Lett. 7, 118 (1961)

Fresser, K., A.R. Bishop, and D.K. Campbell, Phys. Rev. B. 27, 4804 (1983).

Genkin, Y.N., and P.M. Mednis, Zh. Eksperim. I Teor. Fiz. 54 (1968) 1137 English Transl. Soviet Phys. JETP 27 (1968) 609

Gösele, U., Chem. Phys. Lett. 43, 61 (1976); 46, 196(E) (1977).

Harris, D., R. Dorsinville, and T. Mukai Appl. Phys. Lett. 70, 1216 (1997).

Harris, D., E. Royer, R. Dorsinville, NASA Conf. Pub. 3314, Pg. 21, (1995).

Heeger, A.J., Comments Solid State Phys. 10, 53 (1981)

Heeger, A.J., S. Kivelson, J. R. Schrieffer, and W.P. Su, " Solitons in conducting polymers," Rev. Modern Phys. 60, 781 (1988)

Hellwarth, R. W., Prog. Quant. Electron. 5, 1, (1977).

Hermann, J. P., D.Richard, and J. Ducuing, Appl. Phys. Lett. 23. 178 (1973)

Jenekhe, J. A., and J. A. Osaheni, Science 265, 765 (1994)

Jenekhe, S.A., and W. Chen Mat. Res. Soc. Symp. Proc. Vol.173 (1990)

Jenekhe, S.A., W. Chen , S.K. Lo and S.R. Flom, Appl. Phys. Lett.

Jenaekhe, S.A., S.K. Lo, and S.R. Flom, Appl. Phys. Lett.. 54. 2524 (1989)

Kajzar, F., J. Messier, C. Sentein, R. L. Elsenbaumer, and G. G. Miller. Proc. Soc. Photo-Opt. Instrum. Eng. 1147, 36 (1989).

Kaneto. K., S. Hayashi and K. Yoshino, " Kinetics of photoluminescent excitons in polythiphene films during electrochamical doping," J. Phys. Soc. Jpn. 57. 1119-1126 (1988).

Kanner, G. S., X. Wei, B. C. Hess, L. R. Chen, Z. V. Vardeny in press

Keller, H.J., ed., Low-dimensional cooperative phenomena (Plenum Press. New York, 1974); I.F. Shchegolev. Phys. Stat. Sol. 12A (1972) 9

Khyzniak, A., V. Kondilenko, Y. Kucherov, S. Lesnik, S. Odoulov, and M. Soskin J. Opt. Soc. Am. A V. 1, 169 (1984).

Kobayashi, T., S. Nagakura. Mole. Phy. 24 695 (1972).

Kobayashi, T., M. Yoshizawa, U. Stamn, M. Taiji, and M. Hasegawa. J. Opt. Soc. Am. B 7,1558 (1990).

McBranch, D., A . Heys, M. Sinclair, D. Moses, and A.J. Heeger, Phys. Rev. B42, 3011 (1990).

Messier, J., F. Kajzar, P. Prasad and D. Ulrich "Nonlinear Optical Effects in Organic Polymers" Kluwer Academic Publishers pg. 1-12, 1989.

Messier, J., F. Kajzar, P. Prasad and D. Uldich "Nonlinear Optical Effects in Organic Polymers, 375-378, 1989 Kluwer Academic Publishers.

Miller, D.A.B., J.S. Weiner, and D.S. Chemla, IEEE J. Quantum Electron. QE-22, 1816 (1986).

Nakazawa, M., Opt. Lett. 12, 681 (1987)

Neher, D., A. Wolf, M. Leclerc, A. Kaltbeitzel, C. Bubeck. and G. Wegner. Synth. Metals 37, 249 (1990).

Panofsky, W. K. H., and Philips. Classical Electricity and magnetism (Addison-Wesley, Reading, MA,1962).

Pope, M., and C. E. Swenberg, Electronic processes in organic crystals. (Oxford University Press, New York, 1982), p.158.

Powell, R. C., and Z. G. Soos. J. Lumin. 11 1 (1975).

Prasad, P. N., Mat. Res. Soc. Symp. Vol. 109, 271 (1988).

Prasad. P. N., and D. J. Williams, Introduction to Nonlinear Optical Effects in Molecules & Polymers (Wiley. New York. 1991).

Prasad, P.N., J. Swiatkiewicz, and J. Pfleger, Mol. Cryst. Liq. Cryst. 160. 53. (1988)

Priestly, R., A.D. Walser, R. Dorsinville, W.K. Zou. D.Y. Xu. and N.L. Yang Optics Comm. 131. 347 (1996)

Rashba, E. I., "Self-trapping of excitons," in Excitons (selected chapter). E. I. Rashba, and M. D.Struge, eds. (North-Holland, Amsterdam. 1987), pp. 273-332.

Royappa, A.T., M.F. Rubner, and Langmuir, 8 (1992) 3168; C.L. Callender. C. A. Carere, G. Daoust, and M. Leclerc, Thin Solid Films 204 (1991) 451

Ruckh, R., E. Sigmund, C. Kollmar, and H. Sixl, J. Chem. Phys. 85, 2797 (1986).

Rustagi, K.C., and J. Ducuing, Opt. Commun. 10, 258 (1974)

Salem, L., Molecular orbital theory of conjugated systems (Benjamin. New York, 1966).

Samuel, I.D.W., K.E. Meyer, R.H.friend, J. Ruhe, and G. Wegner, Proceedings of ICSM preprint(1990).

Sauteret, C., J. P. Hermann, R. Frey, F. Pradere, J. Ducuing, R.H. Baughman and R. R. Chance. Phys. Rev. Lett. 36, 956 (1976)

Seel, M., C. M. Liegener, W. Forner, and J. Ladik, Phys. Rev. B 37.956 (1988).
Shen,Y. R., The Principles of Nonlinear Optics, (Wiley, New York, 1984).

Shiek, M., A.A. Said, T.H. Wei, D.J. Hagan, and E.W. Styland, IEEE J. Quantum Electron. QE-26, 760 (1990)

Sinclair, M., D. Moses, K.Akagi and A. J. Heeger, Phys. Rev. B 38 10724 (1988).

Singh, B. P., M. Samoc, H. S. Nalwa, P. Prasad J. Chem. Phys., Vol. 92, No. 5 (1990)

Sokolik, I., R. Priestley, A. Walser, R. Dorsinville, Appl. Phys. Lett. Vol. 69, 27 (1996).

Stamm, U., M. Taiji, M.Yoshizawa,T. Kobayashi, and K. Yoshino, Mol. Cryst. Liq.Cryst. 182A, 147 (1990).

Stegeman, G. I., R.H. Stolen, J. Opt. Soc. Am. B 6 (1989) 652

Stepanov, B. I., E. V. Ivakin, and A. S. Rubanov, Sov. Phys. Doklady 16, 46 (1971); R. W. Hellwarth, J. Opt. Soc. Am. 67, 1 (1977)

Swenberg, C. E., and N. E. Geacintov in: Organic molecular photophysics, Vol. 1, ed. J. B. Birks (Wiley-Interscience, London, (1973), p.495.

Sugiyama, T., T. Wada, and H. Sasabe, Synth. Metals 28, 323 (1989).

Sumi, H., M. Georgier, and A. Sumi, Rev. Solid State Science 4, 209 (1990).

Taliani, C., R. Danieli, R. Zamboni, P. Ostoja and W. Porzio, Synth. Meth. 18, 177 (1987).

Vardeny, Z., E. Ehrenfreund, O. Brafman, M. Nowak, H. Schaffer, A.J. Heeter, and F. Wudl "Photogeneration of confined soliton pairs (bipolarons) in polythiophene" Phys. Rev.Lett. 56, 671-674 (1986).

Wang, L., T. Wada, T. Yuba, M. Kakimoto, Y. Imai, and H. Sasabe, J.Appl. Phys. 79 (12) 9321 1996

Weaire, D., B.S. Wherrett, D.A.B. Miller, and S.D. Smith. "Effect of low power nonlinear refraction on laser beam propagation in LnSb", Optics Lett., vol.4, pp. 331-333, (1974).
Worland, R., S. D. Philips, W. C. Walker and A. J. Heeger, Synth.Met. 28. D663 (1989).

Wu, A., T. Akagi, M. Jikei, M. Kakimoto, Y. Imai in Thin Solid Films as proceeding of LB7 Conference, Numana (Ancona) Italy, September 10-15 1995

Wynne, J. J., Phys. Rev. 178,1295 (1969)

Vardeny, Z. V., H.T. Grahn, W.J. Heeger, and F. Wudl, Synth. Metals 28, C299 (1989).

Xuan, N. P., J. L. Ferrier, J. Gazengel, and G. Rivoire, Opt. Commun. 51, 433. (1984)

Yang, L., R. Dorsinville, Q. Z. Wang, P. X. Ye, and R. R. Alfano Opt.Let. V 17, 325 (1992) .

Yang, L., R. Dorsinville, Q. Z. Wang, W. K. Zou, P. P. Ho, N.L. Yang, R. R. Alfano, R. Zamboni, R. Danieli, G. Ruani and C.Taliani, J. Opt. Soc. Am. B 6 753 (1989).

Yariv, A., and P.Yeh, Optical Waves in Crystals (John Wiley & Son, New York. 1984).

Yoshizawa, M., M. Taiji, and T. Kobayashi, IEEE J. Quantum Electron. QE-25 2532 (1989).

Zhoa, M.T., B.P. Singh, and P.N. Prasad, J. Chem. Phys. 89, 5535 (1988)

Zyss, J., I. Ledoux, J. Nicoud "Molecular Nonlinear Optics" Academic Press 1994

IMAGE EVALUATION TEST TARGET (QA-3)

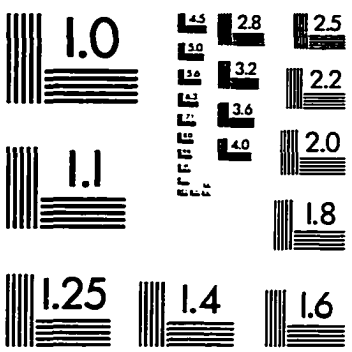

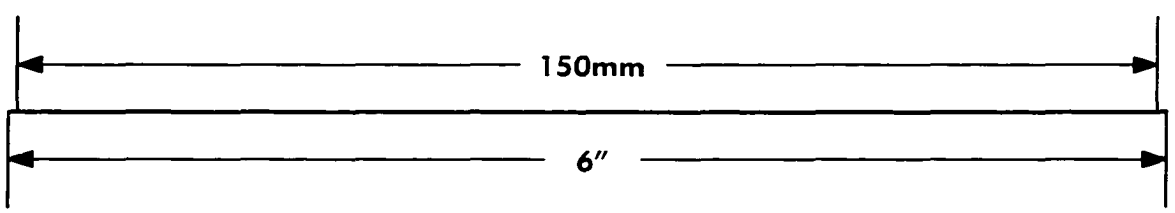

APPLIED IMAGE, Inc
1653 East Main Street
Rochester, NY 14609 USA
Phone: 716/482-0300
Fax: 716/288-5989